博士論文

Remote Cooling Sensation Display by Using Airborne Ultrasound Phased Array

（空中超音波フェーズドアレイによる遠隔冷覚提示）

中島　允

Abstract

Thermal sensation is indispensable to our lives. This sensation responds to temperature change from the outside and enable us to recognize the environment and objects. For example, when we touch the objects whose hardness is the same, the temperature change is different depending on whether it is wood or iron. This difference allows us to determine the material of the target. In addition to audiovisual sensation, a method of displaying tactile sensation has been proposed in VR technology. If thermal sensation can be displayed in haptic feedback devices, we can have a more delicate experience.

There has been growing interest in technology for remotely displaying tactile sensation to the skin surface in a non-contact manner in these days, but, the currently realized modality is mainly vibrotactile. The thermal sensation display has been mainly realized by the contact-based method, and few methods presenting heat from a distance, especially to present the cold sensation, have been proposed.

This paper aims to realize remotely displaying a cooling sensation on the skin surface without contacting the device with the user's body. For that purpose, ultrasound beam or focused ultrasound generated by an ultrasound phased array is used to vaporize the mist floating near the user's skin surface locally and instantly, and the heat of the vaporization cools the skin surface. The cooling sensation is remotely displayed in a non-contact manner.

In the experiment, firstly, the author demonstrated displaying cooling sensation by transporting the mist with ultrasound beam. Secondly, the focused ultrasound was used for the experiment instead of ultrasound beam. During the experiment, we discovered that only the part exposed to the ultrasound was cooled when a focused ultrasound was irradiated in the mist floating in midair. However, the reason has not been known yet. Since this system seems to be sufficiently useful as a haptic display, the author investigated the characteristics in detail and confirmed that it can be used for haptic display.

The result of this study is expected to develop into a more realistic aerial tactile display by applying virtual material feeling such as wood and metal.

Contents

Chapter 1 Introduction 1
1.1 Background 1
1.2 Displaying Thermal Sensation 2
1.3 Application Example of Thesis 3
1.4 Our Approach and Goal of Thesis 4
1.5 Organization of the Thesis 6

Chapter 2 Perceptual Characteristics of Thermal Sensation and Patterns of Displaying 8
2.1 Perceptual Characteristics of Thermal Sensation 8
2.2 Method of Displaying Thermal Sensation and Related Works . . . 16
2.3 Method of Temperature Measurement 19
2.4 Conclusion 20

Chapter 3 Controlling Ultrasound Beam and Focused Ultrasound Using Ultrasound Phased Array 21
3.1 Airborne Ultrasound Phased Array (AUPA) 21
3.2 Ultrasound Beam 24
3.3 Focused Ultrasound 28
3.4 Conclusion 31

Chapter 4 Superiority of Cooling Method Using Mist 33
4.1 Application Example of Mist Cooling 33
4.2 Superiority of Water as Cooling Medium 34
4.3 Droplets Generated by Ultrasound Atomization 35
4.4 Conclusion 37

Chapter 5 Remote Cooling Sensation by Transporting Mist with Ultrasound Beam 38
5.1 Prototype 39
5.2 Experiment 40
5.3 Conclusion 44

Chapter 6 Remotely Displaying Cooling Sensation Controlling Mist in Midair 45
6.1 Prototype . . . 46
6.2 Experiment . . . 48
6.3 Conclusion . . . 51

Chapter 7 Displaying Spatiotemporally Pinpoint Cooling Sensation 52
7.1 Experimental Setup . . . 53
7.2 Experiment 1 . . . 54
7.3 Experiment 2 . . . 56
7.4 Experiment 3 . . . 58
7.5 Discussions . . . 63
7.6 Conclusion . . . 65

Chapter 8 Performance Evaluation as Thermal Display 67
8.1 Heat Transfer When Contacting an Object . . . 67
8.2 Measurement of Heat Flux by Proposed System . . . 69
8.3 Performance Evaluation as Thermal Display . . . 72
8.4 Cooling Effect on Artificial Objects . . . 73
8.5 Conclusion . . . 76

Chapter 9 Interactive Fog Display with Feedback of Cooling Sensation by Focused Ultrasound 77
9.1 Background . . . 78
9.2 Prototype 1 . . . 79
9.3 Experiment 1 . . . 80
9.4 Summary 1 . . . 83
9.5 Prototype 2 . . . 84
9.6 Summary 2 . . . 90
9.7 Conclusion . . . 90

Chapter 10 Conclusion 91
10.1 Summary . . . 91
10.2 Conclusion and Consideration from Experiments . . . 93
10.3 Future Works and Prospects . . . 95

Acknowledgement 97

Bibliography 99

List of Publications 106

A Appendix A: Remote Simultaneous Displaying Cooling and Vibrotactile Sensation 109
A.1 Experimental Setup . . . 110
A.2 Measuring procedures . . . 110
A.3 Result . . . 111
A.4 Conclusion . . . 113

B Appendix B: Noncontact Pain Display by Thermal Grill illusion 115
B.1 Thermal Grill Illusion(TGI) . . . 116
B.2 Experimental Setup . . . 117
B.3 Experiment 1 . . . 118
B.4 Experiment 2 . . . 120
B.5 Conclusion . . . 123

C Appendix C: Sensing and Displaying Odor 124
C.1 Background . . . 124
C.2 Our Approach . . . 125
C.3 Prototype . . . 126
C.4 Experimental Setup . . . 127
C.5 Experiment 1 . . . 128
C.6 Experiment 2 . . . 129
C.7 Conclusion . . . 131

Chapter 1

Introduction

In this thesis, we propose a midair haptic display that provides a cooling sensation using ultrasound phased arrays. The cooling sensation is included in category of thermal sensation, and thermal sensation is included in the tactile sensation. Therefore, this thesis belongs to the field of haptic technology. In this chapter, we first discuss the importance of displaying cooling sensation in haptic technology. Then, we survey some methods of thermal sensation and introduces example of application. Finally, the goal of this thesis is summarized and the organization is described.

1.1 Background

Currently, tactile feedback is used around us like smartphones and tablets. Most of the research has focused on a system for providing a tactile sensation in virtual reality. Virtual reality (VR) refers to a technology that presents the same environment as reality, which is different from the actual thing. VR is expected to be applied to entertainment such as games, robot operation, and remote medical operation. Furthermore, it has expandability in various fields such as advertising, mail order, and ICT (information and communication technology) education.

VR has a history with the development of technology. First of all, in 1990s, the VFX series (Forte Technologies, Inc.) and Virtual Boy (Nintendo) were mentioned as devices that present audiovisual VR. In 2000s, VR games that used large enclosures for arcade began to appear. Then, along with the development of inertial sensors, Oculus Rift (Oculus VR, Inc.) [1] was released in 2012, and Vive (HTC) [2] was also released to follow. With the appearance of Playstation® VR [3] in 2016, VR devices have become popular all over the world. In addition, HoloLens (Microsoft Corp.) [4] was released, showing a dramatic improvement in VR contents. However, these devices basically presented only the audiovisual sensation, and no tactile sensation is presented. Therefore, in order to have a more delicate VR experience, it is essential to add the tactile sensation.

The haptic device does not have an input/output interface like a camera, a mi-

crophone, or a speaker. A wide variety of haptic devices exist because the tactile sensory organs are distributed throughout the body and are not uniform. In addition, the tactile sensation has much information. There is a feature that various tactile information such as force, temperature, vibration, and contact area is input from the skin surface. Here, when we experience the contact of virtual objects in VR, we have an active experience. It has been shown that active tactile sensation is required for shape perception [5], so haptic devices must basically be made for active movement. Most of the haptic devices that have been developed so far are wearable. This is the way that tactile feedback is displayed to the worn part of the body.

In recent haptic device, not only wearable devices but also technology for remotely displaying tactile sensation to the user's skin surface without wearing the device itself has been increasing. Currently, the main method uses focused ultrasound in mid-air [6][7]. Unique application such as visual and tactile interaction with aerial images have been proposed and proceeded by many researchers with the research [8][9][10][11][12]. The tactile sensation of airborne ultrasound generates a localized acoustic radiation pressure on the skin surface, thereby producing vibration and pressure sensation. On the other hand, tactile sensation generally includes sensory modalities such as thermal sensation and pain sensation in addition to vibration and pressure sensation. Thus, it is expected that remotely displaying these sensation will lead to offer us a more realistic and rich haptic experience. In addition to VR, various industrial products focusing on displaying tactile sensation have been commercialized. However, many of these products have been developed focusing on mechanical interactions between human bodies and objects. The development of products that provide tactile sensations such as softness and thermal sensation may make our lives more comfortable. In this thesis, the author focuses on the thermal sensation.

1.2 Displaying Thermal Sensation

As for displaying thermal sensation, the interest as a target of research is increasing [13][14]. This is basically achieved by heat convection with a wearable device such as the Peltier element [15][16]. In addition, a method of displaying thermal sensation has been proposed by using water as the heat medium [17][18]. It is shown that the method can change the temperature more quickly by switching hot and cold water with a solenoid value. Human beings are said to recognize the sense of material by characteristics of heat convection when touching an object, as well as the perception of temperature in the environment such as "hot"and "cold"[19]. Also, a person may feel temperature of the air without touching the object. Using this fact,

a method exists which displays thermal sensation by controlling the humidity of the air [20]. The method uses the liquefaction of steam to control the humidity. It is highly versatile since water is used as the heat medium.

Displaying thermal sensation with noncontact remote manner has advantages that it does not interfere with the user's body movements and the displaying area is wide; although it is fewer compared with contact manner. However, remotely heating or cooling the user's skin surface causes a physical difficulty. The method of transporting heat is mainly conducted and radiated heat. For remote heating sensation, a method using a laser or a halogen lamp was proposed [21]. In addition, since it is easy to heat the user's skin surface selectively and locally, a method using infrared rays was proposed [22]. These methods can control the irradiation position by using a lens or a Galvano mirror. On the other hand, a similar practical method has not been established for a remote cooling sensation. There was no other way to place the medium depriving heat in the cooling area where it was displayed. For this reason, it is difficult to display cooling sensation locally and with high time resolution. Therefore, it remains an unsolved problem. Although there is a method of transporting cooling air in mid-air with a fan or blower, it is difficult to display cooling sensation locally. Furthermore, high spatial resolution is required. A method has been proposed controlling the flow velocity of cold air generated from a vortex tube [23]. The distance displayed in the air is relatively short, since the distance between device and the user's skin surface is about 5cm.

1.3 Application Example of Thesis

In this research, the purpose is to display the cooling sensation. In general, displaying thermal sensation together with heating sensation leads to a sense of immersion in a VR environment or a remote location, an improved sense of presence, and a highly sensitive experience. Furthermore, the technology of displaying thermal sensation in remote control of VR and robots is mainly applied to the reproduction of the environment and the tactile sensation of contacting objects [24].

Regarding the reproduction of the environment, experiencing the temperature of the air in the VR environment more highly reproduces the sensation that exists at that location. For example, reproducing the thermal sensation of the environment is used for attractions such as theme parks. In Orbi Yokohama [25], you can experience a simulated temperature difference between -15 and $20\,^{\circ}$C on your skin. At the International Antarctic Center [26], New Zealand, there is the attraction that recreate the Antarctic climate. By reproducing the temperature and inducing winds that simulate gusts and storms, you can virtually simulate the Antarctic environment. Also, in recent years, the technology for displaying thermal sensation by wind and

splashes according to video contents, such as a 4D theater, is being introduced in movie theaters and museums.

On the other hand, as for reproducing the tactile sensation of contacting object, when a person touches an object, the temperature of skin surface changes due to the characteristics of heat conduction [15]. By detecting the temperature change, it is possible to determine the material and state of the target object. Therefore, reproducing temperature change is considered to be one of the important factors for displaying tactile sensation.

Here, in combination with the method in this research, it is possible to locally reproduce the effect of climate on the skin surface in VR environment. In addition, if an aerial image is combined and the thermal sensation can be displayed at the same time as the haptic feedback, a telexistence with a tactile sensation including the thermal sensation will be realized. Applications for 3D CAD can be expected [27]. Applications other than remote control of VR and robots include interfaces and media art.

In recent years, a method of displaying the tactile sensation of a virtual object has been proposed by combining aerial image and a haptic display [28][29]. Then, the method of this thesis contributes to the improvement of the performance of a haptic display in the future. This improves the texture by reproducing a cold sensation on the virtual object as shown in figure 1.1. For example, it is expected to be applied to a more realistic aerial tactile display by applying virtual material feeling such as wood and metal.

1.4 Our Approach and Goal of Thesis

We proposed a method of displaying cooling sensation by guiding cold air to an arbitrary position on the body by generating acoustic flow driven by an ultrasound beam (Fig. 1.2) [30]. Then we used the ultrasound phased array for controlling the propagation direction and the position of the acoustic beam, which resulted in cold air flow that could be steered to a desired position as a cooling spot. The ultrasound beam can be narrowed down to a comparable size to the ultrasound wavelength, $8.5\,\mathrm{mm}$ in the setup. The narrow beam could successfully transport a cold air mass and generate a localized cold spot on a skin away from the device. However, since dry ice was used as the cold-air source, preparation of the dry ice is a problem, which limits the range of practical applications.

In this thesis, firstly, we propose a method where a mist is transported in the air using the same device and cooled by using the heat of vaporization of water to display cooling sensation. We fabricated a prototype of the system and measured the temperature change of the user's palm exposed to mist. In addition, the measure-

ment was also conducted using the cold air of dry ice, and the cooling effect was compared. As a result, it was shown that the cooling effect was higher when the mist was used than when the cold air of dry ice was used.

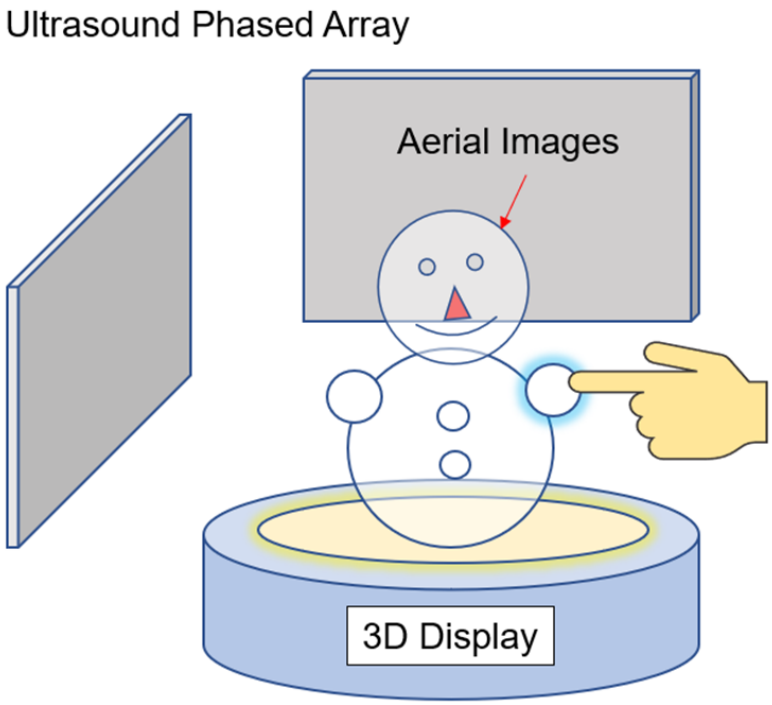

Fig. 1.1. One example of applications in this thesis.

Secondly, we developed a remote cooling method that converges the mist floating near the user's skin using focused ultrasound, and then instantaneously vaporizes mist to display a cooling sensation by the heat of vaporization. Similarly, we describe the prototype of a system that remotely displays cooling sensation by converging mist with focused ultrasound. We confirm that the cooling effect is more likely to be effective when these are combined than when the focused ultrasound or mist is only used. In order to investigate the applicable range of the proposed method, we measure the quantitative relationship between the amount of generated mist and the distance of displaying position. In addition, we investigated the cooling effect in the direction of mist emission. Then, we measured the thermographic spatiotemporal temperature change using focused ultrasound while mist was generated. we measured that a cooling sensation moving in real time was also generated when the focused ultrasound moved on the skin surface.

Finally, we discuss the results and applications of this thesis to haptic technology.

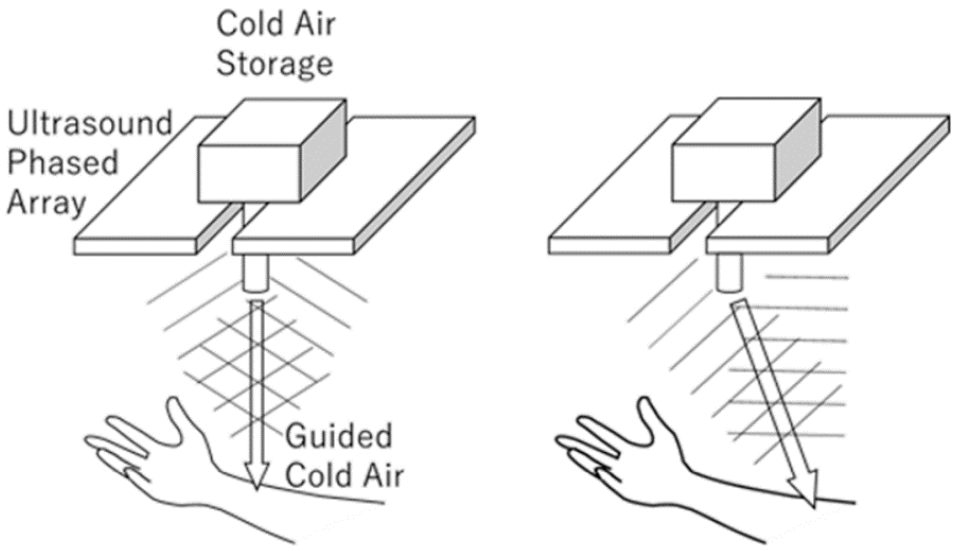

Fig. 1.2. Steerable ultrasound-driven cold air flow can present a cooling sensation on an arbitrary position on the human body [30].

1.5 Organization of the Thesis

This thesis is organized as follows: In Chapter 2, we explain the perceptual characteristics of thermal sensation. Next, we describe patterns of displaying thermal sensation and explain the basic method of temperature measurement.

Chapter 3 describes the method of controlling ultrasound beam and focused ultrasound using the ultrasound phased array. Firstly, we explain how to form acoustic field by controlling the ultrasound phased array. Secondly, we describe the characteristics of ultrasound beam in detail. Finally, we describe the method of forming focused ultrasound.

Chapter 4 describes the characteristics of cooling method using water mist. Firstly, application example of mist cooling is introduced. Next, we explain the superiority of water as cooling medium. we described the generation of droplets by the phenomenon of ultrasound atomization.

Chapter 5 describes the method of remotely displaying a cooling sensation using ultrasound-driven cold airflow cooled by mist vaporization. A prototype of system was created, and the temperature change in the user's palm exposed to mist was

measured. In addition, we measured the temperature change in the case of using cold air of dry ice and compared the cooling effect.

In chapter 6, the prototype used in chapter 5 was improved to enhance cooling effect. The reconstructed system can control the amount of mist generation. Then, we measured the temperature change of the user's palm exposed to mist.

Chapter 7 describes the method of remotely displaying a cooling sensation using a focused ultrasound. By using a focused ultrasound, it can converge the water mist floating near the user's skin surface. In addition, it can instantaneously vaporize mist to display a cooling sensation due to the heat of vaporization. A prototype used in this chapter is the same as that in chapter 6. Using the prototype, we conducted three types of experiments.

Chapter 8 describes the method of evaluating the performance of the system in chapter 7 as a thermal display. The evaluation method was performed by estimating the heat flux. In addition, the heat flux was calculated by measuring the temperature change when the artificial object was cooled.

Chapter 9 describes the application system using a cooling sensation display in chapter 7. The water mist is used not only as a coolant but also as a fog display. We propose an interaction system with a cooling sensation and an image which is projected on a mist screen.

In chapter 10, we finally conclude this thesis.

Chapter 2

Perceptual Characteristics of Thermal Sensation and Patterns of Displaying

Although the proposed method in this thesis is only one of the methods of displaying the thermal sensation, we give an overview of the perceptual characteristics of thermal sensation. In addition, we introduce the pattern of the basic method of displaying thermal sensation through related works. Finally, the method of temperature measurement is described.

2.1 Perceptual Characteristics of Thermal Sensation

In this section, we describe the thermal sensation in the tactile sensation and introduce the mechanism that detects temperature change of human body. In addition, we describe the psychophysical findings. In the system design of displaying the thermal sensation, it is necessary to clarify not only the physical temperature change but also the psychophysical stimulus presentation.

2.1.1 Thermal Sensation in Tactile Sensation

In general, the five senses are the generic term for sight, hearing, tasting, pain, and touching. The present ”tactile sensation” was defined after the end of the 19th century [31]. Previously, many sensory relationship such as hot, cold, hard, and pain were included [32]. Furthermore, since there are many types of sensations, the cause of the ”tactile sensation” was not clearly defined. Therefore, ”tactile sensation” includes many modalities of sensation, and it was argued whether to define it as one sensation. However, the present ”tactile sensation” is defined as a generic term for the following sensations.

- Cutaneous Sensation : Mechanical deformation of skin, skin temperature,

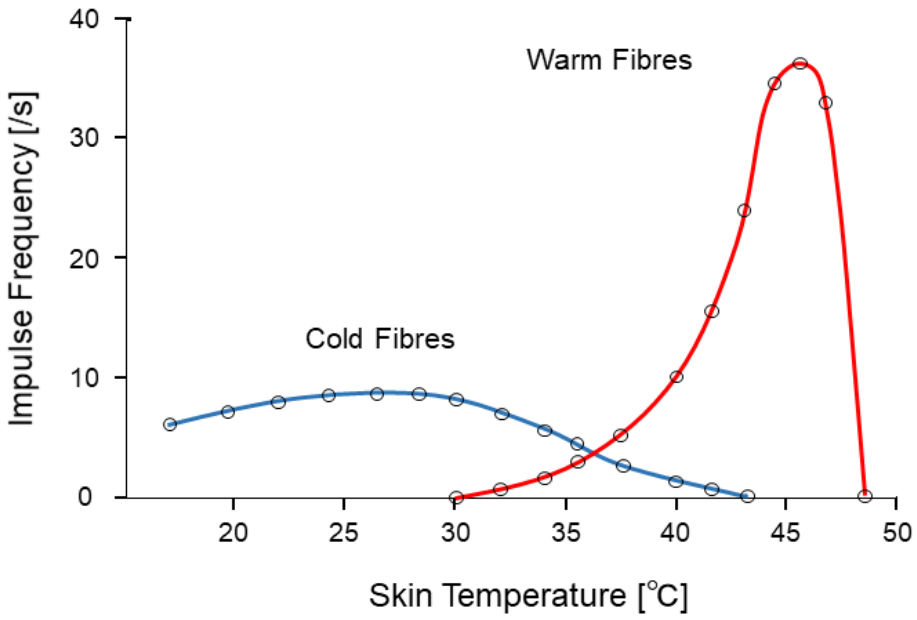

Fig. 2.1. Static response characteristics of warm and cold receptors. Reconstructed and modified from [33].

pain sensation, etc.

- Deep Sensation : Posture of limbs, force acting on joints, etc.
- Balance Sensation
- Visceral Sensation

The thermal sensation we focused on in this thesis is one of the cutaneous sensations. The existence of hot spots and cold spots was classically mentioned as the thermal sensation, but the number of hot spots is smaller than that of pressure or pain points. Depending on the body part, the density of spots may be extremely different and there may be only cold spots like the cornea. However, it is known that there are more receptors than hot spots. When heating sensation occurs at a site with few hot spots, it is considered that spatial weighting is caused by multiple receptors. Therefore, there are many mysteries about the mechanism by which the warm or cold sensation occurs. In the following sections, we explain the temperature change detection mechanism that has been known up to now regarding the thermal sensation.

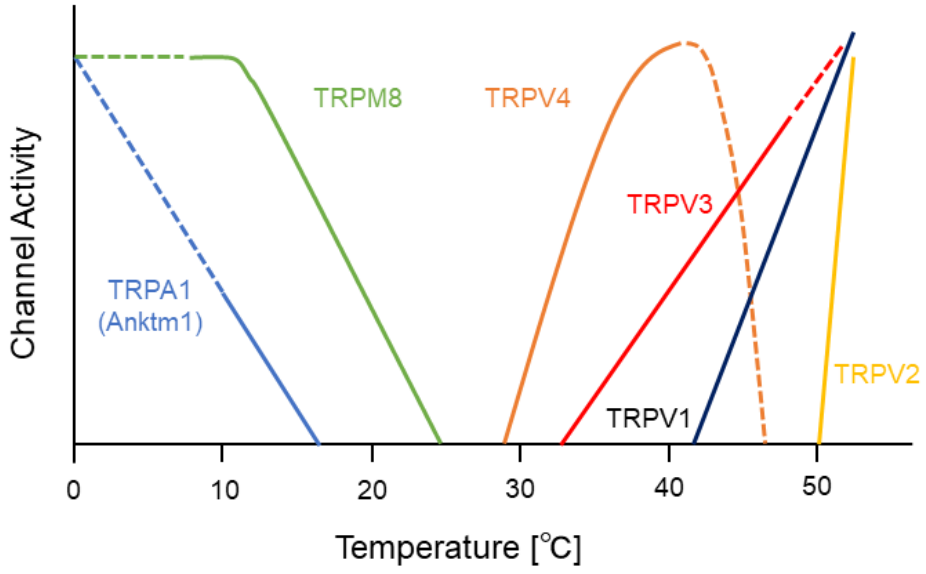

Fig. 2.2. TRP channels and response characteristics. Reconstructed and modified from [33].

Recepter	Temperature sensitivily	Tissue distribution	Non-thermal agonists
TRPV1	≥42 °C	PNS, Brain, Spinal cord, Skin, tongue, bladder	Capsaicin, Lipoxygenase, Acidic pH, Resiniferatoxin, Anandamide, Ethanol
TRPV2	≥52 °C	PNS, Brain, Spinal cord, Widely expressed	Growth factors (mouse)
TRPV3	>33 °C	Skin, PNS	
TRPV4	25~42 °C	Kidney, PNS, Skin, Inner ear, Brain, Liver, trachea, heart, Hypothalamus, Fat, Endothelium	Hypotonic, 4-αphorbol
TRPM8	≤25 °C	PNS, Prostate	Menthol, icilin, eucalyptol
TRPA1	≤17 °C	PNS	Icilin

PNS : Peripheral Nervous System

Fig. 2.3. Properties of TRP channels involved in thermal transduction. Reconstructed and modified from [33].

2.1.2 Detection Mechanism of Temperature Change

There are two types of warm receptors (hot spots) and cold receptors (cold spots) just below the epidermis. The warm receptors are 0.3-$0.6\,\mathrm{mm}$ deep from the skin surface, and the cold receptors are 0.15-$0.17\,\mathrm{mm}$ deep. temperature change on the skin is detected by these two receptors. Although density of thermal receptors varies according to body parts, it has been found that cold receptors are more abundant than warm receptors [34]. In addition, the transmission velocity of cold receptors (5-$30\,\mathrm{m/s}$) is faster than that of warm receptors (0.5-$2\,\mathrm{m/s}$) [35].

Furthermore, the warm and cold receptors show static (steady) and dynamic (instantaneous) responses regardless of warm or cold stimulation. The static response corresponds to the absolute temperature, and the dynamic response corresponds to the temperature change rate. On the other hand, between 30 and $36\,^{\circ}\mathrm{C}$, there is a temperature range where the temperature sensation is not sensed. However, in that area, both receptors spontaneously fire at a low frequency. Then, if the skin temperature changes from this intermediate temperature range, the relative firing frequency of the receptor changes. In fact, an increase in skin temperature promotes firing of warm receptors, and a decrease in skin temperature promotes firing of cold receptors. From figure 2.1, the warm receptors respond at 30 to $50\,^{\circ}\mathrm{C}$, with the highest firing frequency near $45\,^{\circ}\mathrm{C}$. The cold receptors respond at 5 to $43\,^{\circ}\mathrm{C}$, with the highest firing frequency in the range of 22 to $28\,^{\circ}\mathrm{C}$ [34][36]. It is known that nociceptors respond as excessive temperature stimuli that produce pain sensation when skin temperature rises above $45\,^{\circ}\mathrm{C}$ or below $15\,^{\circ}\mathrm{C}$.

When skin temperature changes, warm and cold receptors respond dynamically. An on-reaction is a instantaneous increase in the frequency of action potential release when the temperature receptor heats the skin. The maximum firing frequency depends on the temperature change rate, the temperature change range, and the skin acclimation temperature. In addition, when the skin is cooled, the instantaneous suppression of firing is called off-reaction. Therefore, when the on reaction occurs when the skin is heated, and the off reaction occurs when it is cooled.

There are other processes that convert thermal stimuli into electrical or chemical signals. It is caused by ion channels located in skin cells and thermal receptors. For these ion channels, a total of 6 temperature TRP (Temperature-activated-Transient Receptor Potentials) channels have been discovered: 4 channels that are activated by heating and 2 channels that are activated by cooling. Firstly, TRPV 1 and 2 are activated by heat in the area of pain sensation among two channels activated by heat. TRPV 3 and 4 are activated in painless warmth. On the other hand, among the channels activated by cooling, TRPM 8 is activated at a low temperature at which

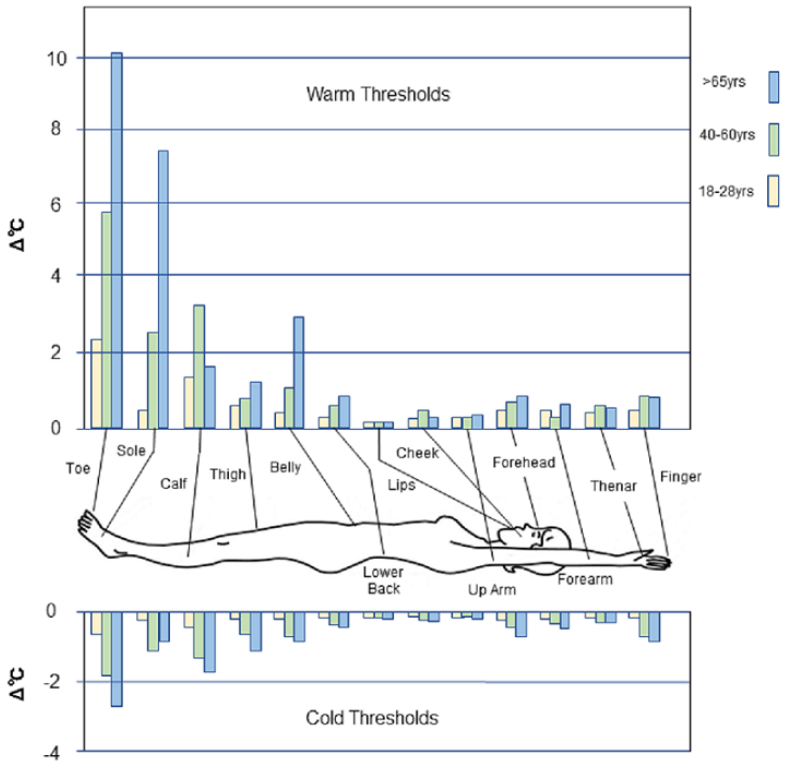

Fig. 2.4. Perceptual sensitivity of warm sensation (upper side) and cold sensation (lower side) in each body part. Reconstructed and modified from [37].

no pain is produced, and TRPA 1 (Anktm1) is activated in the area of pain sensation. In chemical substances, TRPV 1 reacts with capsaicin, the main component of red pepper, and TRPM 8 reacts with menthol, the main component of mint [33]. Figure 2.2 shows the relationship between the temperature TRP channel and the response characteristics. Furthermore, Figure 2.3 shows the properties of ion channels involved in thermal transduction.

2.1.3 Perceptual Sensitivity

In the system design of displaying the thermal sensation, it is necessary to clarify not only the physical temperature change but also the psychophysical stimulus presentation. In this section, we introduce the characteristics of perceptual sensitivity.

In figure 2.4, the upper and lower bars show the body maps of regional warm and cold sensitivity. Figure 2.4 shows that the higher the threshold of warm sensation, the lower the perceptual sensitivity of warm sensation [37]. Similarly, the higher the threshold of cold sensation, the lower the perceptual sensitivity of cold sensation. From the results, the following is shown.

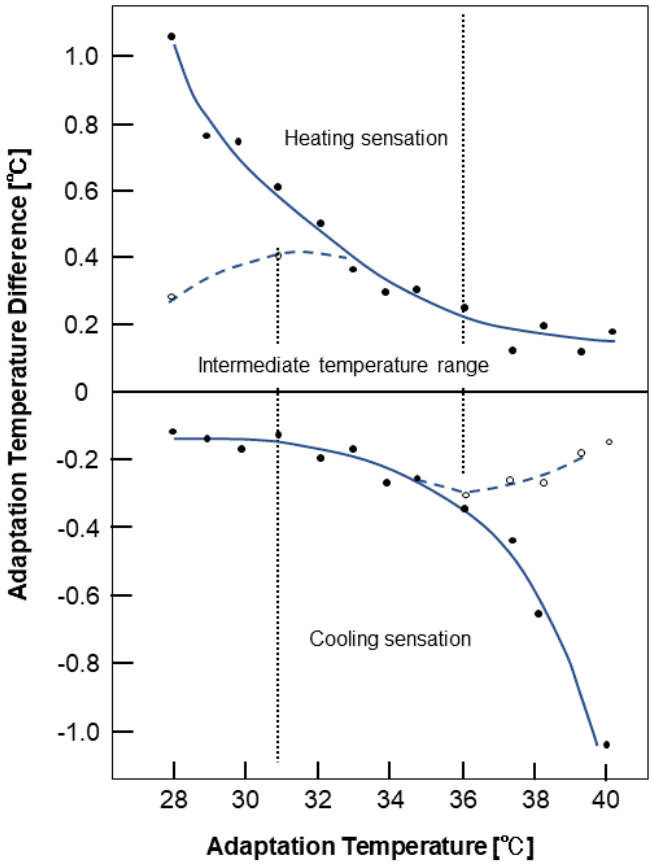

Fig. 2.5. Relationship between adaptation temperature and detection threshold per $15\,\mathrm{cm}^2$ of stimulated area. Reconstructed and modified from [38].

- The perceptual sensitivity of thermal sensation varies depending on the body parts, so the lips have the highest sensitivity in the face, but the limbs are not.
- For any body part, the cold sensation has a higher perceptual sensitivity than the warm sensation.
- Perceptual sensitivities may differ even in the hands. The ball of the palm is more sensitive to both warm and cold sensation than the fingertips.
- All body parts are perceptually sensitive to cold rather than warm stimulation. The higher the cold sensitivity, the higher the temperature sensitivity.
- The perceptual sensitivity to thermal sensation tends to decrease with age.

On the other hand, in figure 2.5, the skin adaptation temperature also affects the detection threshold, as in figure 2.4. The following is shown from figure 2.5 [38].

- Case of low skin temperature : The detection threshold for warmth tends to be larger than that for coldness.

- Case of high skin temperature : The cold sensation is preferentially perceived.
- Case of high adaptation temperature : The detection threshold of warm sensation becomes small and the detection threshold of cold sensation becomes large.

2.1.4 Spatial Characteristics

Here, regarding the perception of thermal sensation, we introduce the spatial characteristics of thermal stimulation, other than the characteristics of perceptual sensitivity. When the thermal stimulation is weak, the characteristic of spatial weighting is shown [39][40][41]. Spatial weighting means that the intensity of the thermal stimulation and the spatial range are transformed so as to maintain a threshold or above threshold sensation. Spatial weighting differs between warm and cold sensations. The degree of spatial weighting in the warm sensation weakens when the stimulus intensity is high. The degree of spatial weighting in cold sensation is similar for the temperature drop in the range of 1.5 to 12 °C [42]. Furthermore, for both warm and cold sensations, the effect of spatial weighting tends to decrease as the thermal stimulus approaches the area of pain sensation [43].

On the other hand, the ability to localize thermal stimulation without contact depends on the intensity of the stimulation. When the intensity of stimulation is low, the localization ability of thermal stimulation is extremely low. When infrared radiant heat is irradiated to the skin surface, spatial thermal information such as position, width, and shape is likely to be ambiguously judged [44][45]. On the contrary, it is known that the localization ability improves as the stimulation intensity increases [41][46][47]. In addition, the localization of the thermal stimulation during the contact between the hand and the object is evaluated by using the object that causes different temperature drops for the fingers [15].

2.1.5 Temporal Characteristics

In addition to the spatial characteristics in the previous section, we introduce the characteristics of the temporal response to thermal stimulation. Adaptation means the loss of response to a thermal stimulation when applied continuously. For example, the warm sensation of taking the bath gradually disappears even if the temperature of the hot water is kept constant. This is called adaptation. Due to this characteristic, when adapted to a certain temperature range, it is possible to operate as in an intermediate temperature in which neither cold feeling nor warm feeling occurs. Then, the temperature change criterion changes. The temperature range in which full adaptation occurs depends on the body part and the stimulation range.

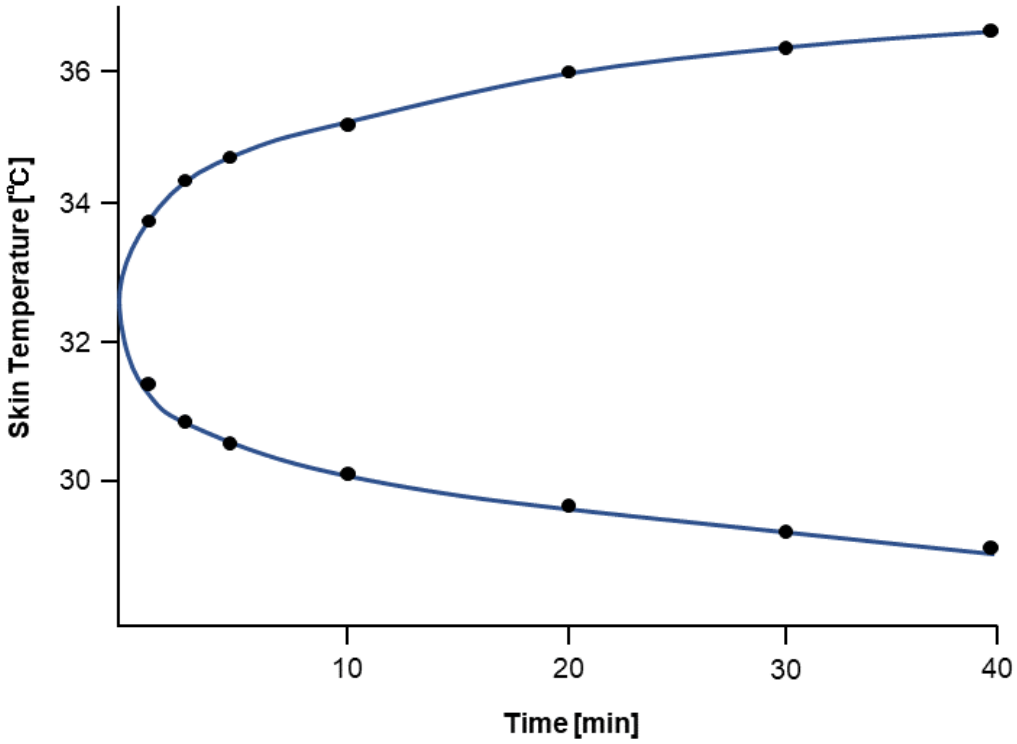

Fig. 2.6. Relationship between adaptation temperature and time in the forearm. Reconstructed and modified from [48].

From figure 2.6, it is 28-37.5 °C when a stimulus of $14.4\,\mathrm{cm}^2$ is applied to the forearm [48]. In the case of a finger, since the stimulation range is small, the temperature range for total adaptation is 17-40 °C [49]. The speed of adaptation depends on the difference between the initial skin temperature and the adaptation temperature. Adaptation occurs as soon as the initial skin temperature is close to the adaptation temperature. Adaptation takes longer if the adaptation temperature is far away.

Also, the duration and intensity of thermal stimulation are transformed to maintain threshold and above threshold sensations similarly to the spatial weighting. This is called time weighting. The characteristics of time weighting have been investigated by thermal stimulation of the face [50]. If the duration of irradiation from infrared rays is less than $1\,\mathrm{s}$, the duration and intensity of stimulation are exchanged with each other. However, if the duration is $1\,\mathrm{s}$ or more, the effect of time weighting is not seen. On the other hand, it is not clear whether time weighting occurs in cold stimulation as well, since no similar study has been done for cold stimulation.

The response time to the thermal sensation is measured for each body part

[51][52]. The results of these studies indicate that cold stimulation has a shorter response time than warm stimulation. Besides, the response time in the temperature characteristic of the material is longer than the simple response time. Furthermore, the determination time of the thermal characteristic is longer than the determination time of the tactile characteristic.

2.2 Method of Displaying Thermal Sensation and Related Works

There are a variety of methods in the technology of displaying thermal sensation. In this section, we classify the method of displaying the thermal sensation. The method of displaying the thermal sensation is roughly divided into two types depending on whether or not the skin temperature is changed. Next, in the method of changing the skin temperature, whether the device for displaying thermal sensation is in contact with the skin or not. That is, it is divided into a contact manner and a non-contact manner. It has been proposed to display the thermal sensation by using one or more of these methods. Furthermore, using the characteristics of human perception, the method of displaying the thermal sensation has also been proposed.

here, the term ”heating sensation” and ”cooling sensation” are defined as follows. These term belong to warm and cold sensations, respectively.

- Heating sensation: The warm sensation when it is physically heated.
- Cooling sensation: The cold sensation when it is physically cooled.

2.2.1 The method of changing the skin temperature

・Contact manner

In many cases, the Peltier device is used as the method of displaying the thermal sensation when wearing the device on the skin [16][19]. The Peltier device is a semiconductor device that uses the Peltier effect, which is the effect of heat transfer from one metal to the other. In this device, the heat transfer direction and the amount of heat transfer can be controlled by the direction and the amount of the electric current. Therefore, both warm and cold sensation can be displayed. The amount of heat can also be electrically controlled. In addition, it is convenient since it has a size of several mm to several hundred mm. However, in order to provide a stable cold sensation, a heat dissipation mechanism has to be provided on the surface opposite to the displaying direction.

As a method other than the Peltier element, a method has been proposed in which

a liquid is made to flow inside a metal and the temperature of the liquid is controlled to display the thermal sensation. Sakaguchi et al. proposed a method of displaying thermal sensation using hot and cold water [17]. This is suitable for displaying a thermal sensation over a wide area since the entire path of the heat medium fluid can be used as a surface of displaying. However, it is necessary to have a mechanism for storing the fluid changing the temperature of the fluid, or for transporting the fluid to the user's body part. In other words, there are issues regarding system design. Furthermore, it is possible to create a device of displaying the thermal sensation by using the Joule heat.

・Non-contact manner

As for a method of displaying thermal sensation without contacting device, an air conditioner that changes the temperature of the air can be used. In addition, a method of heating the skin surface using radiant heat such as infrared rays or a laser to display the thermal sensation has been proposed [21][22]. The method using an air conditioner or a fan can display the cold sensation to a wide area such as the whole body. However, high spatial resolution is required when displaying at any specific position such as fingertip.

Thermal sensation may be affected by mechanical tactile sensation. In the non-contact manner, the warm and cold sensation without mechanical sensation can be displayed.

Here, we introduce some methods of displaying thermal sensation without contacting device and describe them in detail.

(1)Halogen lamp

Saga proposed the method of heating the user's skin surface using a halogen lamp [21][53][54]. This method is the system of remotely displaying heating sensation. The condensing reflector can converge the radiant heat of the halogen lamp and control the irradiation direction. It is shown that it is possible to control the radiant intensity within a certain distance range and display a virtual wall. Further, it has been attempted to use the generation of pain sensation due to the characteristics of the thermal receptor. As described in the perceptual characteristics of thermal sensation, the thermal sensation consists of the responses of several receptors. Each receptor receives a different temperature range. One of them, TRPV1, produces not only heating sensation but also pain sensation.

(2)Laser light

Similarly, Saga proposed the method of displaying heating sensation using a laser light [22][55]. Compared with the method using a halogen lamp, there are signifi-

cant restrictions on the distance and accuracy of displaying heating sensation. The advantage of using a laser light is the high spatial resolution displayed on the user's skin surface. In addition, by using a Galvano mirror, high-speed scanning can be realized, and it becomes possible to display the point heating sensation by laser light in a wider range. Furthermore, in the method using a halogen lamp, the emitted light beam contains light in a wide frequency band. On the other hand, it is possible to emit only a light beam with a very limited frequency by using a laser light. Therefore, an active sensor using infrared light such as Kinect2 can be used for human body sensing. In fact, it is shown that control of the scan area can be easily realized. However, due to the reflection characteristics of the mirror, the high enough radiation heat cannot be obtained.

(3)Vortex tube
Xu et al. proposed the method of non-contact displaying the cold sensation by controlling cold air flow generated from a vortex tube [23]. The method is based on a cooling model that relates the flow velocity of cold air and the heat absorbed from the user's skin. It is known that the factors which affect the cold sensation are the temperature and flow velocity of the environmental air [56]. The vortex tube can produce cold air in a short time only by supplying compressed air. The temperature of the output air is related to the pressure of compressed air. As the pressure of the compressed air increases, the temperature of the air discharged from the cool air outlet decreases, and the temperature of the air discharged from the warm air outlet increases [57]. Therefore, various cold sensation is displayed in a non-contact manner by controlling the flow rate of cold air coming out of the tube and mixing with cold air. It was shown that the measured temperature drop increased as the flow velocity of the cold air increased. However, the distance of displaying needs to be improved, since the distance between device and the user's skin surface is about 5cm. The distance between the user's skin surface and the device is preferably several meters or more in order to display cold sensation remotely.

(4)Focused airborne ultrasound
Kamigaki et al. proposed a non-contact method to display the heating sensation by airborne ultrasound [58]. This method uses ultrasound phased arrays to generate airborne ultrasound. At this time, the heating sensation is displayed in a non-contact manner by irradiating the glove worn by the user with airborne ultrasound. In other words, the heating sensation is due to sound absorption and heat generated by the glove irradiated with ultrasound. Therefore, it is displayed by heat conduction to the skin surface in contact with the glove. In addition, the system can display not only the heating sensation but also vibrotactile sensation at the same time. This is

because the ultrasound phased array can modulate the amplitude at a frequency at which the tactile receptors easily fire. In fact, it was shown that the heating sensation was displayed by the irradiation of airborne ultrasound. Furthermore, it was confirmed that the vibrotactile sensation can be displayed by changing patterns of irradiating ultrasound.

2.2.2 The method which does not change the skin temperature

Some thermal receptors respond to certain chemicals, such as capsaicin for warmth and menthol for coldness [33]. Due to this characteristic, it is possible to display a cold sensation without directly changing the skin temperature.

It has also been reported that thermal sensation is generated from visual information such as the appearance and scenery of objects related to color and temperature [59]. Therefore, it is expected that the use of multi-sensory interaction will illusionally display the thermal sensation.

2.3 Method of Temperature Measurement

It is important to measure the skin temperature when the skin temperature is changed regardless of contact or non-contact manner. Thermistor and thermocouple are mainly used to measure temperature. In addition, a thermography camera is used for measuring the temperature of the object surface. Here, we describe each measurement method in detail.

・Thermistor

A thermistor is an element whose resistance changes when the temperature changes. Electricity flows more easily at higher temperature and becomes difficult to flow at lower temperature. Therefore, temperature information can be obtained by observing the flow of electricity in the thermistor. It is small, resistant to shock and vibration, and highly sensitive to temperature. However, it is not possible to measure accurate temperature depending on the environment temperature.

・Thermocouple

A thermocouple is a temperature sensor composed of two different types of metal conductors. This sensor uses the Seebeck effect, where a voltage corresponding to the temperature difference between the metals is generated when two different kinds of metals are joined. It has advantages such as long life, heat resistance and mechanical strength.

・Thermography Camera
It is a temperature sensor that estimates the temperature distribution from infrared rays which are emitted from the surface of an object. It is possible to measure the temperature of the object surface in a non-contact manner. Therefore, it is suitable for use in combination with methods of displaying the thermal sensation remotely. However, if there is an object that does not transmit infrared rays between the measurement target and the camera, the temperature of the target cannot be measured.

2.4 Conclusion

In this chapter, firstly, we described the perceptual characteristics of the thermal sensation. Secondly, we introduced patterns of displaying the thermal sensation and related works. Finally, the method of temperature measurement is described. Here, in this section, we examine fields suitable for the proposed method in this thesis.

Regarding the purpose of this study, it is to remotely display a cooling sensation on the user's body without wearing the device on the user's skin surface. From the classification of displaying method patterns, it is classified as a method of displaying the thermal sensation in a non-contact manner. In the proposed method of this thesis, the ultrasound beam or focused ultrasound is utilized by using the ultrasound phased array. The beam size can be focused down to about the wavelength. Therefore, a cooling sensation can be displayed with good localization at a distance from the device by a sound source with an appropriate aperture. It means that the spatial resolution is higher than the method of displaying the cooling sensation using an air conditioner. The principle and details of the proposed method using the ultrasound phased array are described in the next section.

Chapter 3

Controlling Ultrasound Beam and Focused Ultrasound Using Ultrasound Phased Array

In this thesis, our proposed method uses the ultrasound phased array. In this chapter, we describe fundamental principle of the ultrasound phased array. First, we introduce the method of creating acoustic field using the ultrasound phased array. Second, we explain how to form the ultrasound beam and related works. Finally, the method of forming the focused ultrasound.

3.1 Airborne Ultrasound Phased Array (AUPA)

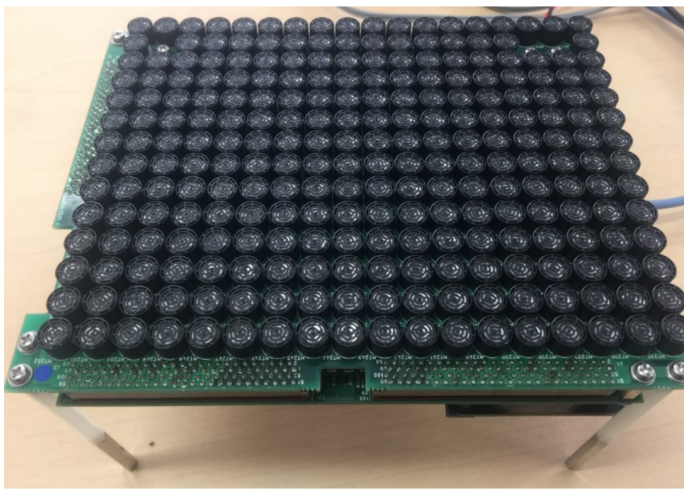

Fig. 3.1. Appearance of the AUPA.

We use the airborne ultrasound phased array (AUPA) developed by Iwamoto et al. as the ultrasound phased array used in our proposed method [6][7][60]. AUPA is a phased array in which ultrasound transducers are arranged in a grid pattern. This

device can make the sound field with various spatial distributions by controlling the phase delay and amplitude of output waveform for each transducer using driving signal control and acoustic metasurface [61]. Thus, the ultrasound beam and focused ultrasound can be formed on arbitrary three-dimensional positions. In addition, by applying amplitude modulation to acoustic radiation pressures of the ultrasound beam and focused ultrasound, the tactile receptors are fired. In other words, the tactile sensation is generated. In this section, we describe the basic theory of acoustic field formed by AUPA (Fig. 3.1).

3.1.1 Acoustic Field Controlled by AUPA

The complex sound pressure formed by the ultrasound phased array consisting of N transducers at time t and position $\boldsymbol{r} = (x, y, z)$ can be represented by the superposition formed by each transducer at $\boldsymbol{r}_n = (x_n, y_n, z_n)$:

$$p(\boldsymbol{r}, t) = \sum_{n=1}^{N} A_n \frac{D(\theta_n)}{\|\boldsymbol{r} - \boldsymbol{r}_n\|} \mathrm{e}^{-\beta\|\boldsymbol{r}-\boldsymbol{r}_n\|} \mathrm{e}^{\mathrm{j}(k\|\boldsymbol{r}-\boldsymbol{r}_n\|-\omega t)} \mathrm{e}^{\mathrm{j}\phi_n} \tag{3.1}$$

where the subscripts $n = 1, 2, ..., N$ is the index of the transducer, $A_n, \phi_n, \boldsymbol{r}_n$ represent the output amplitude, phase, and position of transducer n, respectively, θ_n is an angle from normal direction to transducer, and $D(\theta_n)$ is the directivity of the transducer. In addition, $\beta = 1.15 \times 10^{-1}$ [Np/m] is the coefficient of air damping, and k, ω are the wave number and angular frequency, respectively.

In the case of AUPA used in this research, both the amplitude A_n and the phase ϕ_n have a resolution of 8 bits. The transducer (T4010A1, Nippon Ceramic Co., Ltd.) has a resonance frequency of 40 kHz. It has directional characteristics as shown in figure 3.2. Here, the desired distribution of sound pressure is discretized into M control points. According to the expression(3.1), the distribution of sound pressure and method of driving can be written as follows. Then, the time oscillation component is excluded.

$$\boldsymbol{p} = \boldsymbol{G} \cdot \boldsymbol{q} \tag{3.2}$$

$$\boldsymbol{p} = [p_1, p_2, ..., p_M]^{\mathrm{T}} \tag{3.3}$$

$$\boldsymbol{G} = \begin{pmatrix} G_{11} & \cdots & G_{1N} \\ \vdots & \ddots & \vdots \\ G_{M1} & \cdots & G_{MN} \end{pmatrix} \tag{3.4}$$

$$G_{m,n} = \frac{D(\theta_{m,n})}{\|\boldsymbol{r}_m - \boldsymbol{r}_n\|} \mathrm{e}^{-\beta\|\boldsymbol{r}_m-\boldsymbol{r}_n\|} \mathrm{e}^{\mathrm{j}(k\|\boldsymbol{r}_m-\boldsymbol{r}_n\|)} \tag{3.5}$$

$$\boldsymbol{q} = [q_1, q_2, ..., q_N]^{\mathrm{T}} \tag{3.6}$$

$$q_n = A_n \mathrm{e}^{\mathrm{j}\phi_n} \tag{3.7}$$

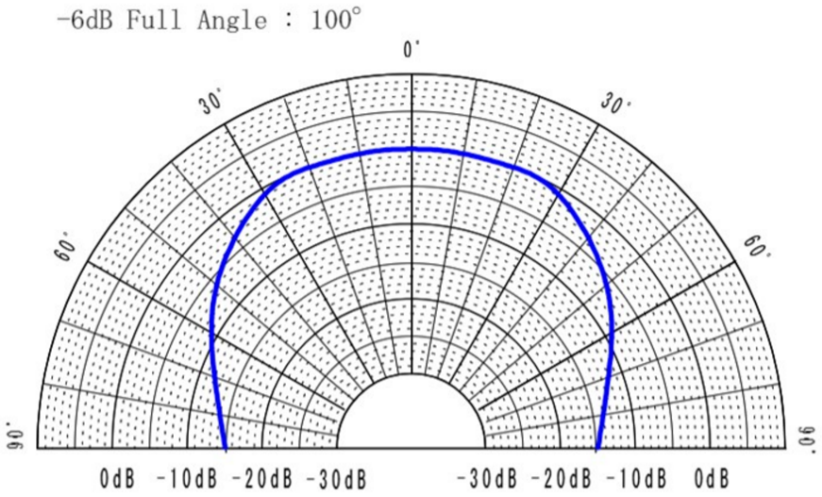

Fig. 3.2. Directivity of T4010A1 from the datasheet.

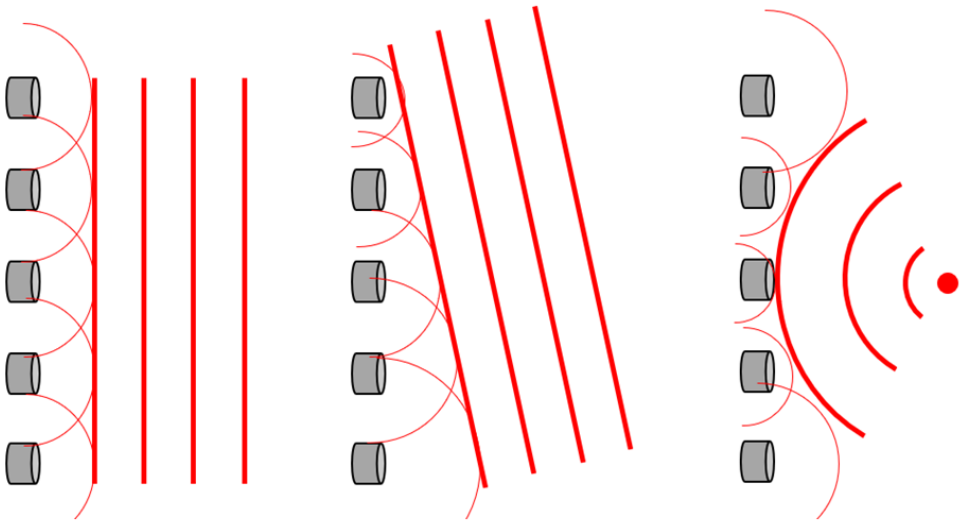

Fig. 3.3. Examples of wavefronts generated by AUPA.

The subscripts $m = 1, 2, ..., M$ is the index of the control point. G is determined as a matrix of the transfer function by arrangement of transducers and control points. $\boldsymbol{q}$ is complex amplitude of the transducer outputs and the amplitude and phase of each transducer can be changed with 8 bit resolution. Therefore, in case of using AUPA, $\boldsymbol{G}$ is physically determined, and $\boldsymbol{q}$ is programmable. Based on the Huygens's principle, AUPA can create arbitrary wave front out of phased-emission from multiple transducers (Fig. 3.3).

3.1.2 Acoustic Radiation Pressure

When displaying tactile sensation by ultrasound, it is desirable that the sound pressure is as high as possible. This is the reason that the acoustic radiation pressure P $[\mathrm{Pa}]$ is proportional to the square of the sound pressure given by

$$P = \alpha E = \alpha \frac{p^2}{\rho c^2} \tag{3.8}$$

where E $[\mathrm{J/m^3}]$, p $[\mathrm{Pa}]$, ρ $[\mathrm{kg/m^3}]$, and c $[\mathrm{m/s}]$ denote the sound energy density, sound pressure, density of the medium, and sound velocity, respectively. α is determined by $\alpha = 1 + R^2$, where R denote the reflection coefficient on the object surface. The value of α is between 1 and 2. If the value of α is 1, the energy is perfectly absorbed by the object. If the value of α is 2, it is perfectly reflected on the object surface. In this study, since we use human skin as the displaying target, we calculate $\alpha = 2$. This is why almost all of the ultrasound is reflected at the boundary.

3.2 Ultrasound Beam

In the section 3.1, we introduced the characteristics of AUPA. In this section, we describe the ultrasound beam generated by AUPA. Since the ultrasound beam can induce small air flow, we use the air flow for transporting cold air in our proposed method. This uses a phenomenon called acoustic streaming.

3.2.1 Acoustic Streaming

As a characteristics of ultrasound, when a liquid containing particles is irradiated with ultrasound, acoustic radiation pressure is generated on the particles. It is known that particles are converged to nodule due to forming of standing waves. When a traveling wave of ultrasound is generated in a fluid, acoustic streaming occurs [62][63][64]. Generally, acoustic streaming is the phenomenon that causes ultrasound-driven air flow [65]. Acoustic Streaming can be classified into the following three types [66][67].

- Rayleigh Streaming
- Schlichting Streaming
- Eckart Streaming

Rayleigh streaming, which is comparable to the wavelength, is a vortex flow induced in a standing sound field. Schichting streaming, which is far shorter than the wavelength, is a vortex flow formed in a viscous boundary layer on the object sur-

face in the sound field. Eckart streaming, which is much longer than the wavelength of the ultrasound, is a straight flow formed in a progressive sound field. These generation have been observed not only in water [68][69] but also in the air [62][70].

In this thesis, we use a straight beam generated in an electronically steerable manner, by means of AUPA.

3.2.2 Generation of Airflow by Ultrasound Beam

Here, we describe a method of generating a steerable, narrow, straight airflow that is located away from the AUPA which generates an acoustic Bessel beam [71]. The ultrasound-driven flow is accelerated during propagation by kinetic energy supplied from the area where ultrasound is generated. Compared to the flow of jets or fans, the farther it propagates, the less it attenuates and dissipate. At the point of maximum velocity, it is possible to place far away from the sound source such as jets or fans is following the flow in the air.

With single-frequency sinusoidal sound sources, the driving force per unit volume exerted by the air is known to be proportional to the acoustic power [62]. At the position $\boldsymbol{r} = (x, y, z)$, the driving force vector per unit volume $F(\boldsymbol{r})$ is given by

$$F(\boldsymbol{r}) = 2\frac{\alpha}{\rho c} I(\boldsymbol{r}) \tag{3.9}$$

where $I(\boldsymbol{r})$, ρ $[\mathrm{kg/m^3}]$, and c $[\mathrm{m/s}]$ denote the acoustic intensity, density of the medium, and sound velocity, respectively. The acoustic intensity $I(\boldsymbol{r})$ is equivalent to the temporally averaged acoustic power. Therefore, by creating a situaton where the acoustic power is localized in a narrow range in the air, it has been found that a straight airflow with a narrow cross-sectional area can be generated away from the sound source [71].

3.2.3 Method of Forming Acoustic Bessel Beam

In the method of generating the acoustic flow in previous section 3.2.2, the Bessel beam is an appropriate example of an acoustic beam when used in the design of the proposed method. Since it can generate a narrow air flow, the proposed method can be expected to have higher spatial resolution than fans such as air conditioners. Generally, the Bessel beam is a long focal depth beam whose amplitude is represented by the Bessel function of the first kind in the cross section in the wave propagation direction. In the optical disciplines, it is mainly formed by using a conical axicon lens [72][73] (Fig. 3.4).

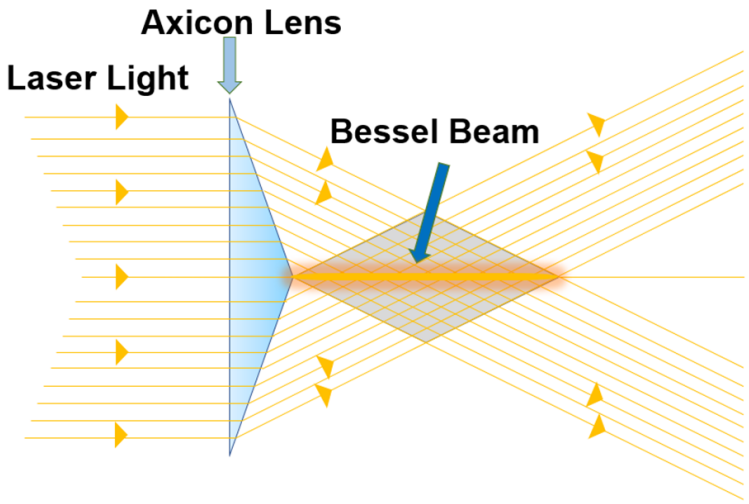

Fig. 3.4. Example of Bessel beam generated by axicon lens in optics.

The Bessel beam has the energy density which is highest around the propagation axis. Coaxial energy is distributed in the beam cross section. In addition, the diameter of the beam cross section can be as small as the wavelength. Therefore, a higher frequency source is required to generate a narrower beam. We explain the basic method of controlling the beam with reference to tha paper by Hasegawa et al. [71].

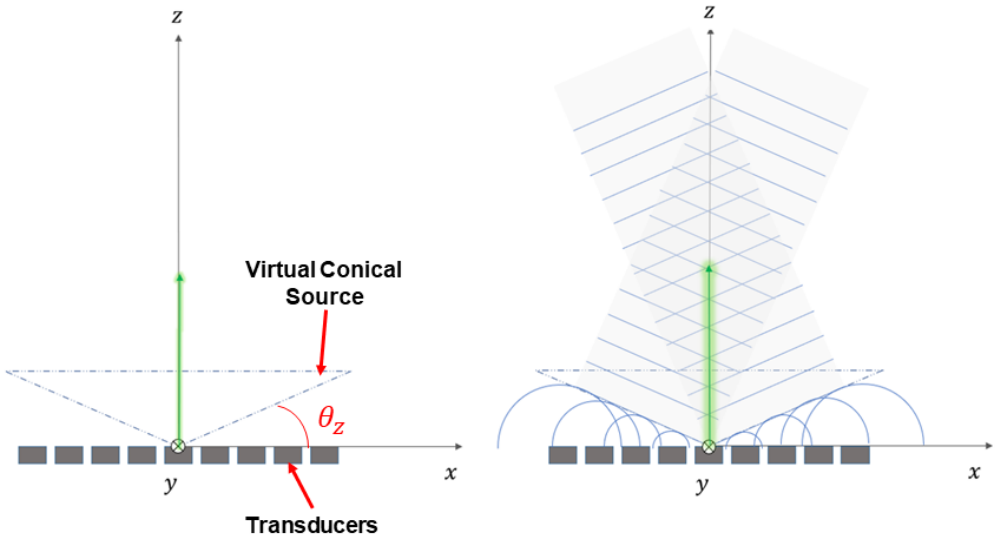

Fig. 3.5. Bessel beam formed by virtual cone-shaped sound source with AUPA.

Bessel beam is generated by making the waves conical. Figure 3.5 shows how the conical source forms a Bessel beam. AUPAs are used to design the system of the proposed method. In the section 3.1, the wave front can be controlled by properly setting the phase delay from multiple emission sources. If each transducer has a phase shift that is proportional to the distance between its position $\boldsymbol{r} = (x, y, z)$ and the cone-shaped virtual sound source, Bessel beam can be formed.

Here, in order to generate the Bessel beam, we describe the phase shift control of the ultrasound transducer forming the conical sound source in detail. Suppose that the vertex of the cone corresponds to the origin, the z-axis is identical to that of the cone with its direction faced towards the bottom. θ_z is the angle between the side of the cone and the xy-plane. Then, a phase shift $\phi(\boldsymbol{r})$ is given by

$$\phi(\boldsymbol{r}) = k\left(\sqrt{x^2 + y^2}\sin\theta_z - z\cos\theta_z\right) \tag{3.10}$$

where k is a wave number. The length of Bessel beam L_{beam} is given by

$$L_{beam} = \frac{A}{2\tan\theta_z} \tag{3.11}$$

where A is the width of array aperture. When it is near the position of $z = \frac{1}{2}L_{beam}$, the acoustic intensity of the beam can take a maximum value. Change of the beam direction can be realized by changing the direction of virtual cone-shaped sound source as shown in figure 3.6. This is detailed in [71].

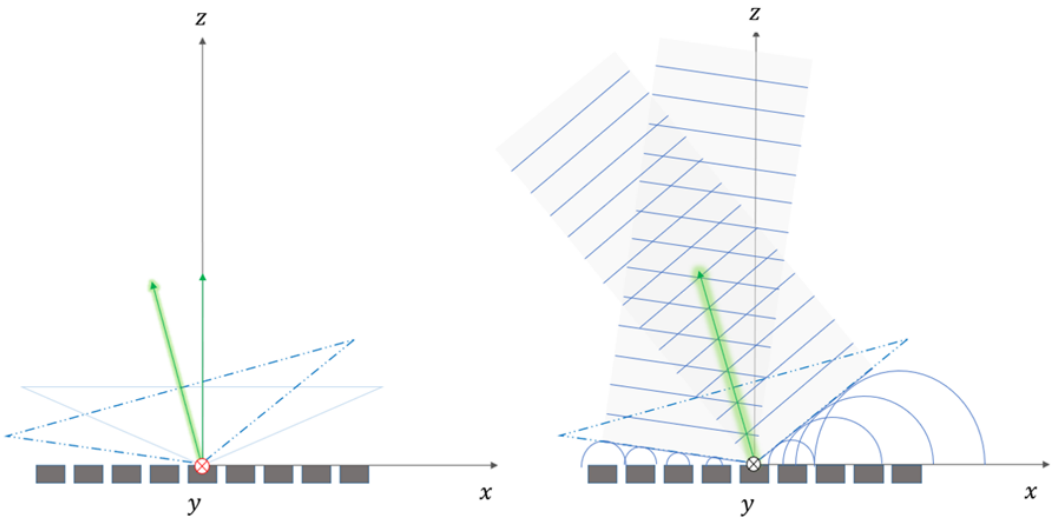

Fig. 3.6. Example of changing the Bessel beam direction.

Furthermore, when the beam irradiation position is not in the center of AUPA, the position $\boldsymbol{r} = (x, y, z)$ should be moved in parallel so that the position $\boldsymbol{r}_0 = (x_0, y_0, z_0)$ is centered (Fig. 3.7).

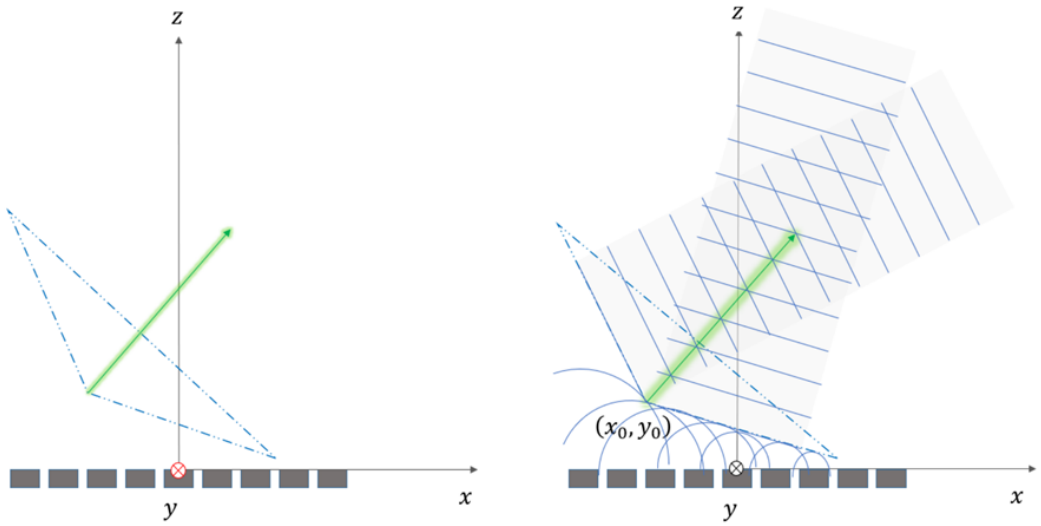

Fig. 3.7. Example of changing the Bessel beam position and direction.

3.2.4 Application Example of Using Bessel Beam

As an application example using Bessel beam in the previous section 3.2.3, Hasegawa et al. developed a technology for transporting odors in the air [74][75]. In fact, it has been shown that steerable narrow airflow is generated, and it can transport odor midair within a certain distance.

On the same principle, we can expect to transport low temperature air instead of odorous substances. The Bessel beam can be narrowed down to a comparable size to the ultrasound wavelength, 8.5 mm in our setup. The narrow beam could successfully transport a cold air mass and generate a localized cold spot on a skin away from the device. Similarly to odorous substances, it was shown that gas such as cold air of dry ice could be transported to the user's skin surface in the air [30].

In this thesis, we use the mist instead of cold air of dry ice and describe in chapter.

3.3 Focused Ultrasound

In this section, we describe the focused ultrasound generated by AUPA. In this thesis, the focused ultrasound is equivalent to focal point of ultrasound. As the section 3.1,

AUPA can create a focused sound at any position in the air by controlling the phase of each transducer. When it is interrupted with the skin surface, acoustic radiation pressure is generated and a vibrotactile sensation is displayed. Also, the relationship between sound pressure and acoustic radiation is shown as the expression (3.8).

3.3.1 Method of Forming Focused Ultrasound

As for the method of forming the focused ultrasound, you can create a proper phase shift similar to the method of forming ultrasound beam (3.10). Let the position of focused ultrasound be $\boldsymbol{r}_f = (x_f, y_f, z_f)$. As shown in figure 3.8, the phase shift $\phi(\boldsymbol{r})$ at the position $\boldsymbol{r} = (x, y, z)$ is given by

$$\phi(\boldsymbol{r}) = \frac{2\pi}{\lambda}\|\boldsymbol{r} - \boldsymbol{r}_f\| \tag{3.12}$$

where λ [m] is wavelength of focused ultrasound. This phase shift can lead to form focused ultrasound.

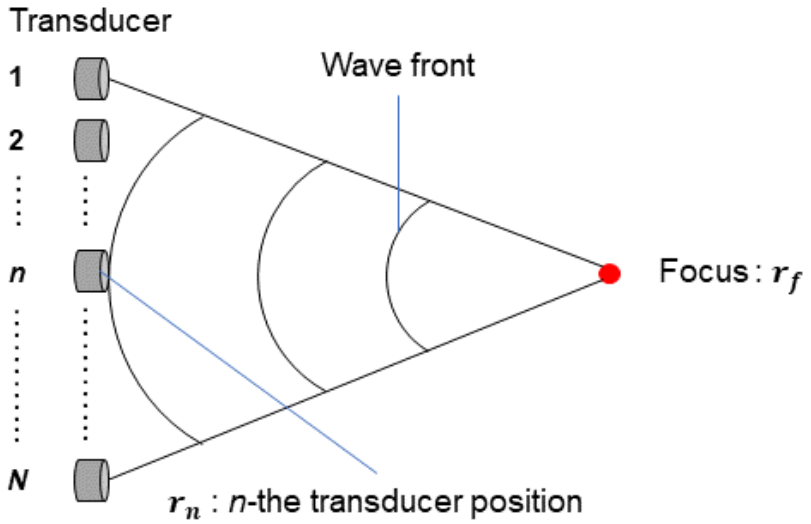

Fig. 3.8. Schematic image of forming focused ultrasound.

3.3.2 Spatial Resolution of Focused Ultrasound

In the AUPA, it is assumed that N transducers are arranged at intervals d [m]. In addition, it is assumed that the focused ultrasound is at a distance h [m] from the

center of the AUPA as shown in figure 3.9 [76]. Here, if $h >> d$ is satisfied, it can be regarded as Fresnel diffraction. The sound pressure distribution is approximated by $sinc$ function. Therefore, the minimum diameter of the focused ultrasound w_f is estimated as

$$w_f = \frac{2h}{Nd}\lambda \tag{3.13}$$

Furthermore, the diameter of the focused ultrasound is proportional to the wavelength λ [m] and inversely proportional to the aperture diameter Nd. On the other hand, The sound pressure distribution in the depth direction is approximated by $sinc$ function. The center diameter w_d is estimated as follows.

$$w_d = \frac{2h}{Nd}w_f = \left(\frac{2h}{Nd}\right)^2 \lambda \tag{3.14}$$

The expression (3.13) and (3.14) show that a proper aperture can provide better localization of the focused ultrasound. Therefore, the spatial resolution of AUPA is determined by the diameter of the focused ultrasound w_f. On the other hand, since the displaying direction is vertical to the user's skin surface, the center diameter w_d shall not be considered.

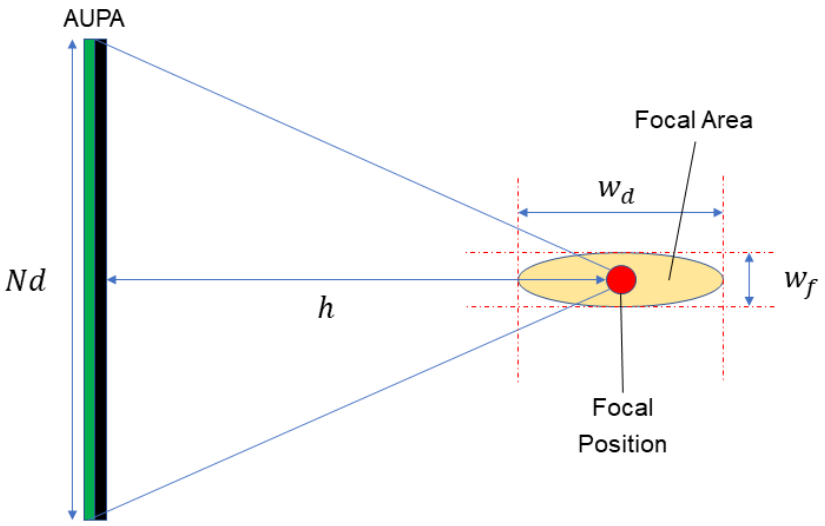

Fig. 3.9. The area of the focused ultrasound. Reconstructed and modified from [76]

3.3.3 Airflow Generation by Focused Ultrasound

Similar to generation of acoustic streaming by ultrasound beam, airflow can also occur when using the focused ultrasound. The cause of this airflow has not been identified, but the main cause is the generation of acoustic streaming [77]. According to (3.2.1), the airflow observed by displaying tactile sensation can be sensed by the finger, it is considered to be the Eckart streaming. The basic equations for the Eckart streaming are described as

$$\nabla \cdot \boldsymbol{v} = 0 \tag{3.15}$$

$$\frac{\partial \boldsymbol{v}}{\partial t} + \boldsymbol{v} \cdot \nabla \boldsymbol{v} = -\frac{1}{\rho}\nabla \bar{p} + \nu \nabla^2 \boldsymbol{v} + F \tag{3.16}$$

$$F = \frac{b}{\rho^3 c^4} \overline{p \nabla \left(\frac{\partial p}{\partial t} \right)} \tag{3.17}$$

where $\boldsymbol{v}$, ρ, p, ν, F, and c denote the particle velocity, density of the medium, sound pressure, kinematic viscosity coefficient, force applied to the medium per unit volume, and sound velocity, respectively [78]. From these equations, it can be seen that F is determined by the time change of sound pressure and the amplitude. When the focused ultrasound waves are irradiated with acoustic radiation pressure, ultrasound generated from each transducer concentrate in the same phase. Therefore, the amplitude and time change of sound pressure increase. In other words, it is considered that F becomes large enough and acoustic streaming is generated.

In this thesis, we also use air flow driven by focused ultrasound for transporting the mist and describe in chapter.

3.4 Conclusion

In this chapter, we described the principle of AUPA. Firstly, we introduced the method of creating acoustic field. This method showed that AUPA can create various arbitrary wave front out of phased-emission from AUPA. Secondly, we described the method of forming the ultrasound beam and application examples. Then, it is explained that the ultrasound beam can cause air flow as small as wavelength. we introduced the acoustic Bessel beam as an appropriate example of the ultrasound beam. It can be expected to have higher spatial resolution than fans or jets. Finally, we described the method of generating the focused ultrasound. The acoustic field of focused ultrasound can be formed by creating a proper phase shift similar to forming ultrasound beam. The spatial resolution is also increased by changing a proper aperture. In addition, airflow may occur when using focused ultrasound.

The cause may be thought to be acoustic streaming. In the chapter 5 and 6, we use the acoustic streaming for transporting the mist similar to ultrasound beam.

Although the methods of using ultrasound beam and focused ultrasound were described, we perform experiments of remote displaying cooling sensation using each method. Each method is basically used for transporting the mist. However, in case of using focused ultrasound, it is aimed to instantly converge the mist and simultaneously vaporize it. As for cooling the user's skin surface, both methods use the heat of mist vaporization. In next chapter, we describe the cooling method with mist.

Chapter 4

Superiority of Cooling Method Using Mist

In this research, the mist is used as a coolant for displaying cooling sensation. When displaying a cooling sensation in the air, it needs to remove the heat from the user's skin surface. The same strategy as heating sensation does not go well with cooling sensation in non-contact manner because the irradiated rays can only raise the temperature on the objects. Airborne cold air is virtually the only way to deprive heat of the users'skin surface. However, since a physical cooling engine is required to create the cold air, it is difficult to implement institutional setup. There is also a method of using cold air such as dry ice, but it limits the range of practical application. The method of using mist is convenient because it is easy to get from water without the need for a cooling engine. In this chapter, we describe the characteristics of cooling method using mist.

4.1 Application Example of Mist Cooling

Generally, an air conditioner using a heat pump is utilized to cool the air in the environment. In recent years, attention has been paid to mist cooling using the heat vaporization of water along with the occurrence of the heat island phenomenon. This method of using mist cooling has the advantage that the power consumption required to lower temperature is less than that of heat pump type. The mist cooling is mainly used for reducing the temperature of environmental air in facilities such as factories, warehouses and farms. In other words, the vast majority is used in large-scale spaces [79][80][81].

On the other hand, there are several examples of using a fan to cool the user's body surface [82][83]. However, there are few methods for cooling localized areas of the body such as the fingertips. In this thesis, we proposed the method of transporting mist using acoustic flow instead of the winds generated by fans. Therefore, we came up with the idea of contributing to the field of haptics technology by taking

advantages of the high spatial resolution of the AUPA described in Chapter 3. In addition, we utilize the water mainly for generating mist. In next section, we describe the characteristics of water.

4.2 Superiority of Water as Cooling Medium

The advantage of using water for mist cooling is that it is easy to get water. In addition, the reason why it is excellent as a medium used for cooling is the following.

- Chemically stable :
  Water does not decompose into different substances by heating under normal temperature environment. Less risk of significantly corroding other substances.

- Large specific heat :
  Specific heat is the amount of heat required to raise the temperature per gram of substance by $1\ ^{\circ}$C. High specific heat means that much heat is required to raise the water temperature. According to the table 4.1, the value of water specific heat is larger than other substances. Therefore, it is shown that cooling efficiency using water is high.

Table 4.1. Table of specific heat. Referenced from [84]. Some substances are calculated.

Name of Substance	Specific Heat [kJ/(kg•°C)]
Water	4.182
Dry air	1.005
Ethanol	2.416
Benzene	1.695
Carbon dioxide	0.837

The standard is 1 atm (1013.25 Pa) and 20 °C (gas : 0 °C).

- Large heat of evaporation :
  The heat of vaporization is the heat required to turn liquids into gases. According to the table 4.2, it can be seen that water has a remarkably high heat of vaporization compared to other substances. The larger the heat of vapor-

ization, the more heat is required to vaporize. In other words, the more heat of evaporation, the more heat it takes from the surroundings when it evaporates. This means that the cooling capacity is large.

Table 4.2. Table of boiling point and heat of evaporation. Referenced from [84]. Some substances are calculated.

Name of Substance	Boiling Point [℃]	Heat of Evaporation [kJ/kg]
Water	100	2257
Ethanol	78.3	838
Mercury	356.7	290
Liquid oxygen	-182.97	213
Liquid nitrogen	-195.8	199

The standard is 1 atm (1013.25 Pa).

4.3 Droplets Generated by Ultrasound Atomization

In this thesis, we use a method to generate mist by irradiating water with ultrasound. This section describes liquid atomization and droplet generation with ultrasound.

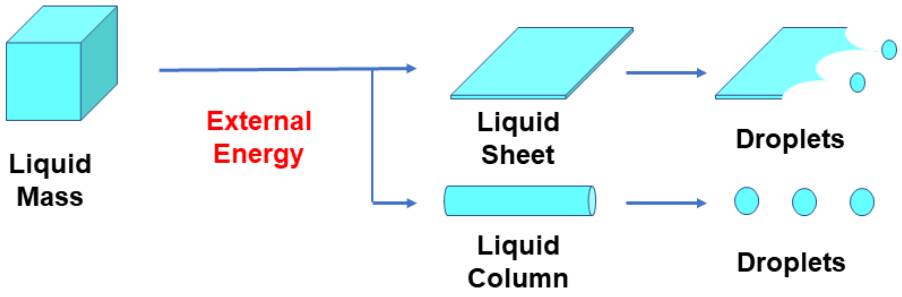

Fig. 4.1. The process of droplet formation.

4.3.1 Liquid Atomization

In the process of atomization, there is a change in the interface shape of the liquid. Liquid atomization involves the processes of turbulence in the liquid, generation of surface waves, deformation of the interface, splitting, and formation of droplets. When external energy (pressure, heat, vibration, etc) is applied to a liquid mass,

it transforms into a liquid sheet or a liquid column. When the interface becomes unstable, atomized droplets split from the interface as shown in figure 4.1.

4.3.2 Ultrasound Atomization

In this subsection, the phenomenon of ultrasound atomization is described with reference to [85]. The ultrasound atomization is the atomization of a liquid by using the vibration energy of ultrasound. The size of droplets depends on frequency, surface tension of the liquid, and density. 2MHz ultrasound is predicted to produce droplets of several micrometer size, and it has been reported that there are much smaller nanometer-sized droplets.

4.3.3 Droplet generation model

This subsection introduces two droplet generation models. They are capillary wave model and cavitation model. These differences are shown in figure 4.2.

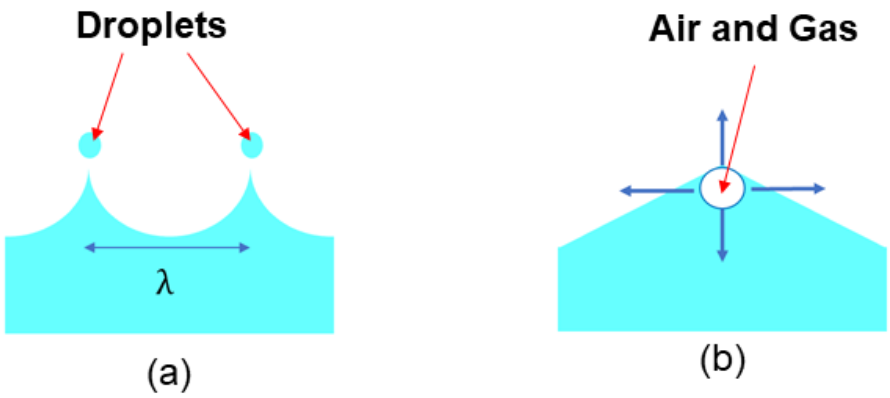

Fig. 4.2. (a) capillary wave model and (b) cavitation model.

- Capillary wave model:
  When the surface of the liquid is vibrated by ultrasound, a capillary wave is formed, and the tip of the wave is split to generate droplets.
  Droplet diameter R [cm] is known to be proportional to the wavelength λ [cm] of the capillary wave given by

$$R = k\lambda = k(8\pi\gamma/(\rho f^2))^{1/3} \tag{4.1}$$

  where ρ [g/cm^3], γ [mN/m], f [Hz] and k [$-$] denote the density of the liquid, surface tension, frequency, and proportional constant, respectively.

- Cavitation model:
  When the liquid is irradiated with ultrasound, the air and gas in the liquid repeatedly expand and insulate. Therefore, high-temperature and high-pressure microbubbles are generated, and droplets are generated by the breakup of the bubbles.
  According to [85], the size of droplets due to cavitation resulting from ultrasound vibration is theoretically unknown. Similar to the capillary wave model, it has been reported that the smaller the frequency, the larger the droplet diameter along with the bubbles.

Generally, the cavitation model is the main factor when several tens kHz ultrasound vibrates. When vibrating at a high frequency, the intensity of cavitation weakens. Thus, the capillary wave model becomes influential.

4.4 Conclusion

In this chapter, we described the superiority of cooling method using mist in this thesis. Firstly, we introduced application example of mist cooling. In many cases, it is used in a large space. although there is a method of cooling the body using the air blown by a fan, the area to be cooled is relatively large. Here, we came up with the idea that can contribute to the field of haptics technology by utilizing the high spatial resolution of acoustic streaming generated from AUPA. Secondly, the characteristics of water were introduced to describe the high effect of water mist cooling used in this thesis. Thirdly, this thesis uses the method of irradiating water with ultrasound for generating the mist. This was described about the generation of droplets by the phenomenon of ultrasound atomization. In addition, we introduced the estimation of the theoretical size of the generated mist.

Chapter 5

Remote Cooling Sensation by Transporting Mist with Ultrasound Beam

Chapter 3 described the method of generating ultrasound beam in section 3.2. This chapter describes a midair haptic display that provides a cooling sensation using ultrasound-driven cold air flow cooled by mist vaporization (Fig. 5.1). Non-contact thermal display using ultrasound-driven cold air flow has been reported, but the system uses dry ice as the cold-air source, which limits the range of practical applications [30]. In this chapter, we propose a method using mist vaporization instead of dry ice to extend the application. Using this system, we investigate transporting the mist to a localized spot on a user's skin. Then, we compare the cooling effect when mist and cold air of dry ice are used.

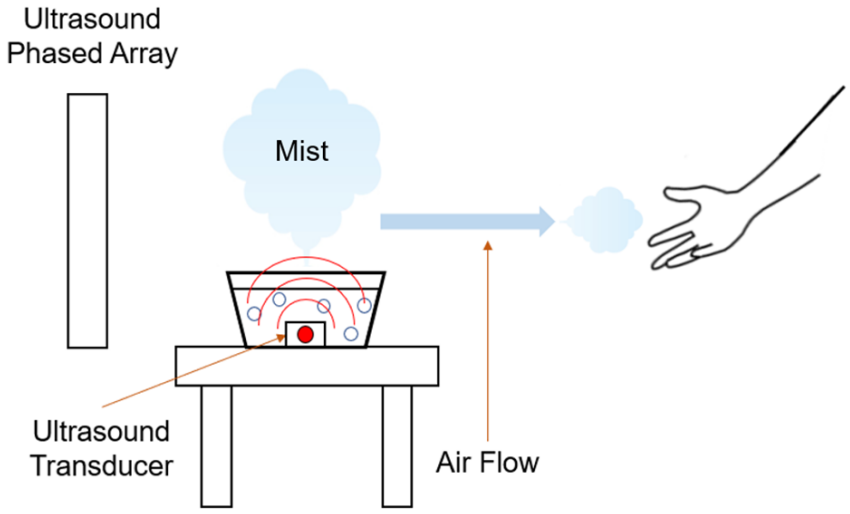

Fig. 5.1. System overview.

5.1 Prototype

The overall system is shown in figure 5.2 and 5.3. This system is composed of the airborne ultrasound phased arrays (AUPA) driven at $40\,\mathrm{kHz}$, ultrasound transducer for generating mist (IM1-24/LW SEIKO GIKEN INC), and water tank.

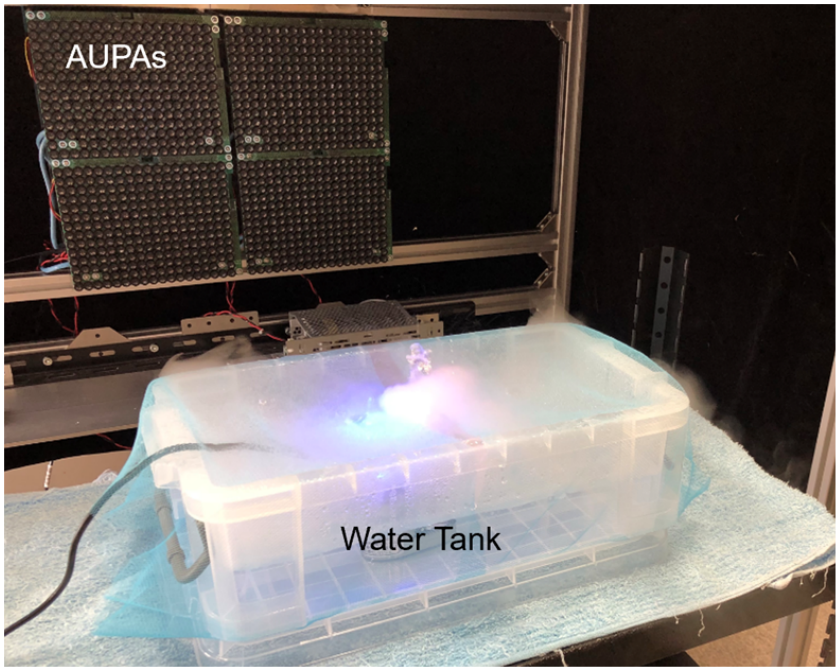

Fig. 5.2. Experimental setup.

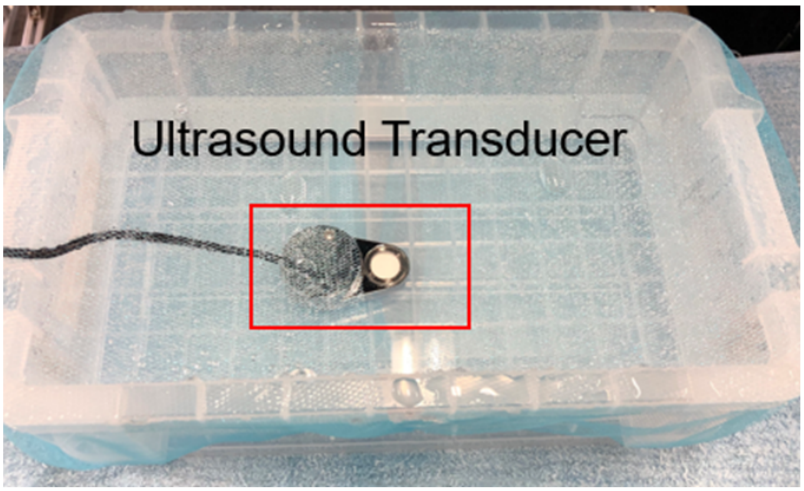

Fig. 5.3. System with a water tank.

The AUPA is set up so that it can radiate ultrasound beam in the horizontal direction toward a water tank. The ultrasound transducer generates $400\,\mathrm{ml}$ mist per hour. The particle diameter of the mist is as small as $4\sim5\mu m$. The ultrasound transducer is set up in water tank which stored 2 liters of water. The transducer produces rich mist as figure 5.4. A part of the mist is transported by the airflow generated from the AUPA.

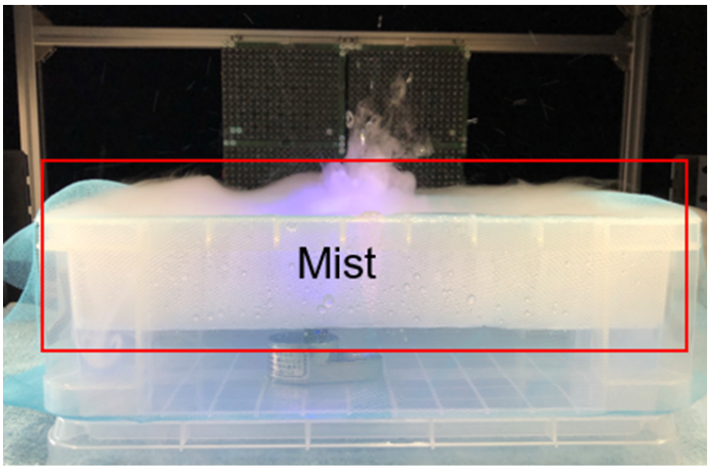

Fig. 5.4. A photo showing the mist generation.

5.2 Experiment

In this experiment, using the prototype system, the mist is transported in the air so that it hits the user's palm due to the airflow. Then, we examine temperature change of the palm surface due to the mist vaporization. As a comparative experiment, a block of dry ice was used. We also measured the temperature change when cold air is generated by dissolving dry ice in water. In this way, we compare the cooling effects of the mist and dry ice.

5.2.1 Measuring Procedures

As shown in figure 5.5, the mist generated from the ultrasound transducer in water is transported to the user's palm by the ultrasound-driven airflow. The cold air of dry ice is also transported by the airflow. Then, we measure the temperature change of palm with a thermography camera (OPTOI450O 29T900) and adjust the airflow so that it hits the center of the palm. As shown in figure 5.6, the measurement area was determined. The measurement area is a circle with a diameter of $3\,\mathrm{cm}$, and the center position is irradiated with the ultrasound beam.

Firstly, the mist or cold air of dry ice is generated before the start of measurement. The airflow is generated from the ultrasound phased arrays 10 seconds after the start of generation of cold air. We continue air transportation to the user's palm for 50 seconds. Then, the ultrasound phased arrays are switched off. Furthermore, the measurement is finished after 30 seconds.

Figure 5.7 shows how the mist and cold air of dry ice are generated from the water tank and transported in the air by ultrasound-driven airflow.

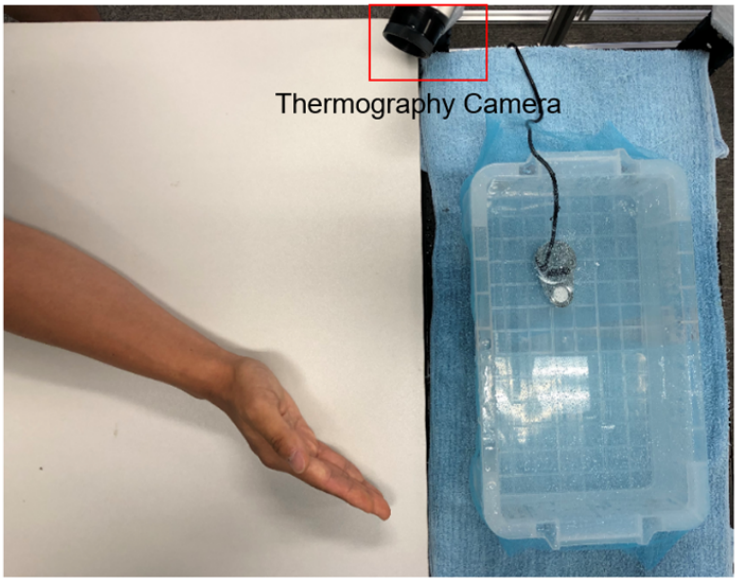

Fig. 5.5. Measurement system.

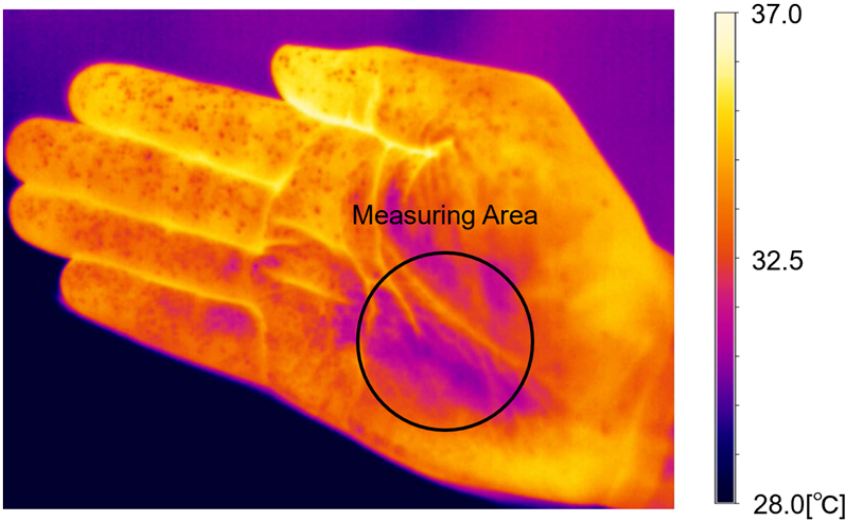

Fig. 5.6. Target parts on the palm shown in the thermographic image.

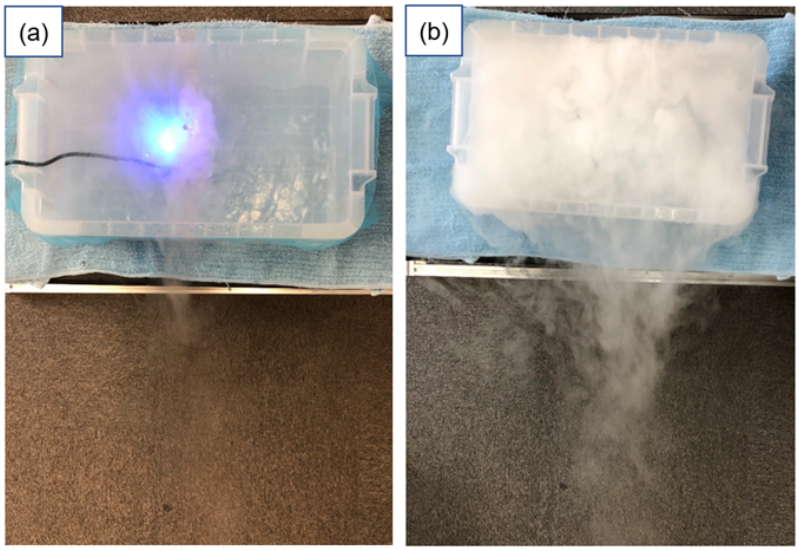

Fig. 5.7. (a)Mist and (b)cold air of dry ice guided by ultrasound-driven airflow.

5.2.2 Experimental Results

Figure 5.8 shows the temperature change when the mist or cold air of dry ice cools user's palm according to the measuring procedures. We let $t\,\mathrm{s}$ be the elapsed time from the start of measurement. The airflow was generated at $t = 10\,\mathrm{s}$. Figure 5.8 shows the image of cooing by the mist and cold air of dry ice at $t = 5, 20\,\mathrm{s}$. In other words, it shows how the palm is cooled before and after the airflow is generated. From this result, compared with using cold air of dry ice, it is found that cold spots are more likely to generate when the mist is used. In addition, a larger temperature drop was observed around the area of airflow irradiation.

The minimum value of the temperature in the palm measured by thermography camera is shown in figure 5.9. When the mist was used, the temperature rapidly dropped $1\,\mathrm{s}$ after the airflow was generated. It dropped 3.5 to $3.8\,^{\circ}\mathrm{C}$ in $50\,\mathrm{s}$. Secondly, when the cold air of dry ice was used, the temperature drop is 1.1 to $1.3\,^{\circ}\mathrm{C}$ compared to the case of using the mist. Therefore, it can be shown that the cooling effect is higher when the mist is used. Even in the subjective experience, we felt cooler with the mist. Since the heat of water vaporization is as large as 2257 kJ/kg, it is considered that the ultrasound beam has the effect of promoting vaporization and effectively cools the skin surface.

On the other hand, there was also an undesired tendency for the temperature change after the acoustic flow was stopped. When the cold air of dry ice was used, there was a tendency of returning to the initial temperature immediately after stop-

ping the flow. When the mist was used, there is a tendency to keep a low temperature. It is considered that water droplets formed by the mist remain on the palm and continue to take the heat from the skin surface. This is because it is necessary to switch the proper thermal sensation as a haptics display. That is the issue in the proposed method.

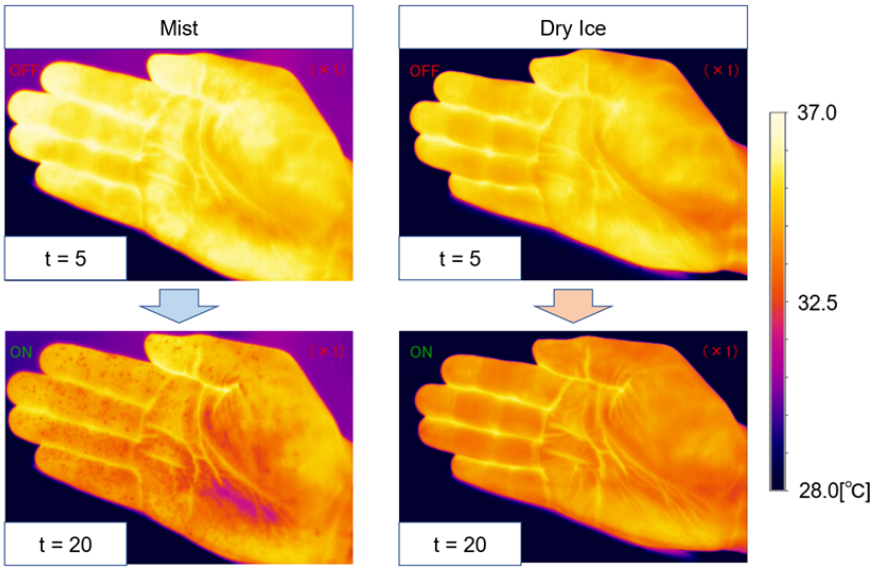

Fig. 5.8. Temperature change of the palm in the thermographic image at $t = 5, 20\,\mathrm{s}$. (Left)Using the mist. (Right)Using cold air of dry ice.

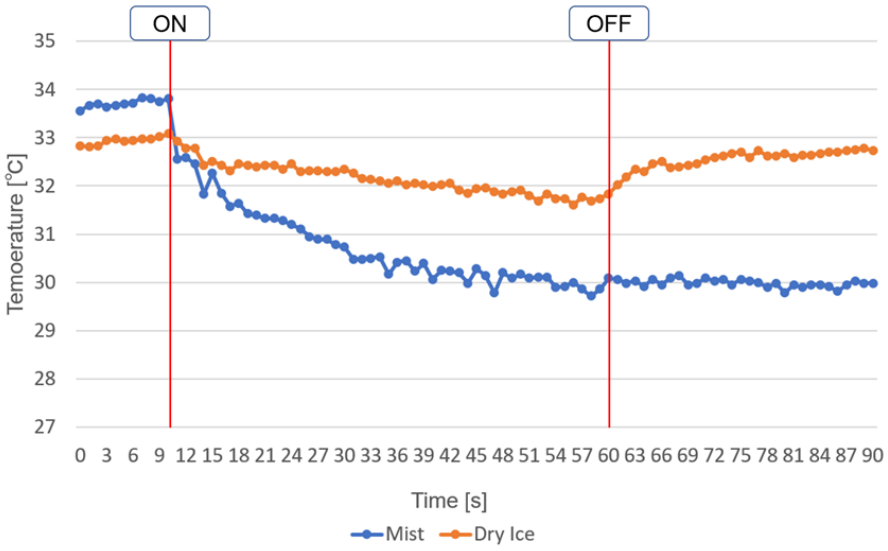

Fig. 5.9. Temperature change in the palm using the mist and cold air of dry ice.

5.3 Conclusion

In this chapter, we proposed a method of transporting the mist to the user's skin surface using the acoustic flow generated by ultrasound beam. This method can play a role in displaying cooling sensation by the heat of vaporization. We created a prototype of the system and measured the temperature change in the user's palm exposed to mist. We also measured the case of using cold air of dry ice and compared the cooling effect. As a result, it was shown that the cooling effect using the mist was higher than that effect using cold air of dry ice. On the other hand, it was also found that the temperature tends to be hard to return to the initial temperature when the airflow is stopped.

In next chapter, we will improve the prototype to further enhance the cooling effect by the mist vaporization. In addition, since the position and the amount of mist generation are fixed, it will be improved so that it can be controlled freely.

Chapter 6

Remotely Displaying Cooling Sensation Controlling Mist in Midair

Chapter 5 described a method to display cooling sensation by transporting mist to the user's skin surface with ultrasound beam and cooling from the heat of vaporization. A comparative experiment was performed as a cooling effect by the mist and cold air of dry ice. It was shown that the cooling effect using the mist was higher. As for the system of prototype, the position and the amount of mist generation were fixed. In this chapter, we build a system that can control the position and the amount of mist generation. Therefore, we reconstruct the system to enhance the cooling effect in chapter 5. The ultrasound beam is also used for transporting the mist. Figure 6.1 shows the schematic image of prototype. The direction of mist emission is determined by the position of the hose outlet. In this chapter, it is fixed at the position where it is emitted from the center of AUPAs. In the experiment, we measure the cooling effect of the system.

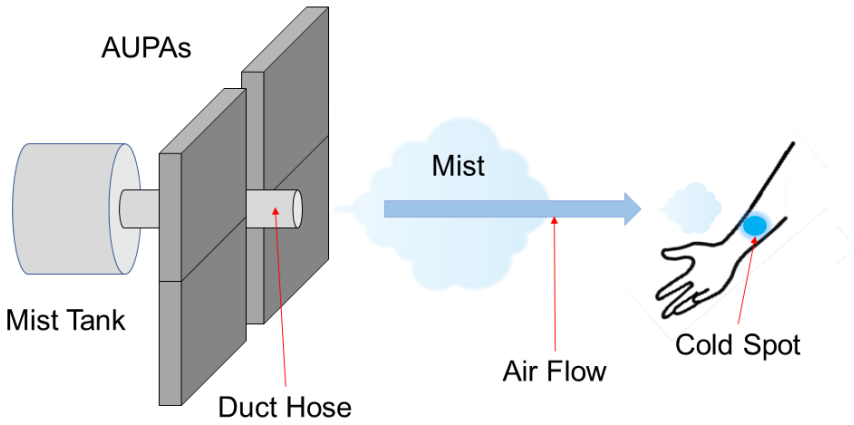

Fig. 6.1. System overview.

6.1 Prototype

The overall schematic of the prototype is shown in figure 6.2, 6.3. This prototype is composed of AUPAs driven at $40\,\mathrm{kHz}$, a duct hose for emitting mist, and a water tank ($20\,\mathrm{L}$) for mist storage.

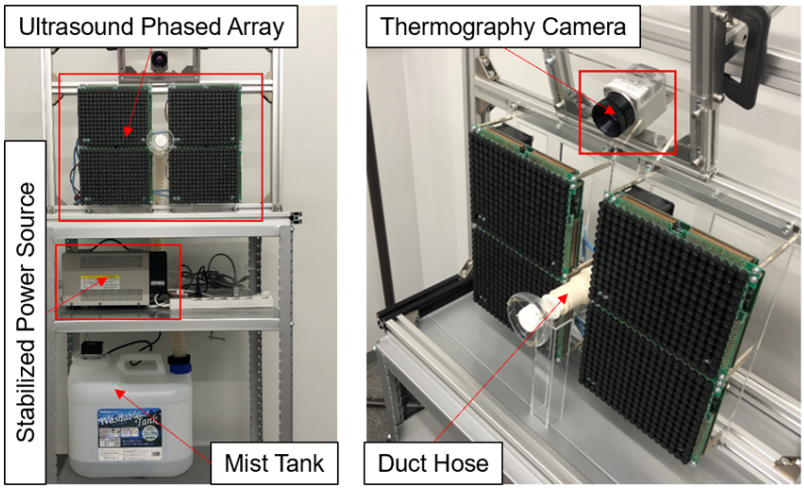

Fig. 6.2. Overall view.

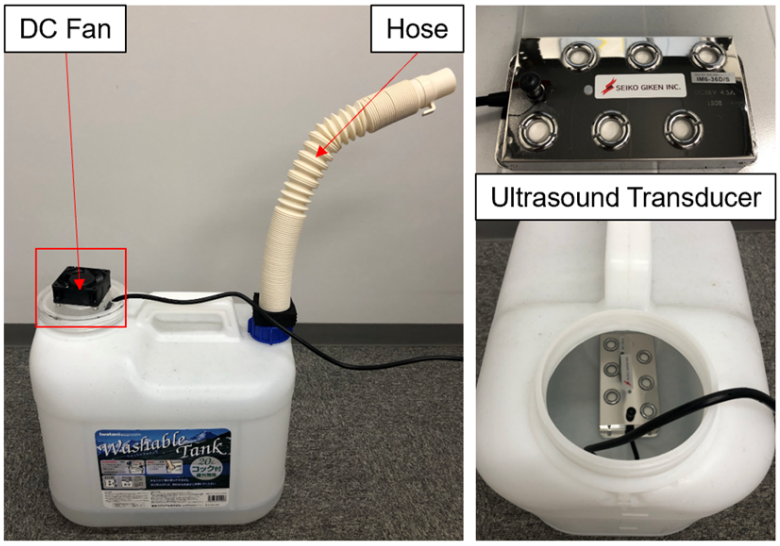

Fig. 6.3. Mist generator.

A duct hose is located at the center of the phased arrays so that it faces the same direction as the AUPAs surface. An ultrasound transducer for generating mist, whose resonant frequency is approximately 1.6 MHz (IM6-36D/S SEIKO GIKEN INC),

is contained in the water tank. At the highest power, the transducer can produce $4000\,\mathrm{ml}$ of water mist per hour. The particle diameter of the generated mist which was measured by the company was $4\sim5\mu m$.

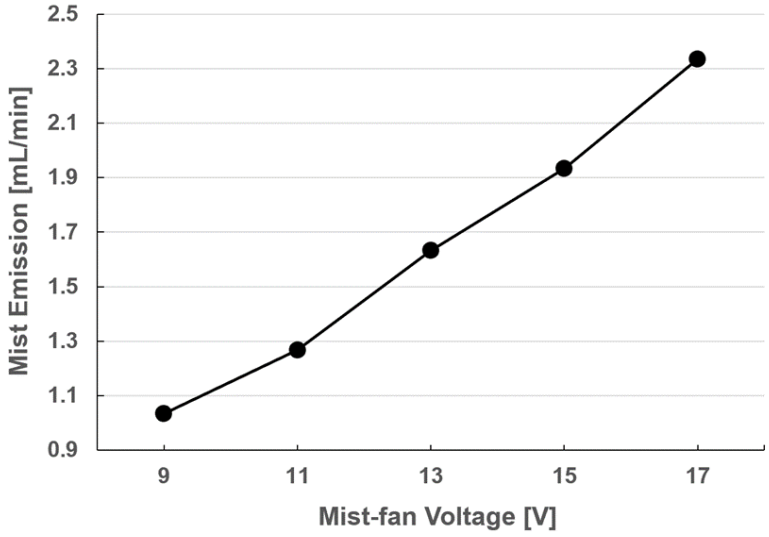

Fig. 6.4. The quantitative relationship between the mist-fan voltage and the amount of mist emission.

The tank is connected to a DC fan (San Ace 60W SANYO DENKI CO) and the duct hose. When the DC fan operates, air is blown into the inside of the tank and the mist is emitted from the duct hose. The fan is connected to the stabilized power source. The amount of mist emission can be controlled by adjusting the driving voltage of the fan. Figure 6.4 shows the quantitative relationship between the mist-fan voltage and the amount of mist emission. A part of the mist emitted from the duct is transported by the airflow generated from AUPAs. Figure 6.5 shows that the mist emitted from the duct is transported by ultrasound beam.

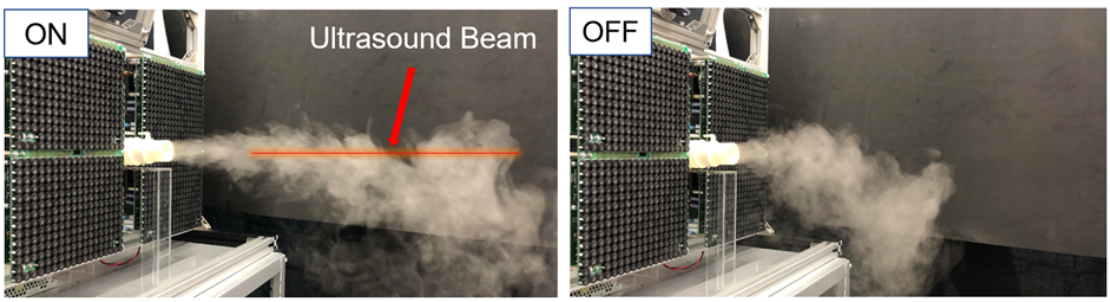

Fig. 6.5. (Left) The mist is being transported by ultrasound beam. (Right) AUPAs are not working.

6.2 Experiment

In this section, using the prototype described in the section 6.1, we report the cooling effect of the prototype. Firstly, we adjusted the applied voltage of the stabilized power source for driving the fan so that the mist emitted from the duct floated in the air near the AUPAs. The current and applied voltage are $0.01\,\mathrm{A}$ and $15\,\mathrm{V}$ respectively. Next, the floating mist is transported so that it hits the user's palm by the ultrasound-driven airflow. As a evaluation of the cooling effect, we measure how the surface of the palm is cooled by the mist vaporization and the temperature changes.

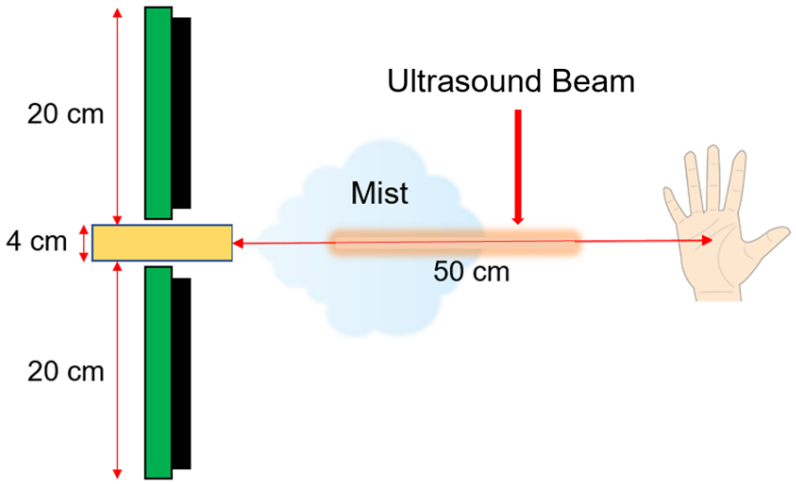

Fig. 6.6. Schematic image of experimental setup and view from above.

6.2.1 Measuring Procedures

As shown in figure 6.6, the mist emitted from the duct is transported in midair by the airflow generated from the ultrasound beam. The mist is applied to the user's palm. As shown in figure 6.7, we adjusted the ultrasound beam to hit the center of circle on the palm. We captured the temperature change on the palm with thermographic camera (OPTOI450O 29T900) in a video format.

We measured the temperature change for $90\,\mathrm{s}$. We let $t\,\mathrm{s}$ be the elapsed time from the start of measurement. First, the mist is generated when $t = 5\,\mathrm{s}$. Second, the ultrasound beam is generated when $t = 10\,\mathrm{s}$. For $50\,\mathrm{s}$ from the start of the airflow generation, the mist is being transported to user's palm. When $t = 60\,\mathrm{s}$, we switched off the AUPAs for stopping the airflow. Finaly, the measurement ends when $t = 90\,\mathrm{s}$.

Figure 6.7 shows the thermographic image and the area inside the circle is determined as measurement area. We measured the minimum value of the temperature

in that area. The diameter of the measurement area is approximately $5\,\mathrm{cm}$.

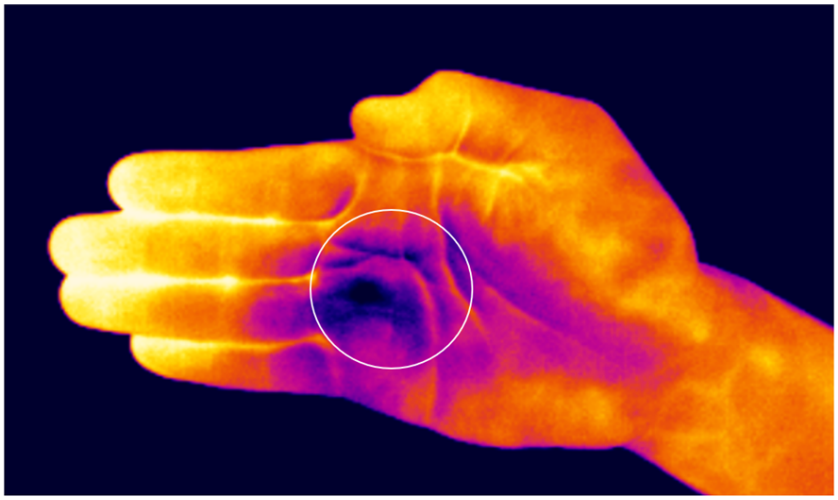

Fig. 6.7. Target area on the palm shown in the thermographic image.

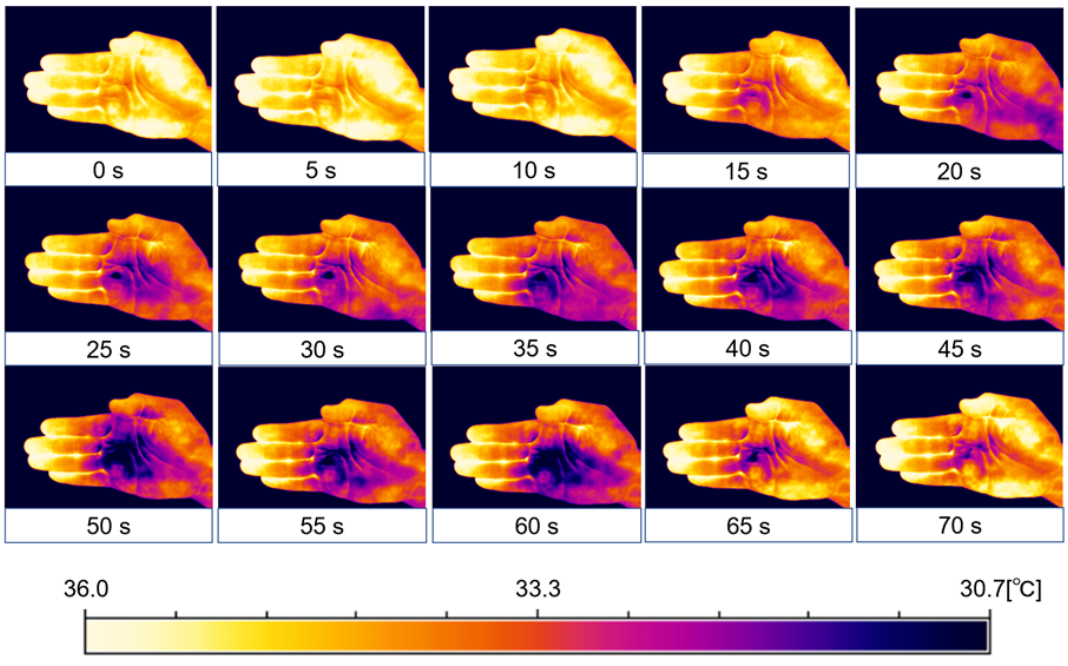

Fig. 6.8. Temporal change of the skin irradiated by the mist and ultrasound beam. The ultrasound beam generated at $10\,\mathrm{s}$ and stopped at $60\,\mathrm{s}$.

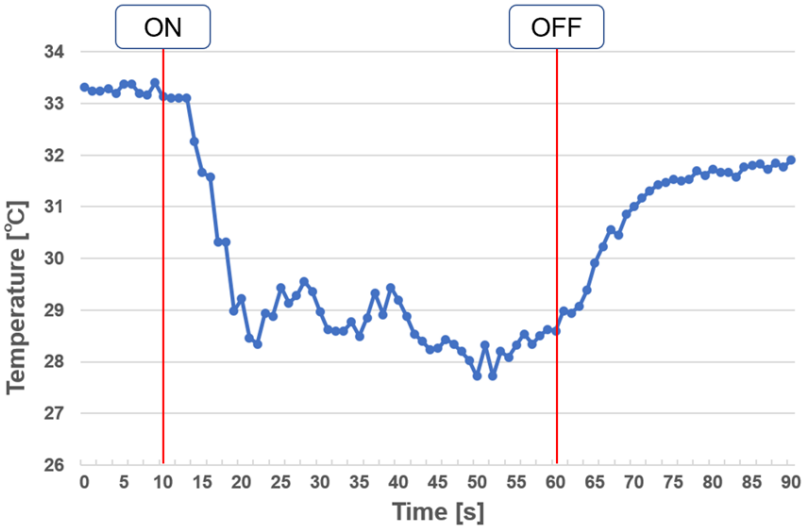

Fig. 6.9. Temperature change in the palm.

6.2.2 Experimental Results

Figure 6.8 shows the temperature change when the mist vaporization cools the user's palm from the measuring procedures 6.2.1. The ultrasound beam generated at $10\,\mathrm{s}$ and stopped at $60\,\mathrm{s}$. It was observed that the mist was converged by the ultrasound-driven airflow, and the cold spot was formed at the position irradiated on the user's palm. In addition, the diameter of the cold spot was gradually increasing. However, we did not feel the spatial spread of the cooling sensation subjectively.

Figure 6.9 shows the minimum value of temperature against time in the target area shown in figure 6.7. The temperature decreased at a rate of $0.7\,^{\circ}$C/s $3\,\mathrm{s}$ after the ultrasound-driven airflow was generated. In addition, it decreased by 4.8〜$5.4\,^{\circ}$C in $50\,\mathrm{s}$. It is shown that this result of the cooling effect is higher than in chapter 5. This is considered to be because the prototype in this chapter can control the amount of mist generation. The system in chapter 5 had the following problems. The amount of mist is fixed and cannot be adjusted. Since water drops with large particle sizes are generated at the position where the mist is generated and the ultrasound beam is directly irradiated, some water drops may be transported and adhered to. Thus, it includes the feeling of getting wet, which is suggested that the cooling effect of displaying cold sensation is insufficient. It means that the system displays cooling and wet sensations at the same time. This is because this research simply focuses on displaying cooling sensation only. Furthermore, it was seen that water drops caused to keep the low temperature. There was no tendency to return to the initial

temperature after the airflow was stopped. As a result, it was shown that the cooling effect depended on the proper amount of the mist.

6.3 Conclusion

In this chapter, we reconstructed a prototype that enhances the cooling effect in chapter 5. We proposed a system that can control the amount of mist generation. We fabricated a prototype of the system and measured the temperature change of the user's palm. As a result, we confirmed that the cooling effect depended on the proper amount of the mist.

In next chapter, we will measure the quantitative relationship between the amount of mist generation and the distance of displaying position. In addition, we will investigate the cooling effect in the direction of mist emission.

Chapter 7

Displaying Spatiotemporally Pinpoint Cooling Sensation

In chapter 5 and 6, we proposed a method of displaying the cooling sensation by transporting the mist with ultrasound-driven airflow. In chapter 5, it was found that the user's skin surface could be effectively cooled by mist vaporization in ultrasound beam. In chapter 6, improvements to the prototype have made it possible to release the proper amount of mist without water droplets.

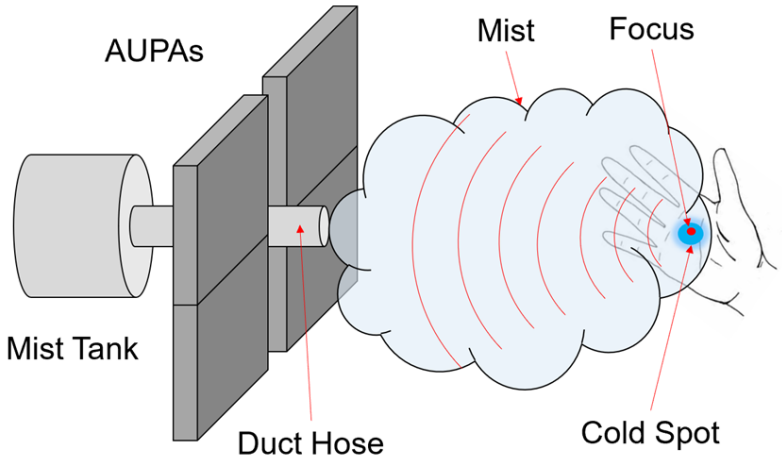

Fig. 7.1. System overview in this chapter. The water mist converged by focused ultrasound can be rapidly vaporized and display cooling sensation.

In this chapter, we propose a remote cooling method that converges the mist floating near the user's skin using focused ultrasound, and then instantaneously vaporizes mist to display a cooling sensation by the heat of vaporization. The key in this chapter is to utilize the focused ultrasound instead of the ultrasound beam used in chapter 5 and 6. The ultrasound beam was mainly used for transporting the mist. The prototype in chapter 6 can generate the mist at any position by changing

the position of the duct. Thus, by filling the workspace near the user's skin surface with mist, an irradiated focused ultrasound can produce a cold spot without a long-distance mist transportation.

The method in this chapter has three advantages. Firstly, since we use water at room temperature, it has no restrictions on the range of applications and is of great versatility. Secondly, due to the characteristics of ultrasound phased array as described in section 3.3, focused ultrasound is generated in arbitrary three-dimensional positions, and the mist is instantaneously vaporized. Therefore, the spatiotemporal resolution of displaying a cooling sensation is high. Finally, it is possible to display a cooling sensation with a complicated spatiotemporal pattern such as a cold spot moving on the skin surface.

In the experiment, we measure the spatiotemporal property of the method in this chapter and clarify the conditions for effectively cooling the skin surface. We also demonstrate that motion of a cold spot is displayed when the focused ultrasound moves on the skin surface.

7.1 Experimental Setup

The prototype used in the experiment is the same as that used in chapter 6 (Fig. 6.2 and 6.3). It is detailed in section 6.1. When a cold spot can be produced by the irradiated focused ultrasound without a long-distance mist transportation, the direction of mist emission should be changed as shown in the figure 7.2.

In the experiment, as subjective perceptions of the authors, we did not feel cooling sensation by merely touching the floating mist in the air. However, we could clearly perceive our skin surface being cooled when focused ultrasound irradiation was superimposed on skin. In Experiment 1, we evaluate and clarify this phenomenon.

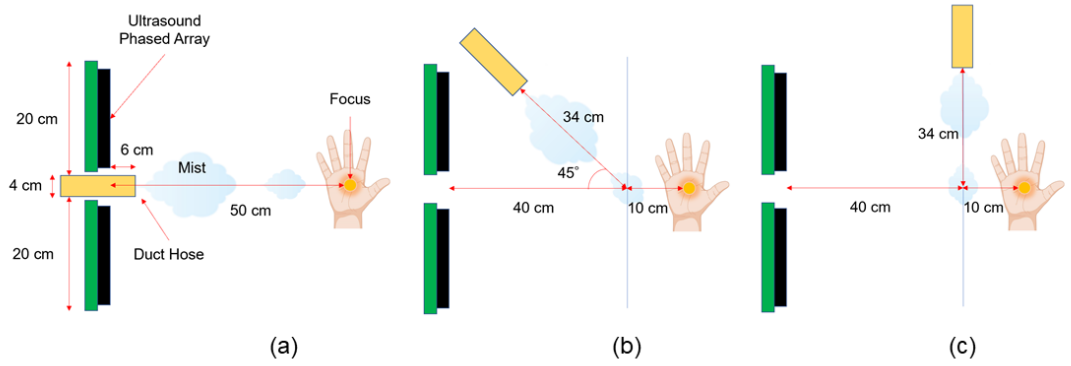

Fig. 7.2. System overview in this chapter and view from above.

7.2 Experiment 1

In this section, using the fabricated prototype, we performed a comparative experiment about the cooling effect of displaying cooling sensation using three cases: irradiation of focused ultrasound, exposure to mist, and simultaneous combination of them. The palm used in the experiment was the author (male, 27 years old). This palm was also used in another experiments. For the experimental environment, the room temperature and humidity were $25\ ^{\circ}$C and $60\ \%$, respectively.

7.2.1 Measuring procedures

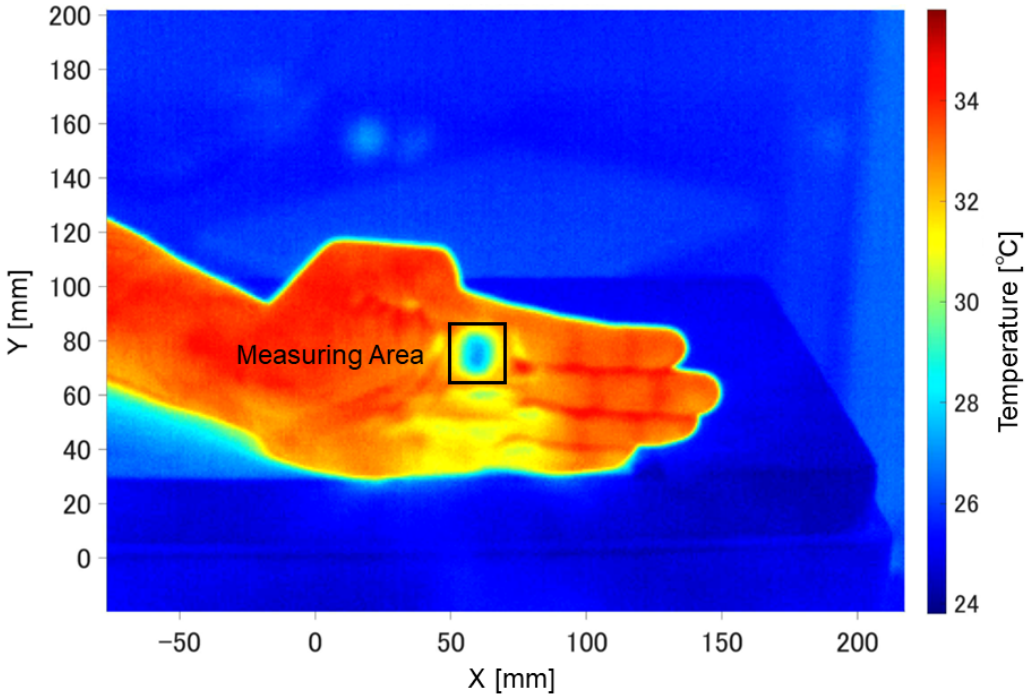

Fig. 7.3. Target parts on Measuring Area in the thermographic image.

For each of the three cases of using focused ultrasound, mist, or both of them, we place our hand 50 cm away from the AUPAs surface as shown in figure 7.2(a). At this time, we adjusted the position of displaying cooling sensation to match the center of the palm so that the plane of the user's palm and the phased array are parallel to each other.

We evaluated the cooling effect in the three cases by the temperature change on the skin surface after irradiation. We captured the entire palm cooled by the system with a thermographic camera (OPTOI450O 29T900, Optris) in a video format. We

determined the measurement area ($50\,\mathrm{mm} \leq \mathrm{X} \leq 65\,\mathrm{mm}$, $64\,\mathrm{mm} \leq \mathrm{Y} \leq 88\,\mathrm{mm}$) as shown in figure 7.3, when measuring. The area is the position where the mist is converged and cooled by the focused ultrasound.

For measurement with thermographic camera, the captured data is saved as binary data and converted to csv data. We performed sophisticated measurement using numerical analysis software (MATLAB R2019b). In chapter 5 and 6, measurement was performed by only manipulating thermographic camera.

7.2.2 Result 1

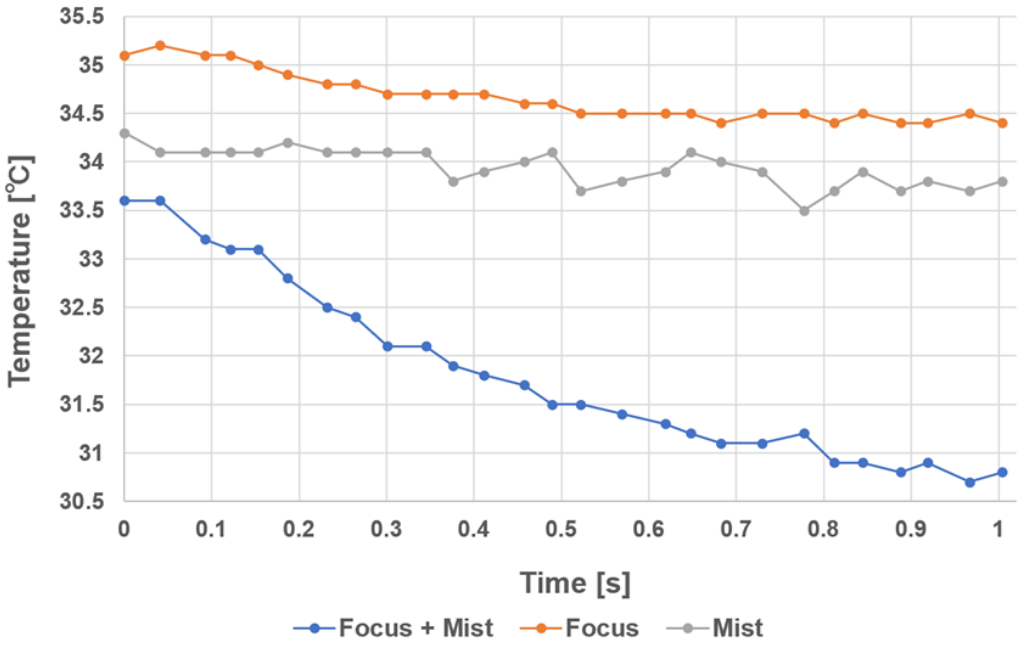

Fig. 7.4. Temperature change in the cases of using focused ultrasound, mist, or both of them.

Figure 7.4 shows the temperature changes for three cases and each of the plots shows the minimum value of temperature in the measurement area at each time. We defined the time origin for each of the three cases as follows.

In the Mist condition, the origin is the moment when the air blowing fan is turned on and the mist is sent out into the space when there is no mist in the space. In the Focus condition, the origin is the moment when the focused ultrasound is turned on. When the sound velocity is assumed to be $340\,\mathrm{m/s}$, the time required to propagate a distance of $50\,\mathrm{cm}$ is approximately $1.5\,\mathrm{ms}$, which is sufficiently short compared to sampling interval of the temperature change. In the Focus+Mist condition, the ori-

gin is the moment when the focused ultrasound is turned on while the workspace is filled with mist.

It was found that the temperature rapidly decreased when the focused ultrasound was displayed on the skin surface exposed to the mist. For that case we observed surface temperature drop by nearly $2\,^{\circ}\mathrm{C}$ in $0.5\,\mathrm{s}$ and $3\,^{\circ}\mathrm{C}$ in $1\,\mathrm{s}$. This result demonstrated that the cooling sensation with our system is indeed caused by physical cooling effects.

7.3 Experiment 2

In this section, we measured the temperature changes on the skin surface to obtain the relationship between the amount of ejected mist and the position of focused ultrasound using a system similar to Experiment 7.2. The purpose of this experiment was to clarify the valid spatial range of the proposed system. The amount of mist emission was controlled by the applied voltage to the fan supplied with a stabilized power source. By measuring the temperature change varying the mist-fan voltages, we indicated the quantitative relationship among the temperature drop on the skin surface, the amount of mist, and the skin position from the device. For the experimental environment, the room temperature and humidity were $25\,^{\circ}\mathrm{C}$ and $60\,\%$, respectively.

We also performed another measurement of the temperature changes in the cases of (a), (b), and (c) in figure 7.2. We evaluated the cooling effect of the discharge direction of the mist under a constant mist flow.

7.3.1 Measuring procedures

In each measurement, we first placed the palm on a hot plate (NHP-M30N) heated to $36\,^{\circ}\mathrm{C}$ for $60\,\mathrm{s}$. After that heating process, we measured surface temperature distribution of the palm with a thermographic camera while cooling sensation was displayed by focused ultrasound as we performed in Experiment 1 (7.2).

First, we investigated five cases where the distances between the palm and the AUPAs were 35, 40, 45, 50, 55, 60, 65, 70, 75 and $80\,\mathrm{cm}$. We evaluated the temperature drop changing the mist-fan voltage across 9, 11, 13, 15, and $17\,\mathrm{V}$. The temperature-drop is defined as the temperature change from the initial time of cooling process to $1\,\mathrm{s}$ later.

Next, the same measurement was performed by changing the mist directions in the three directions in figure 7.2. The position of the focused ultrasound was $50\,\mathrm{cm}$ from the AUPAs surface. The mist-fan voltage was $13\,\mathrm{V}$.

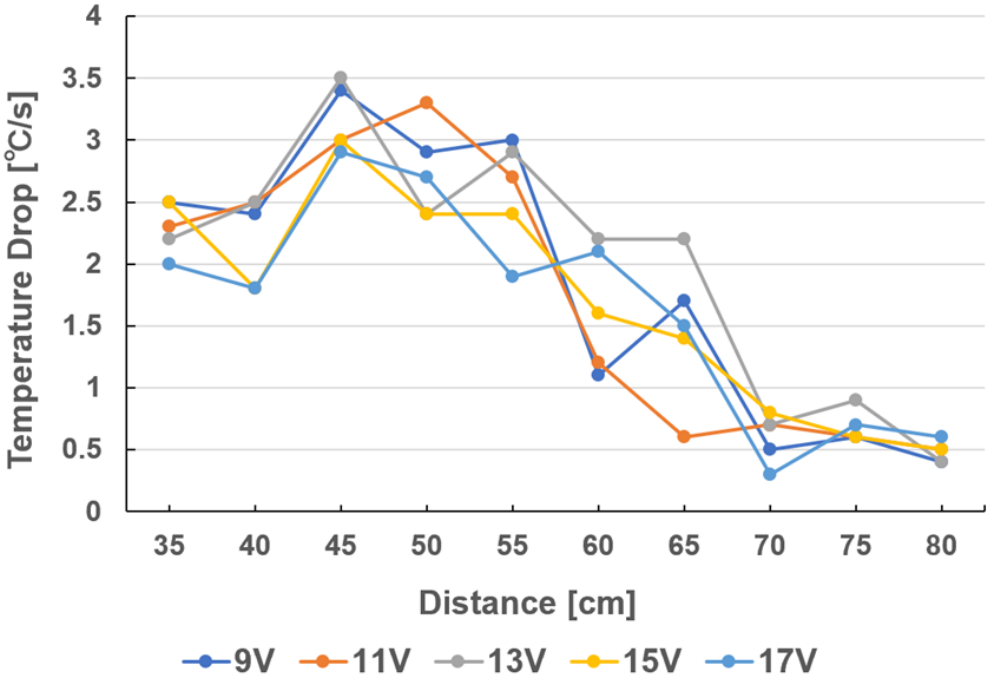

Fig. 7.5. Temperature drops versus the distance from the AUPAs surface.

7.3.2 Result 2

Figure 7.5 shows the temperature drop at each mist-fan voltage against the distance from the AUPAS surface and the amount of mist emission. The amount of mist emission depends on the mist-fan voltage as shown in figure 6.4. In cases of distances between 35 and $50\,\mathrm{cm}$, the difference in temperature drop was less than $1\,^{\circ}\mathrm{C}$ regardless of the mist-fan voltage conditions. In contrast, for distances between 55 and $65\,\mathrm{cm}$, a larger variance was observed. At distances greater than $70\,\mathrm{cm}$, the temperature drop was less than $1\,^{\circ}\mathrm{C}$. Based on the results of the temperature drop, the feasible distance was found to be 45 to $50\,\mathrm{cm}$. Up to that distance, the performance of the cooling effect was stable regardless of the mist generation as far as the tested voltage was concerned.

Figure 7.6 shows the temperature change with respect to the direction of mist emission. In cases (a), (b), and (c), the temperature change increases in this order, which is presumably due to the difference in the amount of mist supplied.

Therefore, we conclude that the proposed system requires a certain amount of mist supplied to the position of the focused ultrasound in order to display stable cooling sensation. In addition, the delay of displaying cooling sensation is not related to the distance to the system provided that the mist is sufficiently supplied.

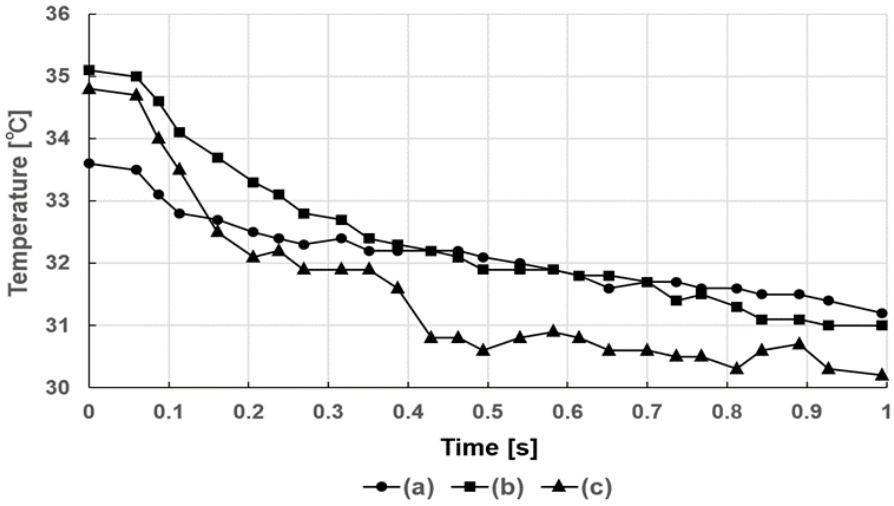

Fig. 7.6. Temperature change when the direction of mist emission was changed as in figure 7.2 (a), (b), and (c).

7.4 Experiment 3

In this section, we measured the spatiotemporal temperature distribution on the palm for a long term using a thermographic camera with a still ultrasound-driven cold spot on the palm.

We offer two types of measurement results: temporal temperature changes in the spot region and horizontal temperature distributions with a cross-sectional axis that passed the spot center. We also performed a measurement where the cold spot travelled on the palm. For the experimental environment, the room temperature and humidity were $24\,^{\circ}$C and $55\,\%$, respectively.

7.4.1 Measuring procedures

We set the position of focused ultrasound at $50\,\mathrm{cm}$ away from the surface of the phased array as in Experiment 1 (7.2). Also, similar to the former experiments, we placed the palm so that the focused ultrasound hit the center of the palm as shown in figure 7.2 (a). Then, we captured the video image of palm while it was cooled by the mist vaporization.

The measuring time was $20\,\mathrm{s}$. We started irradiation of focused ultrasound at $5\,\mathrm{s}$ after the measurement began. Irradiation continued for $10\,\mathrm{s}$ and ceased in the last $5\,\mathrm{s}$. We defined the measurement area here in after as a rectangular region that contained the moving cooling spot as seen in figure 7.3. Figure 7.7 shows the measuring

axis (Y = $73\,\mathrm{mm}$) that represents a specified position for cross-sectional measurement of the temperature distribution on the palm.

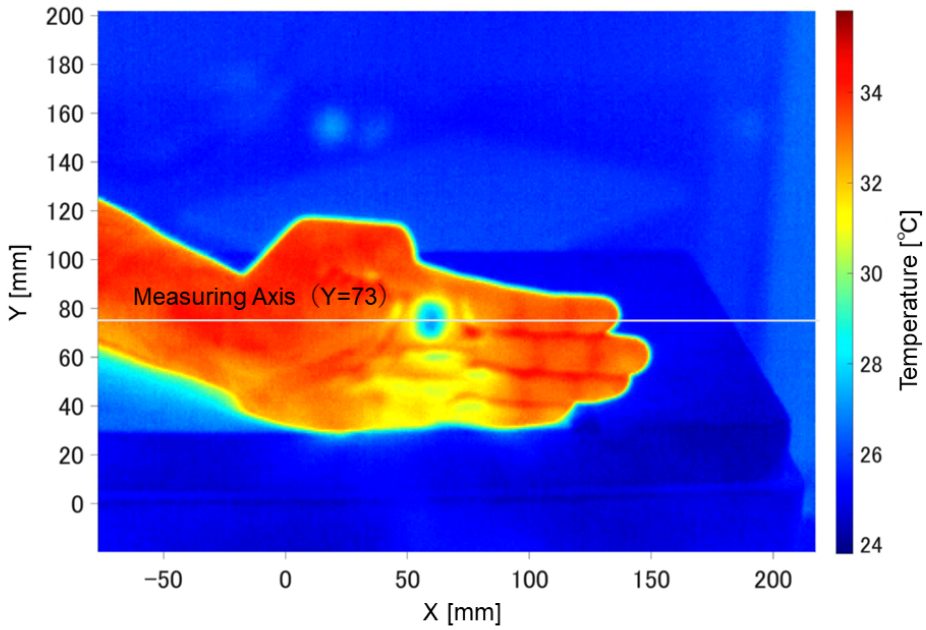

Fig. 7.7. Target parts on Measuring Axis in the thermographic image.

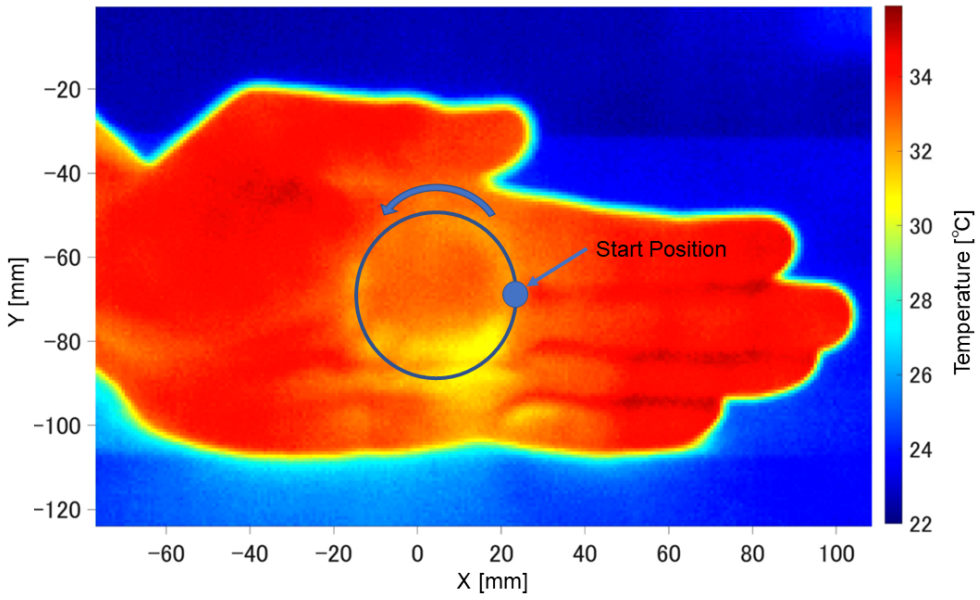

Fig. 7.8. The start point of the cold spot, circular trajectory and motion direction are shown in the thermographic image.

Next, the focused ultrasound repetitively travelled counterclockwise on a circle whose radius is $2\,\mathrm{cm}$ with a rotation period of $5\,\mathrm{s}$. The start position, the rotational position, and the rotational direction are as indicated in figure 7.8. We shot a video where the ultrasound focus travelled during the single period.

7.4.2 Result 3

Figure 7.9 and 7.10 show the long-term temperature change for a still cooling spot. Figure 7.11 shows the minimum value of temperature against time in the Measuring Area. It is clearly indicated that the irradiation of focused ultrasound yielded a cold spot causing rapid temperature drop within $1\,\mathrm{s}$. After that, the temperature drop reached $3.3\ ^{\circ}\mathrm{C}$ in $500\,\mathrm{ms}$ and $4.6\ ^{\circ}\mathrm{C}$ in $1000\,\mathrm{ms}$. The temperature was continuously lowered while focused ultrasound was being irradiated. After irradiation for 10 seconds, the temperature finally dropped by $7.8\ ^{\circ}\mathrm{C}$. It is observed that the temperature of the skin started to increase after ultrasound irradiation stopped.

Figure 7.12 shows the cross-sectional temperature distribution on the Measuring Axis in figure 7.7. The temporal changes of the temperature pattern are plotted during t = 5 to $15\,\mathrm{s}$. The size of cold spot was kept at about $2\,\mathrm{cm}$, while the peripheral semi-cold area was gradually formed around the cold spot.

Figure 7.13 shows sequential images when the cold spot moved for one period on the circular path. A circular trace on the palm is clearly observed, which demonstrates a continuous movement of a cooled spot on the palm.

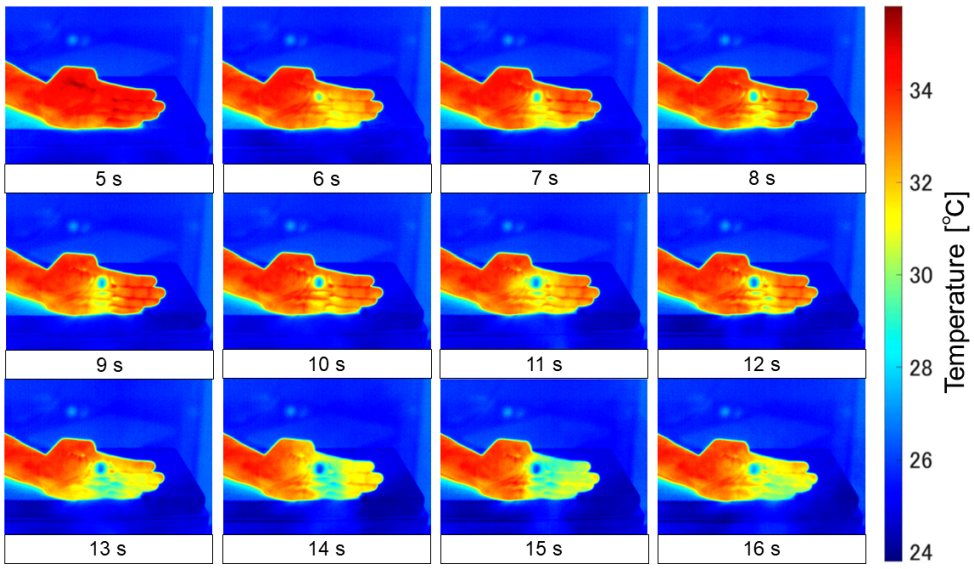

Fig. 7.9. Temporal change of the skin cooled by converged mist. The focused ultrasound was generated at $5\,\mathrm{s}$ and was stopped at $15\,\mathrm{s}$.

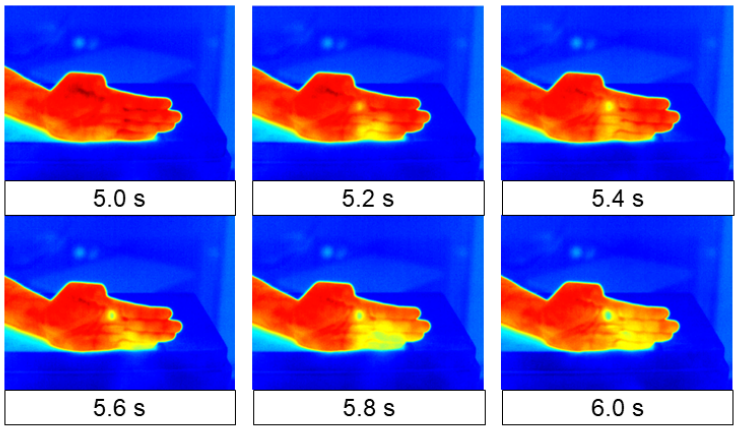

Fig. 7.10. Temperature change of the skin cooled by converged mist at $0.2\,\mathrm{s}$ intervals between $5\,\mathrm{s}$ and $6\,\mathrm{s}$.

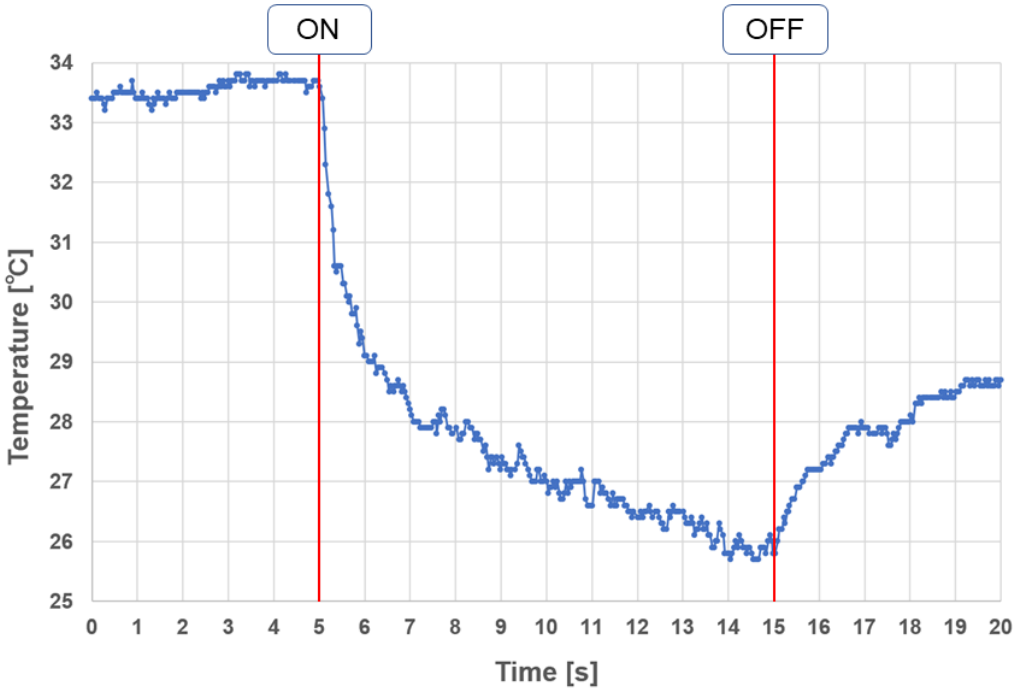

Fig. 7.11. Temperature change by the focused ultrasound.

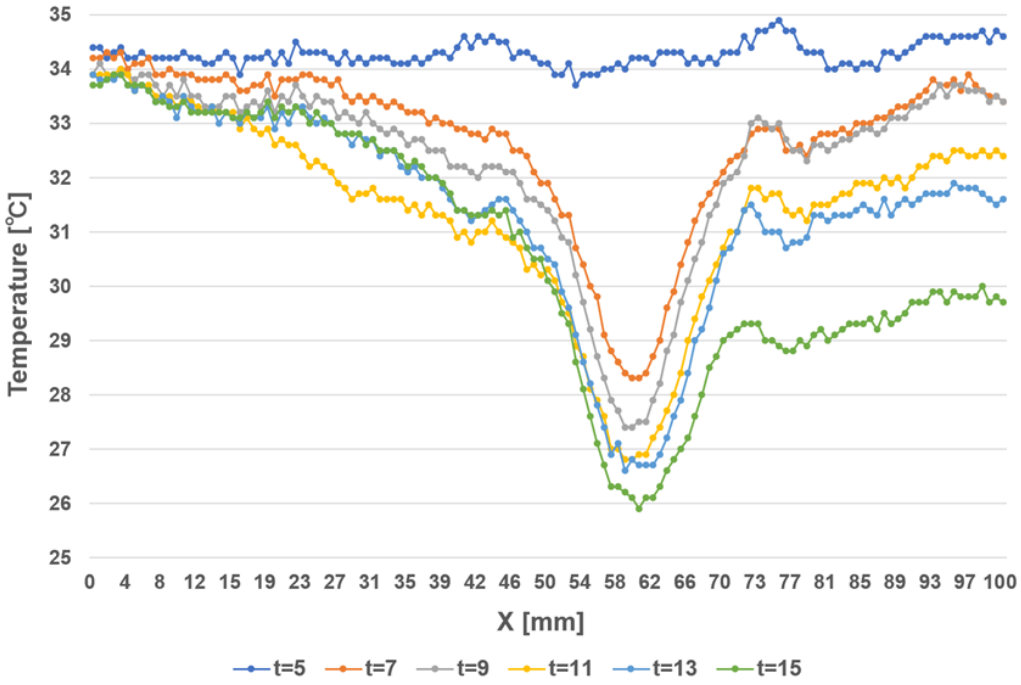

Fig. 7.12. Temperature distribution along Measuring Axis.

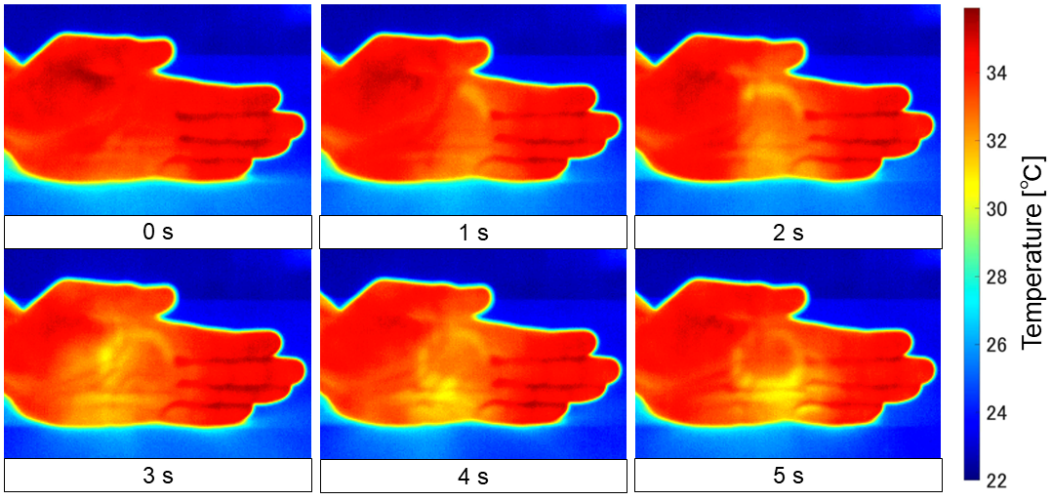

Fig. 7.13. Temporal change on the skin while cold spot rotates one round. The movement of cold spot started at $0\,\mathrm{s}$. At $5\,\mathrm{s}$, cold spot reached one lap.

7.5 Discussions

7.5.1 Experiment 1

This result of figure 7.4 showed that the rapid cooling effect was achieved only when the ultrasound was irradiated in the presence of mist.

In the previous study [30], the steepest temperature drop was $0.5\,^{\circ}$C/s when cold air of dry ice was transported by ultrasound beam and hit the skin surface. In contrast, the temperature drop in figure 7.4 was $3.0\,^{\circ}$C/s. It suggests that this is a faster phenomenon than the heat conduction caused by the contact of a cold medium to the skin surface. Rapid cooling in figure 7.4 is thought to be achieved by the vaporization heat of the mist.

In chapter 6, the steepest temperature drop was $1.3\,^{\circ}$C/s when using a ultrasound beam and the water mist. Since the mist itself was not cooled, it was also likely to be caused by the vaporization heat. However, the rate of decrease in temperature was higher in the result of figure 7.4 than in the one of chapter 6. We consider that this is because the ultrasound energy given per unit area is higher when the ultrasound is focused. In addition, it is considered that the water mist evaporated before reaching the skin surface while the mist was transported by the ultrasound beam.

7.5.2 Experiment 2

From the result of figure 7.5, the cooling effect decreases when the distance is longer than 50 cm. It is considered that the intensity of the ultrasound and the amount of mist supply can decrease depending on the distance.

When the distance between AUPAs surface and the user's skin surface is within $50\,\mathrm{cm}$, the amount of mist supply did not affect the cooling effect. On the other hand, even if the distance between the hand and the AUPAs surface was constant, the cooling effect was found to vary depending on how the mist was supplied. This is because if the palm is located in a position that obstructs the conveyance of the mist airflow, the reflection of the airflow may reduce the mist delivered to the surface of the hand. Hence, the cooling effect was highest when the mist was supplied parallel to the orientation of the palm.

7.5.3 Experiment 3

From the figures 7.9, 7.10, and 7.12, the area cooled by mist vaporization is as small as $2\,\mathrm{cm}$. From the figure 7.11, the temperature drop was $3.3\,^{\circ}$C at $500\,\mathrm{ms}$ and $4.6\,^{\circ}$C at $1000\,\mathrm{ms}$. It is known that the spatial resolution of the cooling sensation is much lower compared with the vibrotactile and pressure sensation. In addition, the cooling re-

sponse time takes more than $500\,\mathrm{ms}$ [51][52]. Therefore, the smaller cold spots and rapid temperature drop are sufficient to display various thermal sensation, such as material sensations with different thermal conductivity.

As shown in figures 7.9, 7.10, and 7.12, the size of the cold spot gradually increases. However, although this is a subjective report by the authors, the spatial spread of the cold sensation was not felt. In addition, as for the movement of cold spot on the palm, in spite of the low spatial resolution of thermal sensation the authors could feel the motion of cooling sensation subjectively. The purpose of this paper is to clarify the basic physical properties of the proposed methods, and thus we have not conducted subjective experiments, however, we believe that it is necessary to investigate how such rapid changes of non-contact cold stimuli are subjectively perceived by subjects as a future work.

7.5.4 Confirmation of measurement error

In this subsection, we check the measurement error with thermographic camera. In the Experiment 1, 2 and 3, there are three data performed under the same conditions: the case of the Focus+Mist condition in figure 7.4, the case (a) in figure 7.6, and in figure 7.11. These data have a maximum difference of $2.1\,^{\circ}$C/s. It is considered that the difference is within the inevitable fluctuation of the system. The temperature and humidity slightly varied within $1\,^{\circ}$C and $5\,\%$, respectively. We consider that it does not seem to cause the difference in cooling performance depending on the system.

The concern for temperature measurement with a thermographic camera is the influence by the mist image. The white water mist is visible on the thermographic image. It is possible to influence the temperature estimation of the skin surface by the thermographic camera. In order to confirm the measurement error, the palm surface temperature was measured with the mist flow in front of the palm surface while applying the focused ultrasound to the palm surface. The focused ultrasound cooled the mist but did not irradiate the palm surface. That is, we created a situation where the cooling mist was flowing in front of the palm surface, but the temperature of the palm was clearly constant. Figure 7.14 shows the temperature change measured by the thermographic camera in that situation. In this case, the difference in temperature change was less than $1.5\,^{\circ}$C during irradiation of focused ultrasound. The temperature decrease was not observed during the measurement. This indicates that the mist image does not significantly affect the measurement with a thermographic camera.

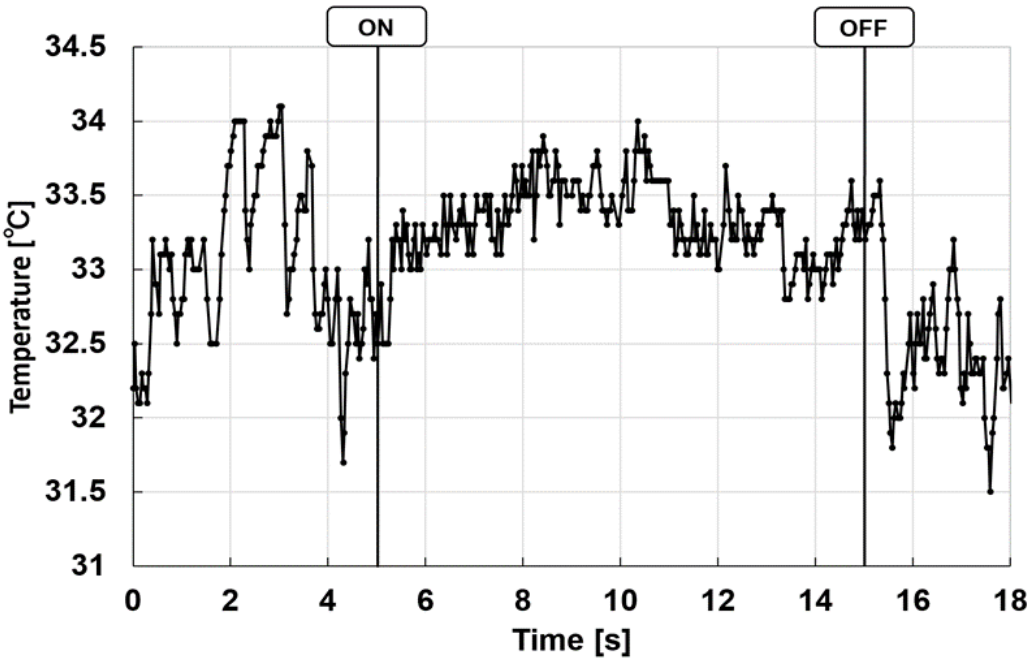

Fig. 7.14. Temperature change on the palm when the focused ultrasound is applied to the mist from the side.

7.6 Conclusion

In this chapter, we proposed a method of remotely displaying cooling sensation, where the mist is instantly vaporized in a spot area on the user's skin surface by the focused ultrasound. We used the same prototype as in chapter 6. Whereas the ultrasound beam was used in chapter 6, the focused ultrasound was used in this chapter. These can be generated on the same AUPAs, as mentioned in chapter 3. Using the prototype system, we examined the basic properties in displaying a cooling sensation.

First, we confirmed that cooling effect was achieved by combining the mist with the irradiation of the focused ultrasound. Next, it was found that a certain amount of mist supply was required depending on the position of the focused ultrasound. We also found that the cooling performance depended on the distance between the AUPAs surface and the target skin surface. Then, we confirmed that the emitted mist was transported to the skin surface in mid-air with the generation of focused ultrasound, and the converged mist was instantly vaporized and cooled. In addition, by continuously shifting the position of the focused ultrasound along the path of travel, we succeeded in creating a cooling spot that moves on the skin surface in real time. Therefore, we have validated that the system in this chapter can display a pinpoint

remote cooling sensation. It is of particular interest that the cooling effect demonstrated by the system can coexist with conventional ultrasound-driven vibrotactile stimuli.

Chapter 8

Performance Evaluation as Thermal Display

Chapters 5, 6 and 7 proposed an approach to display cooling sensation in the air. They were evaluated by the temperature change when displayed on the user's skin. As a result, it was found that the method proposed in chapter 7 had a high temperature change. In this chapter, we verified whether the proposed system in chapter 7 has enough performance to display contact with an object. As an example of metal, we examine the situation when it comes into contact with iron and estimate the heat flux at the time of contacting. We also estimated the heat flux when cooled by the proposed system. By comparing these heat fluxes, we evaluated the reproducibility of the object temperature.

First, we describe a method for analyzing heat flux at the time of contact with an object. Next, we describe a method for estimating the heat flux when cooled by the system. In addition, we estimate the heat flux when cooled to an object as well as the skin surface.

8.1 Heat Transfer When Contacting an Object

This section describes how to analyze heat transfer phenomena related to contact with object. Physical quantities that indicate the difference in thermal sensation include the temperature of the contact surface and heat flux. This is expressed as an index of thermal sensation at the time of contact by theoretically analyzing heat transfer to wood and metal.

First, we consider an object that has no internal heat source and is not stationary. T [K], q [W/m^2], ρ [g/cm^3], c [J/(gK)] and λ [W/(mK)] denote the temperature, the heat flux, the density of the object, the specific heat, and the heat conductivity, respectively. The index S, M, cs S_0 and M_0 denote the skin, the object, the contact surface, the initial skin and the initial object, respectively. In addition, it is assumed that $T_{\mathrm{S}} > T_{cs} > T_{\mathrm{M}}$.

The basic formula of the temperature T [K] at the time t [s] and the position $x(>0)$ [m] can be given as follows.

$$\frac{\partial^2 T_{\mathrm{S}}(t,x)}{\partial x^2} = \frac{c_{\mathrm{S}}\rho_{\mathrm{S}}}{\lambda_{\mathrm{S}}}\frac{\partial T_{\mathrm{S}}(t,x)}{\partial t} \tag{8.1}$$

$$\frac{\partial^2 T_{\mathrm{M}}(t,x)}{\partial x^2} = \frac{c_{\mathrm{M}}\rho_{\mathrm{M}}}{\lambda_{\mathrm{M}}}\frac{\partial T_{\mathrm{M}}(t,x)}{\partial t} \tag{8.2}$$

- Initial condition (at $t = 0$):

$$T_{\mathrm{S}}(0,x) = T_{\mathrm{S}_0}, \quad T_{\mathrm{M}}(0,x) = T_{\mathrm{M}_0} \tag{8.3}$$

- Boundary condition (at $x = 0$):

$$T_{\mathrm{S}}(t,0) = T_{\mathrm{M}}(t,0) = T_{\mathrm{cs}}(t) \tag{8.4}$$

$$\lambda_S \frac{\partial T_{\mathrm{S}}}{\partial x} = -\lambda_M \frac{\partial T_{\mathrm{M}}}{\partial x} \tag{8.5}$$

These solutions are as follows.

$$T_{\mathrm{S}}(t,x) = T_{\mathrm{cs}} + \left(T_{\mathrm{S}_0} - T_{\mathrm{cs}}\right) \mathrm{erf}\left(\frac{x}{2\sqrt{\alpha_S t}}\right) \tag{8.6}$$

$$T_{\mathrm{M}}(t,x) = T_{\mathrm{cs}} + \left(T_{\mathrm{M}_0} - T_{\mathrm{cs}}\right) \mathrm{erf}\left(\frac{x}{2\sqrt{\alpha_M t}}\right) \tag{8.7}$$

$$\alpha = \frac{\lambda}{c\rho} \tag{8.8}$$

Gauss's error function is as follows.

$$\mathrm{erf}(x) = \frac{2}{\sqrt{\pi}} \int_0^x e^{-t^2}\, \mathrm{d}t \tag{8.9}$$

The heat flux is given by

$$q = -\lambda \left(\frac{\partial T}{\partial x}\right). \tag{8.10}$$

By substituting these solution (8.6 and 8.7), the following relationship can be obtained.

$$T_{cs} = \frac{T_{\mathrm{S}_0} - T_{\mathrm{M}_0}}{1 + \mu_M/\mu_S} + T_{\mathrm{M}_0} \tag{8.11}$$

$$q_{cs}(t) = \frac{\mu_M}{\sqrt{\pi t}} \frac{T_{S_0} - T_{M_0}}{1 + \mu_M/\mu_S} \tag{8.12}$$

The thermal effusivity is as follows.

$$\mu = \sqrt{\lambda c \rho} \tag{8.13}$$

Therefore, by using equations (8.11) and (8.12), the temperature and heat flux at the time of contact with the object are calculated.

8.2 Measurement of Heat Flux by Proposed System

This section describes how to measure heat flux when the skin surface is cooled by the method proposed in chapter 7. Section 8.1 assumed the case of contact with an object. In this section, it is assumed that the surface of a flat object is cooled. Its object also does not have a heat source inside. By considering the heat flux due to the heat conduction of the object, we estimate the amount of heat absorbed when cooled by the system.

8.2.1 Temperature distribution and heat flux in the flat plate

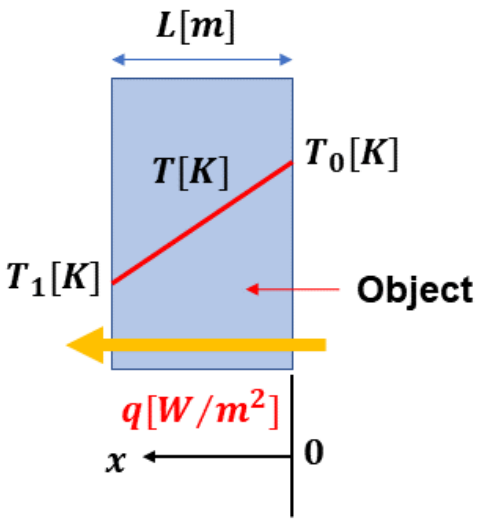

Fig. 8.1. Temperature distribution and heat transfer in the flat plate.

We consider a flat plate with a thickness of L [m] as shown in figure 8.1. The surface temperature on one side of the plate is T_0 [K], the surface temperature on the other side is T_1 [K], and the thermal conductivity λ of the plate is constant. Here, we would

like to get the information of the temperature distribution inside the plate and the heat flux passing through the plate.

Assuming a steady state, the heat flux q is constant, so the following equation is obtained.

$$\frac{\mathrm{d}T}{\mathrm{d}x} = -\frac{q}{\lambda}(= const.) \tag{8.14}$$

- Boundary condition:

$$\left.\begin{array}{ll} x = 0: & T = T_0 \\ x = L: & T = T_1 \end{array}\right\} \tag{8.15}$$

Integrating equation (8.14) gives

$$T = C_1 x + C_2. \tag{8.16}$$

C_1 and C_2 are constants of integration. These are obtained from boundary condition (8.15), and the temperature T is given by

$$T = T_0 - \frac{(T_0 - T_1)}{L} x. \tag{8.17}$$

Therefore, the internal temperature distribution is a straight line as shown in figure 8.1, and the heat flux on the plate vertical to the x-axis is given by

$$q = -\lambda \left(\frac{\partial T}{\partial x}\right) = \frac{T_0 - T_1}{L/\lambda}. \tag{8.18}$$

As shown in figure 8.2, the heat flux q' when the plate on one side is cooled by the mist and drops to the temperature T_2 [K] ($T_2 < T_1$) is given by

$$q' = \frac{T_0 - T_2}{L/\lambda}. \tag{8.19}$$

From (8.18) and (8.19), the heat flux during cooling by the system is as follows.

$$\Delta q = q' - q = \frac{T_1 - T_2}{L/\lambda} \tag{8.20}$$

Let $\Delta T = T_1 - T_2$ be the temperature difference while cooled by the mist, and (8.20) is given by

$$\Delta q = \frac{\lambda}{L}\Delta T. \tag{8.21}$$

This is used to estimate the heat flux when the skin surface is cooled by the system in chapter 7.

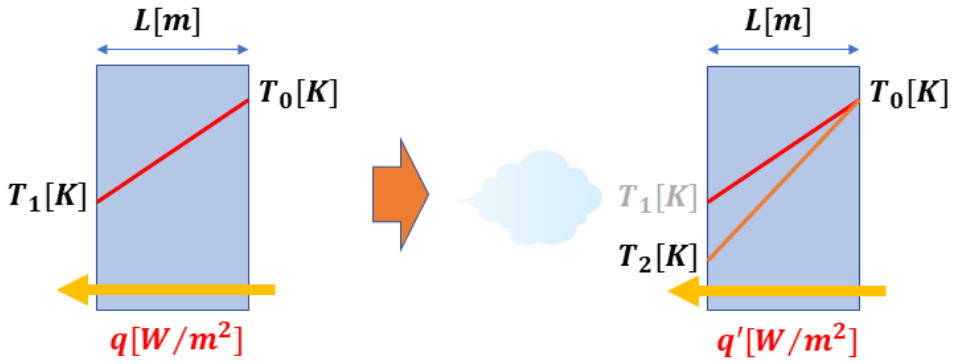

Fig. 8.2. Temperature distribution and heat transfer in the flat plate when cooled by the system.

8.2.2 Time constant in temperature change of an object

The previous subsection described the theoretical method of heat flux. In this subsection, we described the calculation of the time constant in the temperature change while cooled by the system. The time constant is an indispensable factor for estimating the speed of change until the temperature change becomes a steady state.

As shown in figure 8.1, we consider an object which have a thickness L [m], a cross-sectional area A [m^2], a thermal conductivity λ [W/(mK)], a mass m [g], a density ρ [kg/m^3], and a specific heat c [J/(gK)].

Thermal resistance R and heat capacity C are expressed by

$$R = \frac{L}{\lambda A} \tag{8.22}$$

$$C = mc. \tag{8.23}$$

Thus, the time constant is expressed by

$$t_c = RC = \frac{mcL}{\lambda A}. \tag{8.24}$$

Using the time constant t_c, the temperature $T(t)$ of the object at time t is given by

$$\frac{T(t) - T_{ini}}{T_\infty - T_{ini}} = 1 - exp\left(-\frac{t}{t_c}\right) \tag{8.25}$$

where T_{ini} and T_∞ denote the initial and steady temperature. here, it is assumed that the temperature inside the object is uniform.

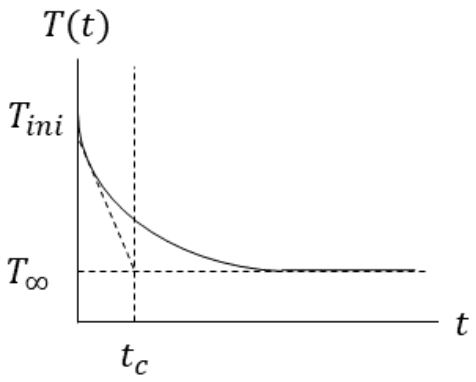

Fig. 8.3. The graph representing (8.25).

8.3 Performance Evaluation as Thermal Display

This section discusses the reproducibility of the method in chapter 7 when we touch an object. Here, assuming that we touch the metal such as iron, the evaluation is performed using the heat flux calculation method described in section 8.1 and 8.2. Then, the average temperature of the skin surface is assumed to be $33\ ^\circ$C.

For example, we consider when touching the iron at $25\ ^\circ$C for 10 seconds. According to the method in section 8.1, $T_S = 306$, $T_M = 298$, $\mu_S = 1334.88$, and $\mu_M = 15591.05$. Thus, the temperature of the contact surface is $T_{cs} = 25.63$ and the heat flux is $q_{cs} = 1753.99$.

On the other hand, in the result 7.11 in chapter 7, the endothermic heat flux is $\Delta q = 1755$ based on section 8.2. This indicates that it is the same situation as touching the iron at $25\ ^\circ$C for 10 seconds. In addition, the heat flux when touching the iron at $15\ ^\circ$C for 50 seconds is $q_{cs} = 1766.90$. Evaluating only by the heat flux, the situation is the same as the result 7.11.

The physical property values used to estimate each heat flux are shown in figure 8.4. This is because the thickness of the dermis is 2×10^{-3}, while the thickness of the epidermis is 80×10^{-6}, which is much smaller. It is also because thermal receptors are located in the dermis.

Iron	Dermis	Epidermis
$\lambda = 67.0\ W/(m \cdot K)$ $\rho = 7870\ \mathrm{kg}/m^3$ $c = 0.461\ \mathrm{J}/(\mathrm{g} \cdot K)$	$\lambda = 0.45\ W/(m \cdot K)$ $\rho = 1200\ \mathrm{kg}/m^3$ $c = 3.30\ \mathrm{J}/(\mathrm{g} \cdot K)$	$\lambda = 0.24\ W/(m \cdot K)$ $\rho = 1200\ \mathrm{kg}/m^3$ $c = 3.59\ \mathrm{J}/(\mathrm{g} \cdot K)$

Fig. 8.4. Physical properties used to calculate heat flux [84][86]

8.4 Cooling Effect on Artificial Objects

In this section, heat flux was measured when cooled to artificial objects other than the skin surface. The purpose of this measurement is to compare the heat flux when the object is cooled in order to display the material sensation by the proposed system. This makes it possible to estimate the heat flux required to display thermal sensation of the object. The objects used in the experiment are acrylic, paper, and natural rubber.

First, the time constant is estimated using the calculation method (8.24) based on the physical properties of each object. Next, we measured the heat flux when each object was cooled for a time sufficiently longer than the time constant. We also evaluated the mist supply dependence when targeting objects as well as the skin surface.

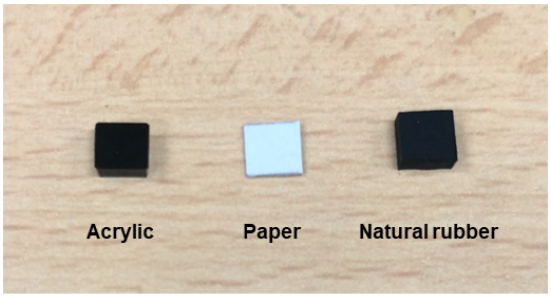

Acrylic	Paper	Natural rubber
$L = 2[mm]$ $A = 5 \times 5[mm^2]$ $\lambda = 0.21[\mathrm{W}/(m \cdot \mathrm{K})]$ $m = 0.052[\mathrm{g}]$ $c = 1.50[\mathrm{J}/(\mathrm{g} \cdot \mathrm{K})]$ $t_c = 29.71$	$L = 0.5[mm]$ $A = 5 \times 5[mm^2]$ $\lambda = 0.06[\mathrm{W}/(m \cdot \mathrm{K})]$ $m = 0.009[\mathrm{g}]$ $c = 1.30[\mathrm{J}/(\mathrm{g} \cdot \mathrm{K})]$ $t_c = 3.90$	$L = 2[mm]$ $A = 5 \times 5[mm^2]$ $\lambda = 0.134[\mathrm{W}/(m \cdot \mathrm{K})]$ $m = 0.008[\mathrm{g}]$ $c = 1.88[\mathrm{J}/(\mathrm{g} \cdot \mathrm{K})]$ $t_c = 8.98$

Fig. 8.5. Thermal physical properties, size, and time constant used in the measurement.

8.4.1 Measuring procedures

With the same setup as (a) in figure 7.2, we measure the temperature change when each object is cooled for 50 seconds by the system in chapter 7. Each measurement is performed after heating the object on a hot plate for 5 minutes in advance. The preset temperature of the hot plate is 34 °C.

The physical characteristics, size, and time constant of the objects to be measured are shown in figure 8.5. The measurement setup is shown in figure 8.6. The object is surrounded by foamed styrol without any gaps so that one side is in contact with the hot plate. It is contacted by applying grease between the object and the hot plate. In addition, by contacting with the hot plate, the temperature on one side is kept constant.

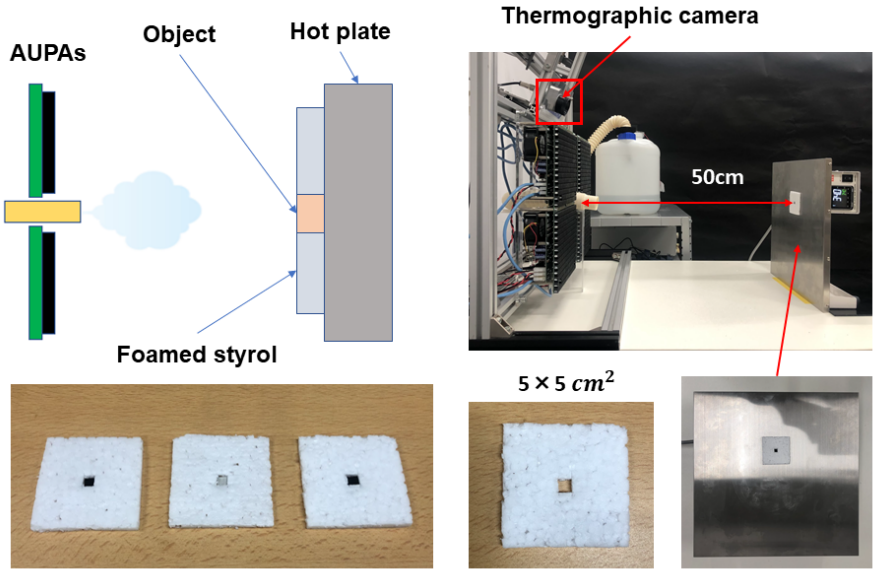

Fig. 8.6. Experimental setup.

8.4.2 Result

Figure 8.7 shows the temperature change and heat flux while each object is cooled. The mist-fan based on (6.4) voltage is set to 13 [V] for the amount of mist generated by the system. $q_{acrylic}$, q_{paper}, and q_{rubber} denote the heat fluxes of acrylic, paper, and natural rubber, respectively. Each heat flux is $q_{acrylic} = 787.5$, $q_{paper} = 1176$, and $q_{rubber} = 723.6$, respectively. Therefore, some heat fluxes required for an object which has no heat source inside could be estimated, and we obtained the information of heat flow required for displaying the material sensation of some objects.

Figure 8.8 shows the rate of temperature change immediately after cooling with respect to the mist-fan voltage of each object. For values of skin surface, result 7.5 was applied. From this result, it was found that the temperature change of the object also does not depend on the supply of mist.

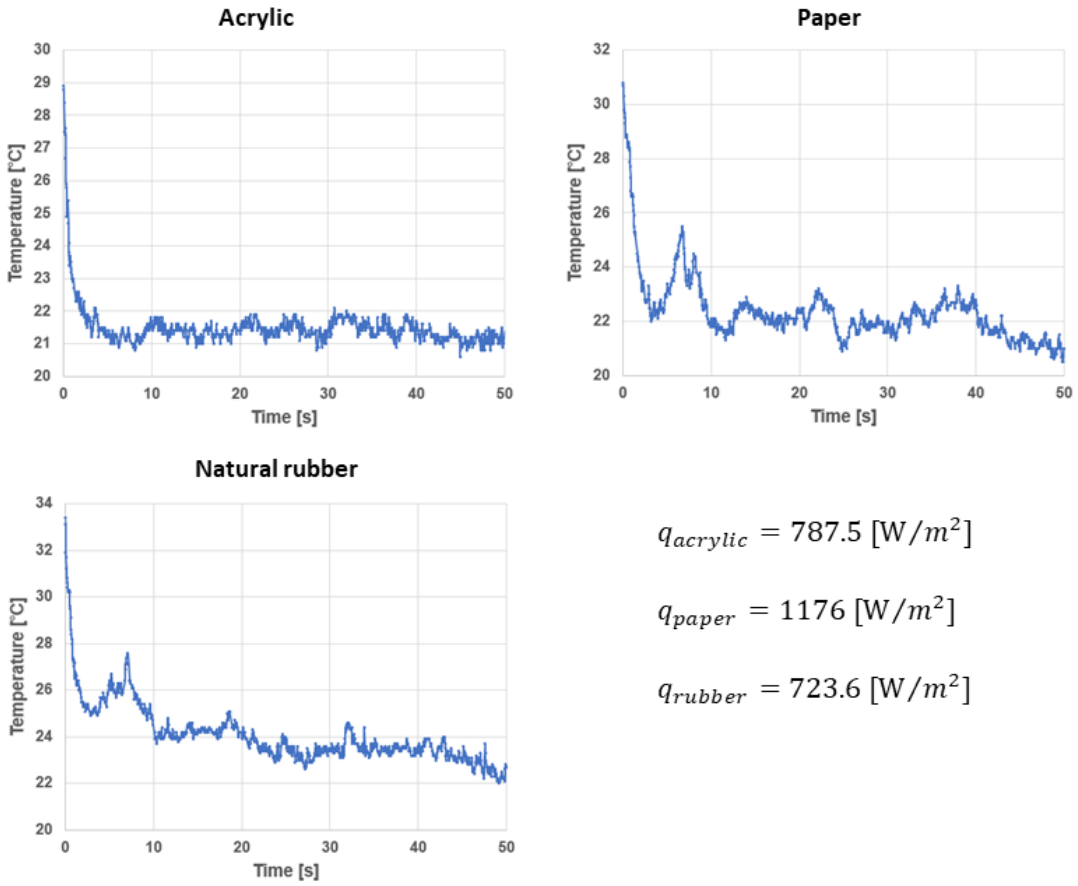

Fig. 8.7. Temperature change and heat flux of each object.

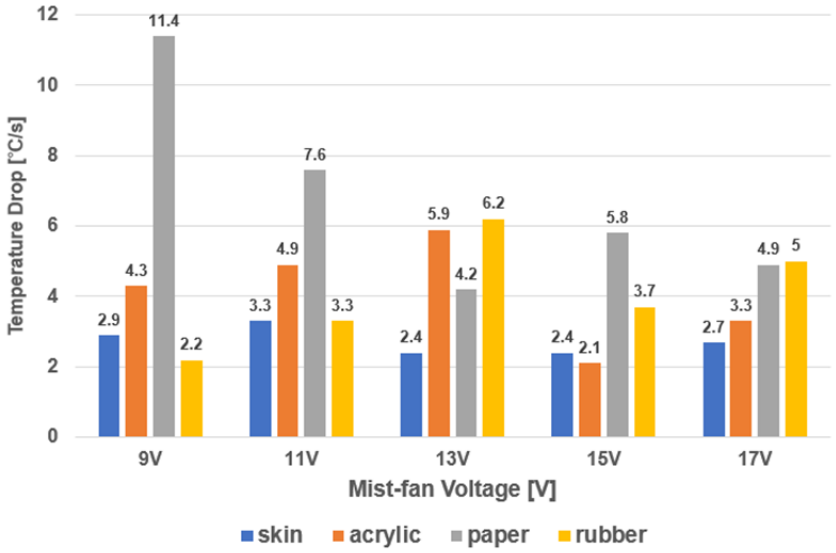

Fig. 8.8. Temperature drops versus the mist-fan voltage.

8.5 Conclusion

In this chapter, we described the method of evaluating the performance of the proposed system in chapter 7 as a thermal display.

First, we described the theoretical measurement method of temperature and heat flux when in contact with an object. Next, the method of estimating the heat flux absorbed by the cooling of the system was described. In addition, the time constant of temperature change required for cooling to an artificial object was explained.

Based on the measurement method of each heat flux, we evaluate that cooling by proposed system has the performance to reproduce contact with an object. As a result, it was found that cooling by the system for 10 seconds was equivalent to touching iron at 25 °C for 10 seconds.

Finally, we measured the heat flux when cooled to objects other than the skin surface. It was also confirmed whether the temperature change depends on the amount of mist supply. From these result, we obtained the information on the heat flux required for displaying the thermal sensation of the object, and it was found that it did not depend on the amount of mist supply. The rest work is the control of heat flux.

Chapter 9

Interactive Fog Display with Feedback of Cooling Sensation by Focused Ultrasound

In this chapter, we present application system using the method in chapter 7. The mist was used as a coolant, but it is used for fog display in this chapter. Fog display is one of the spatial projection technologies that use the semi-transparence of mist. We propose a system that can provide cooling feedback to the fog display. This is achieved by irradiating a local area on the fog display with focused ultrasound generated from the AUPAs, which cool that area using instantaneous mist vaporization. We construct a prototype and performed a demonstration of cooling feedback.

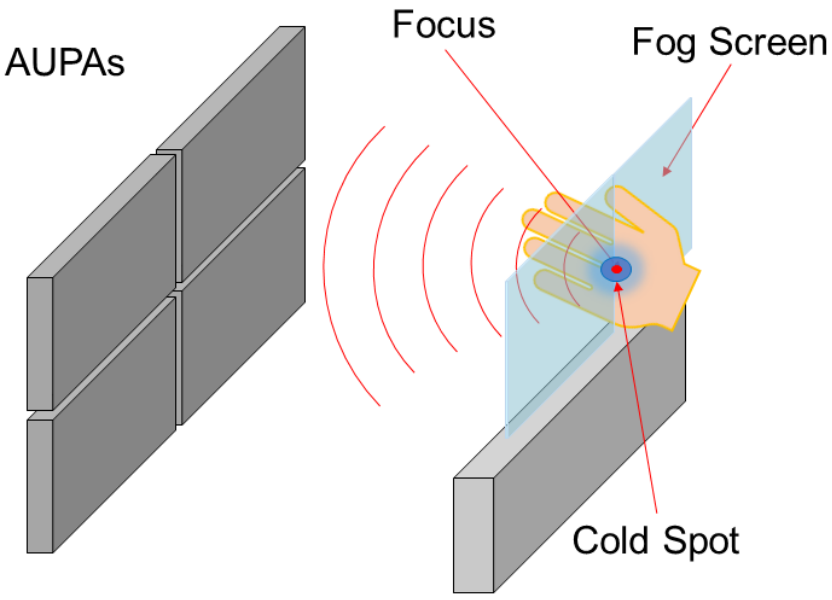

Fig. 9.1. Example of interactive fog display with cooling sensation feedback by focused ultrasound.

9.1 Background

With the spread of 3D displays and HMDs, there has been increasing interest in systems that interact with aerial images and tactile stimulation. A system that operates a virtual object on an aerial image in the same way as a real object has the potential to improve operational performance such as remote operation of medical surgery, simulation of car driving, and telexistence.

In such a system, one example is a method in which an aerial image and a tactile interaction are performed by using ultrasound. For example, HaptoMime [8] and HaptoClone [9] were proposed. The former is a system operated by touching a display imaged in the air using a micro mirror array. The latter is a system that interacts with an aerial mage generated using two micro mirror arrays. In these methods, the positions of the hands and fingers are sensed, and focused ultrasound is generated at the positions which contact with the aerial image. As a result, we have succeeded in displaying only mechanical tactile sensation.

In chapter 7, the mist floating on the user's skin surface was instantaneously vaporized in a local area on the skin, and the heat of vaporization showed the possibility of displaying cooling sensation. In this chapter, remotely displaying cooling sensation and fog display are utilized simultaneously by using water mist. A focused ultrasound is applied to the aerial image displayed on the fog screen using AUPAs. When a user touches this aerial image, the heat vaporization of water mist realizes an interaction with a cooling sensation (Fig. 9.1).

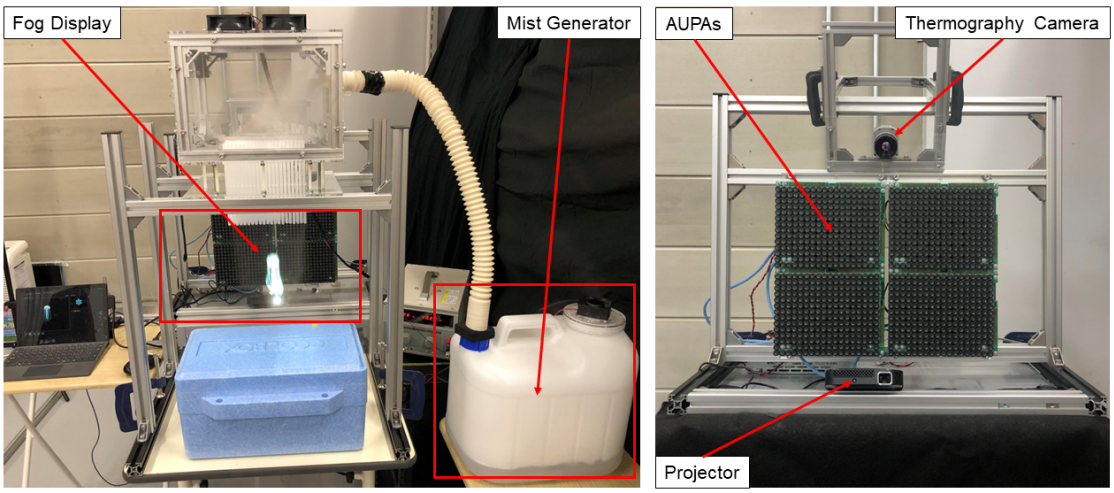

Fig. 9.2. System overview of interactive fog display.

9.2 Prototype 1

Figure 9.2 shows overview of prototype system. It consists of AUPAs, a fog display, projector, and mist generator.

・Mist Generator and Fog Display

The mist generator is the same as that we used in chapter 6 and 7. It is a supply source for use as a fog display. Figure 9.3 shows a prototype of fog display. There is a duct hose connected to the mist generator on the side of the box, and the mist is emitted by the fan at the top. There are 4 fans in the upper of the box, and 189 pipes (Diameter: Approximately $6\,\mathrm{mm}$, Length: Approximately $170\,\mathrm{mm}$) are arranged in the lower. The mist released from the duct hose is stored in the box. The downward flow by the fan causes the mist to be released as a flat layer through the pipes. It is used as a fog display by projecting an image onto a mist that flows in layers with a projector.

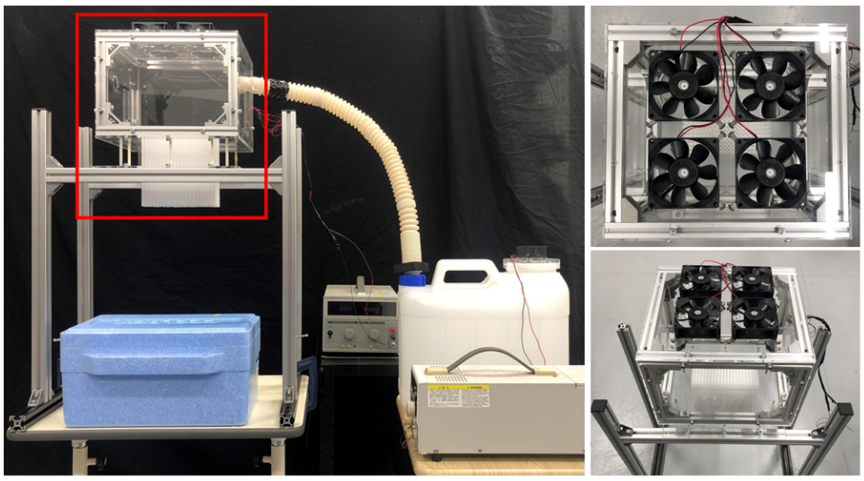

Fig. 9.3. Prototype system of fog display. The part surrounded by the red square shows the box for storing the mist emitted from the mist generator and discharging it with the upper 4 fans.

・Feedback of Cooling Sensation by Focused Ultrasound

We use the method described in chapter 7 to display cooling sensation on the fog screen. The position was set so that the focused ultrasound was irradiated on the fog screen. The heat vaporization of the mist causes interaction with the cooling sensation.

9.3 Experiment 1

Using the prototype 9.2, we measured the temperature change when focused ultrasound was applied to the palm exposed to the mist of the fog display. We also observed the image projected on the fog screen by a projector.

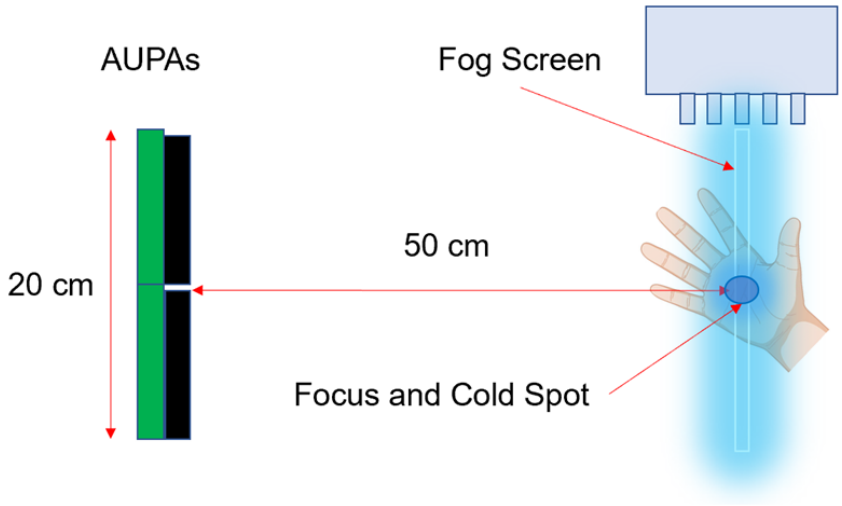

Fig. 9.4. Experimental setup.

9.3.1 Measuring procedures 1

As shown in figure 9.4, the distance between the AUPAs and the fog screen is $50\,\mathrm{cm}$. We place our palm on the table and adjust the position of the palm so that it is directly below the fog display.

When the focused ultrasound was irradiated, the temperature change is measured in a video format with a thermographic camera (OPTOI450O 29T900, Optris). We determined the measurement area ($61.4\,\mathrm{mm} \leq \mathrm{X} \leq 76.8\,\mathrm{mm}$, $84.6\,\mathrm{mm} \leq \mathrm{Y} \leq 100.0\,\mathrm{mm}$) as shown in figure 9.5. The center of the Measuring Area corresponds to the position where the focused ultrasound is irradiated. The measurement with the thermography camera is started at the same time as the irradiation is started. The measurement time is $10\,\mathrm{s}$.

9.3.2 Result 1

Figure 9.6 shows images at the start ($0\,\mathrm{s}$) and the end ($10\,\mathrm{s}$) of irradiation. From this result, it can be seen that the temperature drops at the irradiated position. Figure 9.7 shows the temperature change during irradiation, which indicates the change in the minimum temperature in the determined measurement area. The temperature

decreased at a rate of $0.1\,^{\circ}$C/s after irradiation. In addition, The temperature of the skin surface decreased by $2\,^{\circ}$C in $10\,$s.

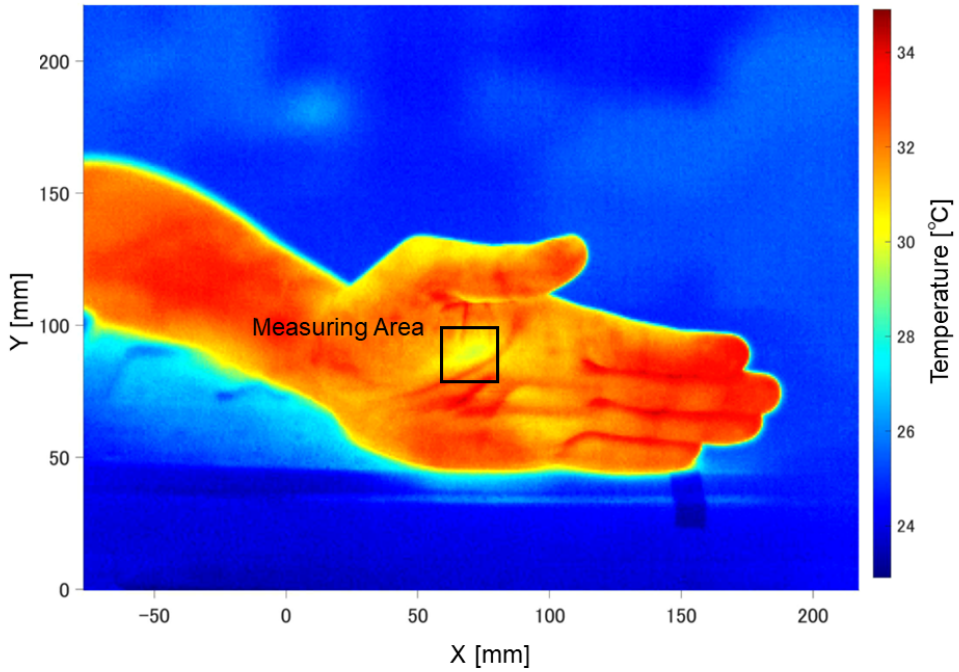

Fig. 9.5. Target parts on Measuring Area in the thermographic image. The Measuring Area can be determined in the same way as the method when measuring with a camera in chapter 7.

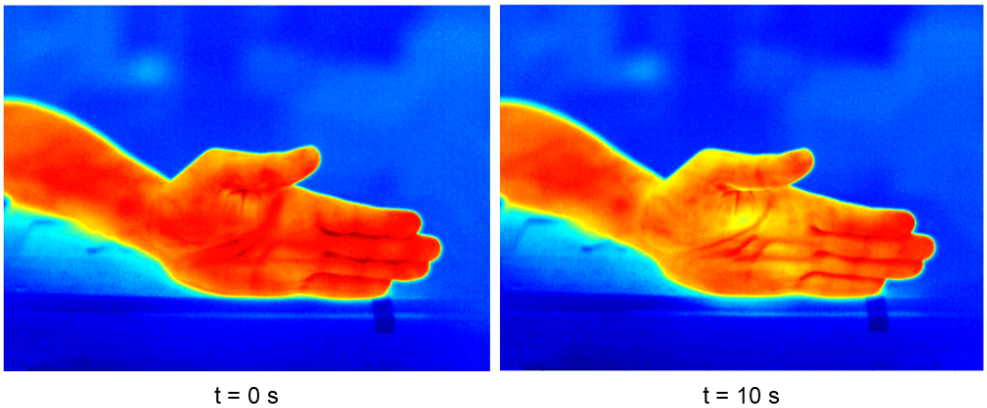

Fig. 9.6. Temperature change of the palm when measuring with a thermographic camera.

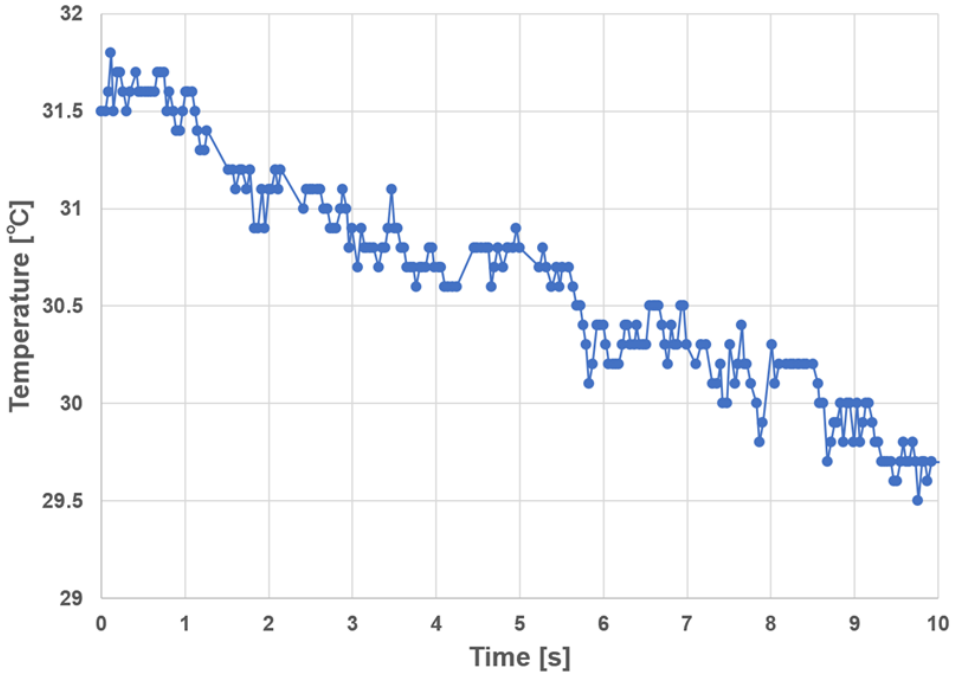

Fig. 9.7. Temperature change from the focused ultrasound on the fog screen.

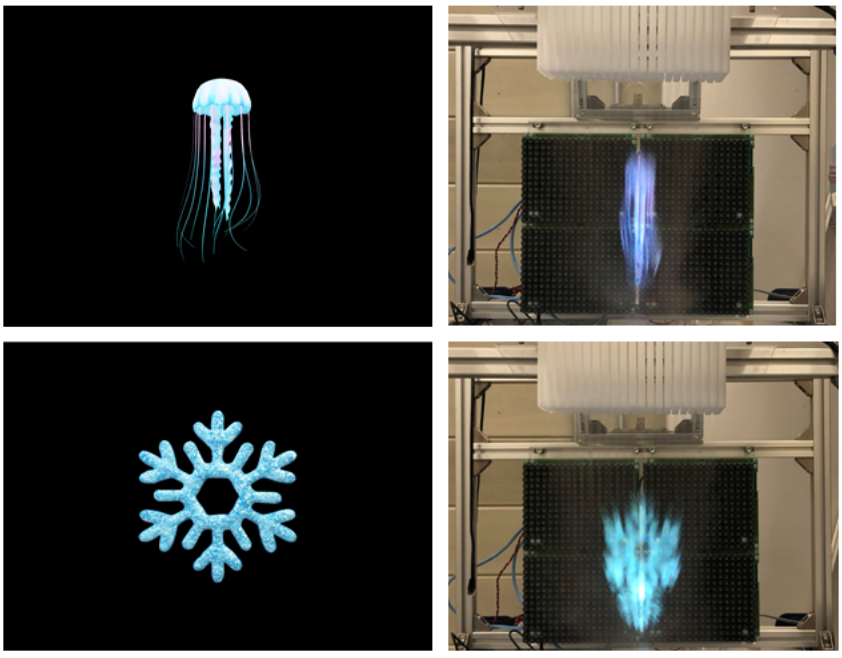

Fig. 9.8. Two kinds of images are projected on the fog screen.

9.3.3 Image Projection on Fog Screen

In this subsection, we investigated the performance of video display by the prototype of fog display. For that purpose, we prepared two kinds of images and projected them with a projector. As shown in figure 9.8, we projected images on the fog screen using mist and confirmed that it was visible. However, since the fog has not been stably trapped on a single thin screen, the image is projected so that the image is blurred around the fog screen. Therefore, it was confirmed that the prototype system has a function as a fog display.

9.4 Summary 1

We fabricated a prototype and evaluated the cooling effect of the system. We measured the temperature change to evaluate the cooling effect when focused ultrasound was applied to the palm on the fog display. It was confirmed that the temperature at the irradiated position decreased and the image projected on the fog display was visualized.

In next section, we propose a more sophisticated version of a interactive fog display with feedback of cooling sensation. As shown in figure 9.9, we add a system that detects the position on the screen where user touches and irradiates a focused ultrasound at that position.

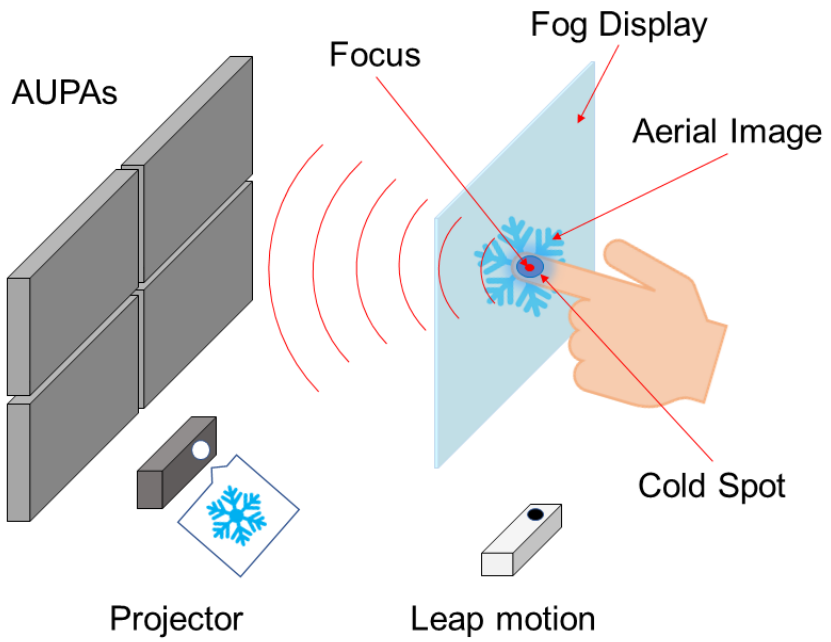

Fig. 9.9. A sophisticated version of the prototype system.

9.5 Prototype 2

The prototype 9.2 was individually equipped with a cooling sensation display and fog display. However, it was not equipped with a sensing system for the position where user touched the fog screen. In this section, we introduce a sensing system for interaction with feedback of cooling sensation. Therefore, it is possible not only to detect the position information of touching the fog screen, but also to implement operation system such as handling and deformation of the image on the screen. We also make improvements to prevent the image on the fog screen from bleeding.

The improved prototype is shown in figure 9.10. It consists of a fog display, a sensing unit, and a cooling sensation display.

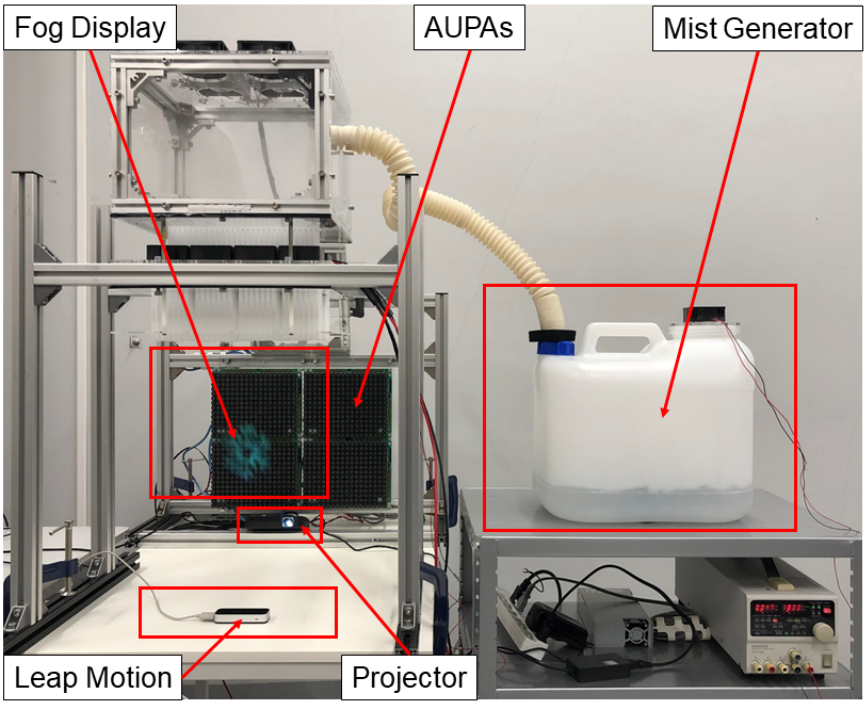

Fig. 9.10. The improved prototype system.

9.5.1 Improved Fog Screen

Figure 9.11 is an overall view of an improved version of prototype 9.2. Similarly, a duct hose connected to the mist generator is on the side of the box. The 4 fans at the top emit the mist through 63 small pipes. As in prototype 9.2, mist flows vertically downward from the pipes in a flat layer to form a mist screen. This prototype 9.5 has a system that sends air around mist screen in order to keep the flatness of the

screen. It has the role of preventing image from bleeding by sandwiching it between layers of airflow on both sides of a mist screen. There are 8 fans around the pipes at the bottom of the box. The airflow is blown from the pipes connected to the bottom of the fans. Figure 9.12 shows when the image is projected on the fog screen.

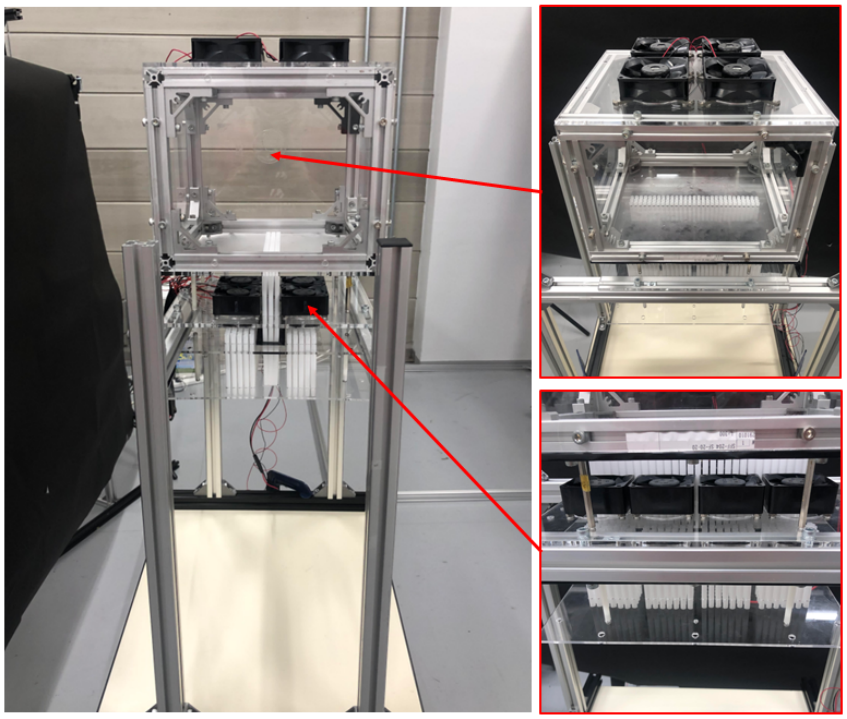

Fig. 9.11. Overview of fog display.

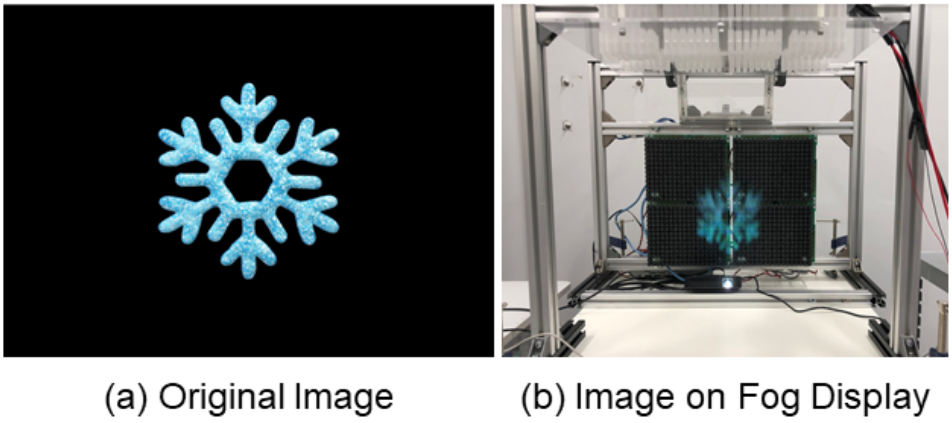

Fig. 9.12. Projection with fog display.

9.5.2 Sensing System

In the sensing system, the position of the user's hand and finger are sensed and modeled in the 3D modeling tool (Unity). We set the screen synchronized with the 3D image and the modeled hand to interact. For that purpose, this interaction on Unity (hand model and 3D Screen) is synchronized with the interaction in real space (user's hand and aerial image on fog screen). That is, we adjusted the following positional relationships.

- An aerial image and a sensor in real space.
- A model and a virtual screen in Unity.

We employed the Leap Motion as the depth sensor (Fig. 9.13(a)). As shown in figure 9.13(b), this sensor can identify not only the shape of the hand but also each finger and joints. Since this system only interacts with the user's hand, it is suitable for implementing applications that require finger identification. However, it may not be recognized if part of the hand is shielded by its angle.

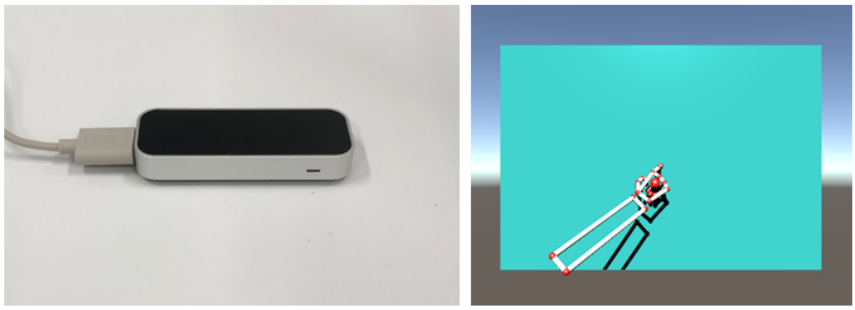

Fig. 9.13. (a)Appearance of Leap Motion. (b)3D model of the hand scanned by Leap Motion.

The main characteristics of Leap Motion are summarized as follows.

- Tracking speed: 60 fps (Precision mode).
- Depth recognition range: 25 to $600\,\mathrm{mm}$.

9.5.3 Displaying Cooling Sensation

We applied the method in chapter 7 to display a cooling sensation as in prototype 9.2. Similar to experiment 9.3, we measured the temperature change when focused ultrasound was applied to the palm exposed to the mist of the fog display. The irradiation time is $10\,\mathrm{s}$.

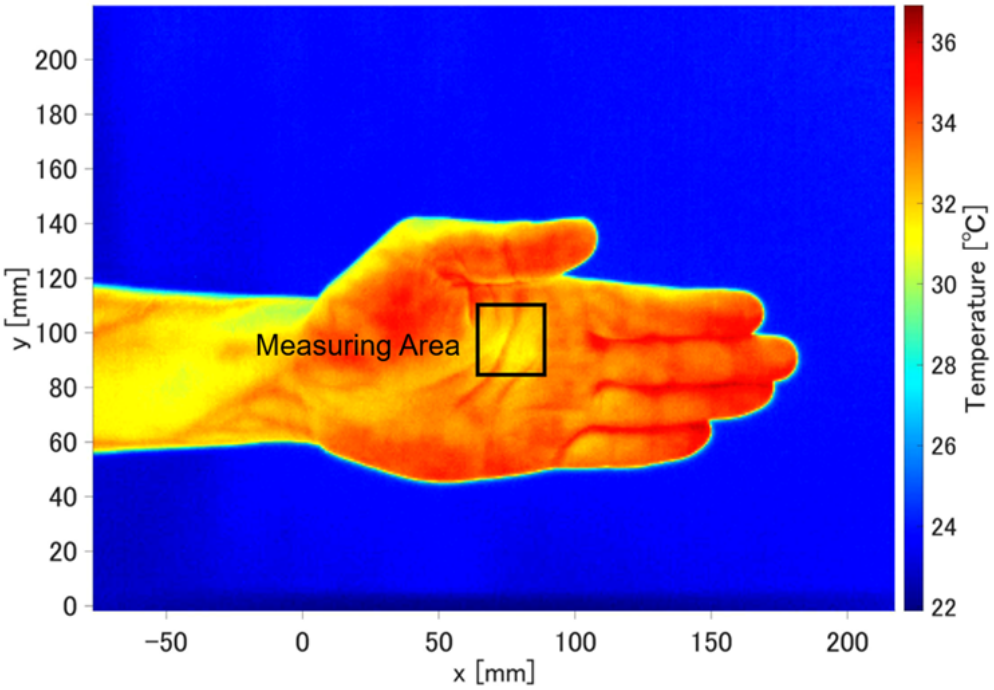

Fig. 9.14. Target parts on measurement area in the thermographic image.

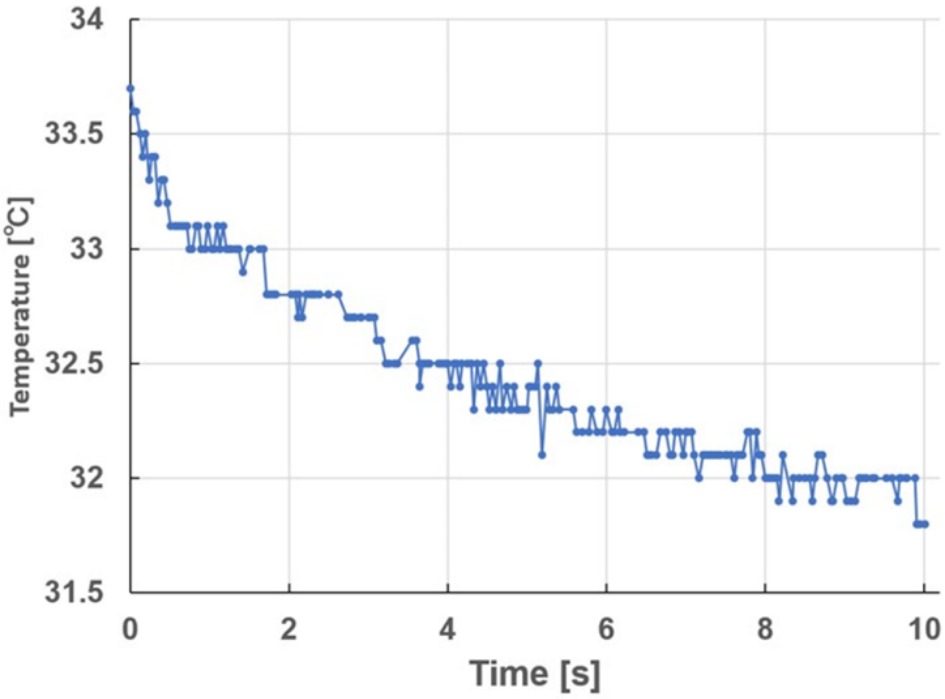

Fig. 9.15. Temperature change in the palm on the fog screen.

As in measuring procedures 9.3.1, we determined the measurement area ($61.4\,\mathrm{mm}$

$\leq$ X $\leq$ 84.6 mm, 90.0 mm $\leq$ Y $\leq$ 131.1 mm) as shown in figure 9.14, and measured the temperature change in that area with thermographic camera.

Figure 9.15 shows the temperature change during irradiation, which indicates the change in the minimum value in the determined measurement area. After the irradiation, the temperature dropped at a rate of 0.7 °C/s, and a temperature drop of 1.9 °C was observed in 10 s. Similar to prototype 9.2, it shows that the temperature drop by the improved system is working. The rate of temperature drop after irradiation was higher. However, there was no significant difference in the change when irradiated for 10 s.

9.5.4 Mutual Relationship in Prototype 2

This subsection describes the exchange of information in the system. Figure 9.16 summarizes the relationships among the user, each system, and the PC controller in a flowchart.

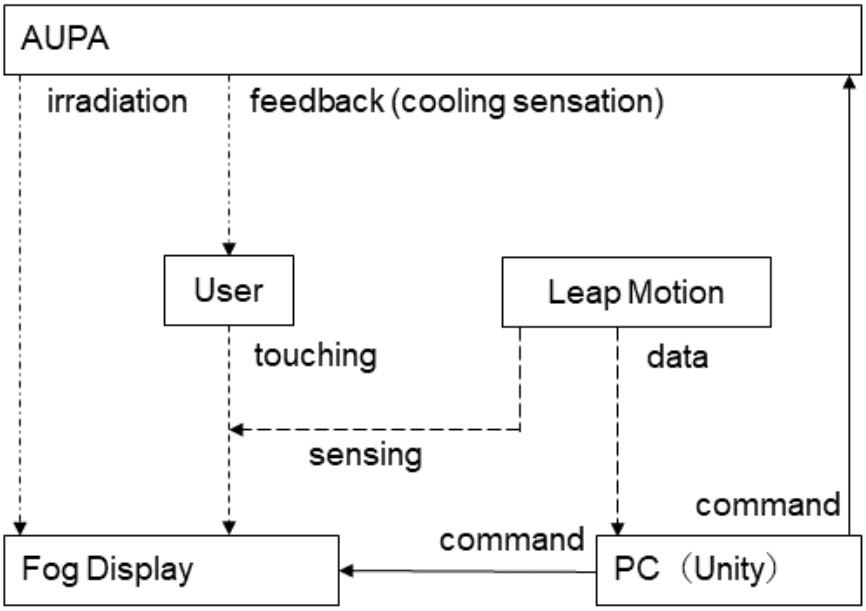

Fig. 9.16. Diagram of prototype system.

First, the user touches the aerial image on the fog screen. Leap Motion senses the position information that the user touches the screen and sends it to the PC. Then, it synchronizes with the interaction on Unity. A hand modeled as a virtual screen synchronized with a fog screen on Unity interacts in the same as in real space. The contact position information of the virtual screen is obtained in real time. The data is sent to the AUPAs. The AUPAs that receives the data generates a focused ultrasound in real space corresponding to that position. At this time, since the position

where focused ultrasound is generated is on the fog screen, a cooling sensation is displayed at the same time by mist vaporization. By repeating this procedure, real-time and programmable interaction is achieved.

9.5.5 Interaction Implementation

As shown in figure 9.17, we implement the interaction using a 3D image of a screen. In other words, a system created in which the focused ultrasound is applied to the position touched on the screen. The algorithm of the interaction system procedure is shown in figure 9.18.

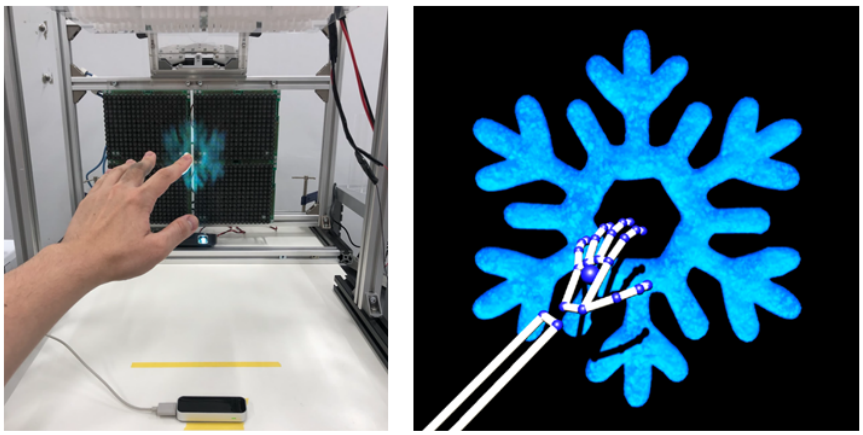

Fig. 9.17. Interaction in real space(a) and in Unity(b).

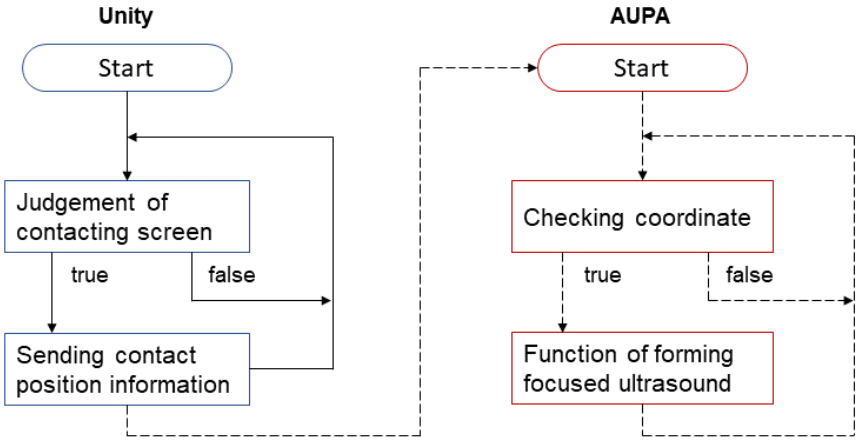

Fig. 9.18. Interaction system flowchart.

Although this system can project some kind of image on the fog screen, we plan to implement an interaction system for real objects and pseudo-shaped virtual objects.

Furthermore, when a 3D object can be freely deformed, we plan to propose a system that displays handling and deformation to soft objects.

9.6 Summary 2

In addition to prototype 9.2, we proposed an interaction system between an image on a fog screen and cooling sensation. By using a hand tracking sensor, it was implemented to display a cooling sensation at the position where the user touched an aerial image on the fog screen.

Similar to experiment 9.3, in order to evaluate the cooling effect of the system, we measured the temperature change when focused ultrasound was applied to the palm in the fog display. It was shown that it has the function of lowering the temperature similar to prototype 9.2. The projection of the image was subjectively more clearly visible. In the future, we will consider evaluating the resolution of the image on the fog screen.

9.7 Conclusion

In this chapter, we described application system using a cooling sensation display in chapter 7. We proposed the application of mist to not only coolant but also fog screen. We fabricated the prototype of fog display. First, the temperature changed during irradiation with focused ultrasound while touching the fog screen. We also observed the image projected on the screen. Second, in addition to the fabricated prototype, we built a system that detects the position information that the user touched the screen, which irradiated that position with focused ultrasound. We also improved the prototype so that the image on the screen does not blur. In the same way, we measured the cooling effect. As a result, it was shown to have a cooling effect.

In the future, we will implement an interaction system for freely shaped objects. We also evaluate the sensation of ”coldness” through psychophysical experiments. Furthermore, we will consider evaluating the resolution of the image on the fog screen.

Chapter 10

Conclusion

In this chapter, firstly, we address summary of this thesis. Next, the conclusions drawn from the experiments are described. Finally, we describe the future prospects and conclude this paper.

10.1 Summary

This thesis presents a method of remotely displaying a cooling sensation on the skin surface without contacting the device with the user's body. For that purpose, we employed the ultrasound phased arrays (AUPAs). The AUPAs can generate an ultrasound beam and a focused ultrasound. In addition, the water mist was used as cooling medium. The vaporization of water mist contributed to display a cooling sensation.

In chapter 1, the significance of thermal sensation was described through haptics technology, and methods of displaying a thermal sensation were shown. Application examples of displaying thermal sensation were also introduced. Here, we introduced previous research and explained our approach of this thesis.

In chapter 2, we described the perceptual characteristics of thermal sensation and the patterns of the displaying. Firstly, by presenting the perceptual characteristics of thermal sensation, we gained an understanding of the detection mechanism of temperature changes and psychophysical findings. Next, we classified the patterns of displaying thermal sensation and related works. The method of temperature measurement was also described. Finally, we investigated the elements suitable for the proposed method of this thesis.

In chapter 3, we described the principle of controlling AUPAs. Firstly, the method of creating acoustic field using AUPAs was explained. It was also shown that acoustic radiation pressure caused the tactile sensation. Secondly, the principle of creating the ultrasound beam was described. It was explained that ultrasound beam caused acoustic airflow. In addition, application examples of using ultrasound beam were introduced. Finally, the principle of forming the focused ultrasound. It was shown

that the spatial resolution of focused ultrasound depended on a proper aperture.

In chapter 4, the advantages of using water mist was described. The example of mist cooling was introduced. In addition, superiority of water as cooling medium was explained through chemical characteristics of water. For mist cooling to the human body surface, an example was given in which the mist was blown by a fan. Expectations for a high cooling effect of the water mist led us to the idea of transporting the mist in the air using an acoustic flow. Finally, we described the principle of mist generation and the estimation of the mist size when the liquid is irradiated with ultrasound.

In chapter 5, we described the midair haptic display that provides a cooling sensation using ultrasound-driven airflow and the water mist. When the mist is transported by acoustic flow and hits the skin surface, a cooling sensation is provided by the heat of vaporization. We fabricated the prototype and compared the cooling effect using the water mist and cold air of dry ice. The result demonstrated high cooling performance by heat of mist vaporization.

In chapter 6, we improved the prototype used in chapter 5, which can control the amount of mist generation. The prototype in chapter 5 sometimes transported not only mist but also water droplets in the air. In contrast, the reconstructed prototype can transport the mist which does not contain water droplets. In the experiment, we measured the temperature change of the user's palm. The result suggested that the cooling effect depended on the proper amount of the mist.

In chapter 7, we described the method of remotely displaying a pinpoint and instantaneous cooling sensation. We employed the same prototype as in chapter 6. The AUPAs, which is part of the prototype, generated a focused ultrasound instead of an ultrasound beam used in chapter 5 and 6. Using the focused ultrasound expedites the vaporization of the water mist floating near the user's skin surface locally and instantaneously, resulting in a sudden and pinpoint cooling sensation. In the experiment, we found that a part of the skin surface exposed to a focused ultrasound with floating mist was selectively cooled with a negligible delay. In addition, we demonstrated that cold spot was traveling on the skin surface in real time while the position of the focused ultrasound was continuously shifting along the path of travel.

In chapter 8, we described the performance evaluation as thermal display. The heat flux was used as a physical index of cooling sensation. As for the theoretical measurement method of heat flux, we first assumed the case of contact with an object. Next, we considered the transfer of heat inside the object. From these heat flux measurement methods, we evaluate the reproducibility of displaying thermal sensation by the system when we touch an object. In previous chapters, we measured

the temperature change when cooled to the human body. The temperature change when cooled to an artificial object was also measured to calculate the heat flux. As a result, the heat flux required to display the material sensation of some objects was estimated. It was also found that, like the skin surface, it does not depend on the amount of mist supply.

In chapter 9, we described an application using the method of chapter 7. We focused on the use of mist as a fog display in addition to the coolant. When the hand on the fabricated fog screen was irradiated with focused ultrasound, the temperature of skin surface was dropped by promoting the vaporization of mist in the same way. We observed the image projected on the fog screen, but it sometimes blurred. In addition, we introduced a system that detects the information of the position where the user touched the screen. Therefore, by irradiating the detected position with focused ultrasound, the aerial image on the screen interacts with the cooling sensation. At the same time, we also improved the fog display. It was shown to cool as well, and the projected image on the fog screen was clearer. As for the implementation of the interaction system, the strategy was described using a hand tracking sensor and 3D modeling tool.

10.2 Conclusion and Consideration from Experiments

This thesis aims to realize remotely displaying a cooling sensation on the skin surface without contacting the device with the user's body. We proposed roughly two types of methods. One was a method using an ultrasound beam (chapter 5 and 6). The other was a method using a focused ultrasound (chapter 7).

These methods take the advantage of AUPAs control method and its spatial resolution. In this section, we concluded and consider what was obtained from the experimental results conducted in each chapter.

10.2.1 Transport of mist by ultrasound beam

In chapter 5, we conducted a comparative experiment on the cooling effect of water mist and cold air of dry ice. For that purpose, we measured temperature change when water mist or cold air of dry ice was transported in the air and hit the skin surface. In the comparative experiment, the maximum difference in temperature drop in $50\,\mathrm{s}$ was $3.5\,^{\circ}\mathrm{C}$. This result shows the cooling effect using water mist is higher than that using cold air of dry ice. From the chemical characteristics of water described in chapter 4, it is shown that efficient cooling of the skin surface can be achieved by using water mist. On the other hand, the system had several problems. Since the generated mist was directly irradiated with an ultrasound beam, water droplets

with a large particle size were also transported. When the ultrasound beam was turned off, it remained low temperature without returning to its initial temperature. The mist generation position was also fixed. The prototype in chapter 5 required to control the amount of mist generation and change the position of mist generation. This suggests that proper mist supply cools the skin surface more efficiently.

In chapter 6, we reconstructed a sophisticated version of the prototype in chapter 5, which can control the amount of mist supply. Although the position of mist supply could be changed, the position was fixed in the experiment. Using the improved prototype, we measured the temperature change when the mist was transported by the ultrasound beam and hit the palm surface. Compared with the results in chapter 5, it was found that the temperature drop in $50\,\mathrm{s}$ was $1.9\,^{\circ}\mathrm{C}$ lower at the maximum. In addition, when the ultrasound beam was turned off, there was a tendency to return to the initial temperature. It is considered that the cooling efficiency could be higher by appropriately supplying the mist without water droplets with a large particle size. In other words, the cooling effect depends on the proper amount of the mist.

10.2.2 Displaying a spatiotemporal pinpoint cooling sensation

In chapter 7, we proposed a method of remotely displaying a pinpoint and instantaneous cooling sensation on the skin surface. For that purpose, we employed the prototype used in chapter 6, where the AUPAs generated a focused ultrasound instead of ultrasound beam.

We conducted three experiments. Firstly, we confirmed that the cooling effect was more likely to be effective by combining the mist with the irradiation of the focused ultrasound. Secondly, it was found that a certain amount of mist supply was necessary but the effect was saturated in a certainly feasible zone. We also found that the cooling performance depended on the distance between the AUPAs surface and the target user's skin surface. Thirdly, we measured the spatiotemporal temperature distribution on the palm. The temperature dropped by $3.3\,^{\circ}\mathrm{C}$ in $500\,\mathrm{ms}$ and $4.6\,^{\circ}\mathrm{C}$ in $1000\,\mathrm{ms}$ on the skin surface rapidly after irradiation. The diameter of the cold spot was approximately $2\,\mathrm{cm}$. The size of cold spot was comparable to that of the ultrasound focus. In addition, we succeeded in creating a cooling spot that moves on the skin surface in real time. This was achieved by continuously shifting the position of the focused ultrasound along the traveling path. Therefore, we demonstrated that our proposed system could display a spatiotemporal pinpoint cooling sensation.

10.2.3 System performance

The method proposed in chapter 7 had a large temperature change. In chapter 8, we evaluated whether this has the performance to display the contact with the object. The heat flux was calculated as an index of the thermal sensation. As a result, it was demonstrated that the proposed system has a performance capable of displaying contact with a metal colder than the skin surface. In addition, we obtained some estimates of the heat flux required to display the material sensation of other artificial objects.

10.3 Future Works and Prospects

This thesis demonstrated the method of remotely displaying a cooling sensation by controlling airborne ultrasound. Since the focused ultrasound can display mechanical tactile stimuli by modulating, it suggested that the cooling effect by our system can coexist with ultrasound-driven vibrotactile stimuli. We believe that there is the room for further development. We list up future works and prospects as follows:

10.3.1 Future works in this thesis

The experiments in this thesis were conducted with a thermographic camera. Each experiment was evaluated by temperature change and distribution. The purpose of this thesis is mainly to clarify the basic physical properities of our proposed system.

In the future, we will evaluate the effect of displaying a cooling sensation on user's skin surface in perspective of psychophysical aspects. In addition, we will research to clarify at what stage mist generation, transportation, and palm cooling are mainly performed by heat of vaporization. In the experiment conducted in chapter 7, the reason why the cooling effect was high by using focused ultrasound and water mist at the same time was not yet known. A possible mechanism for the cooling effect is that the heating effect of sound energy may have promoted the vaporization of mist. As described in Chapter 4, it is possible that the mist was split into smaller particles by ultrasound to generate more mist, and vaporized on the surface of the skin to remove heat. However, it is necessary to discuss how the effect of ultrasound changes due to change of mist particle size.

10.3.2 Future prospects

Application examples of this thesis were introduced in section 1.3. Mostly, displaying a cooling sensation can contribute to the reproduction of the experience in an environment with temperature change.

Since the proposed system in this paper has the potential to coexist with mechanical tactile and cooling sensation, the development of multi-modal display system can be expected. An aerial image system that can obtain tactile feedback using AUPAs has already been proposed as in section 1.3. In chapter 9, we proposed to use the mist not only as a coolant but also as a fog display. As a result, it was shown that a cooling sensation was displayed and that an aerial image on the screen was projected. From these results and the coexistence of vibrotactile sensation, we will integrate all those technical elements for creating a system of haptic feedback to virtual object.

Acknowledgement

This research was based on a great deal of support by current members and seniors of Shinoda-Makino laboratory.

Firstly, I would like to thank Professor Hiroyuki Shinoda. He gave me a lot of suggestions for my research. At regular meetings, he gave me technical advice and essential ideas for advancing research. When writing my thesis, his advice on making it easy to understand was also surprising to me. Thanks to that, I could learn more about writing science and technology papers and thinking about the logic for that purpose.

Secondly, I would like to thank Associate Professor Yasutoshi Makino who is my supervisor for 5 years in the master and doctor course. He often gave me comments after the presentation at the conference etc. His advice gave me the courage to take part in the conference. In addition, his way of accurate presentation and expression is always impressive me.

Thirdly, I am grateful to Masahiro Fujiwara who is now Project Assistant Professor in Shinoda-Makino laboratory. He gave me his technical advice for my research. His advice was very clear and easy to understand.

I am grateful to Keisuke Hasegawa. He is now Assistant Professor in Nara-laboratory and he was Project Assistant Professor in Shinoda-makino laboratory. Particularly, I was indebted to him when I was in the master course. His advice and comments are very essential and clear, and encourage me to notice the importance of seeing things deeply. These have greatly contributed to this research.

I am grateful to Yuichi Masuda, Takaaki Kamigaki, and Takuro Furumoto. They are Project Researcher in Shinoda-Makino laboratory. They gave me a lot of advice for proceeding research.

I am grateful to Yasuko Konagai. She is secretary in Shinoda-makino laboratory. She supported the laboratory members by purchasing goods and administrative procedures etc. Thanks to her support, I could proceed my research smoothly.

From here, I would like to express my gratitude to my colleagues. Daichi Matsumoto is doctoral students in the same grade and in the same lab. Since the master course, he is a companion who has worked hard with each other. Ya Zhu is doctoral students in the same grade and in the same lab. She is trilingual and very diligence.

Thank you for her help in business trips overseas and communication with overseas guests. Yuki Ninomiya is doctoral students in the same grade and in the same lab. He gave me proper advice on how to handle the equipment and tools in laboratory. Ansheng Wang is doctoral students in the same grade and in the same lab. I enjoyed talking with him sometimes. Since he is studying machine learning, I respect the strength of his expertise. Shun Suzuki is doctoral students in the same lab. He has outstanding programming skills. His skill helped me solving the problems of my research. I think he greatly contributes to other member's research.

Finally, I would like to thank other members in Shinoda-makino laboratory. They made my research life very enjoyable.

Bibliography

[1] Oculus Rift, https://www.oculus.com/rift/.

[2] HTC VIVE, https://www.vive.com/.

[3] Playstation® VR, https://www.jp.playstation.com/psvr/.

[4] Microsoft HoloLens, https://www.microsoft.com/En-US/hololens/.

[5] J. J. Gibson, "Observations on active touch." *Psychological review*, vol. 69, no. 6, p. 477, 1962.

[6] T. Iwamoto, M. Tatezono, and H. Shinoda, "Non-contact method for producing tactile sensation using airborne ultrasound," *Haptics: Perception, Devices and Scenarios*, pp. 504–513, 2008.

[7] T. Hoshi, M. Takahashi, T. Iwamoto, and H. Shinoda, "Noncontact tactile display based on radiation pressure of airborne ultrasound," *IEEE Transactions on Haptics*, vol. 3, no. 3, pp. 155–165, 7 2010.

[8] Y. Monnai, K. Hasegawa, M. Fujiwara, K. Yoshino, S. Inoue, and H. Shinoda, "Haptomime: mid-air haptic interaction with a floating virtual screen," in *Proceedings of the 27th annual ACM symposium on User interface software and technology*. ACM, 2014, pp. 663–667.

[9] Y. Makino, Y. Furuyama, S. Inoue, and H. Shinoda, "Haptoclone (haptic-optical clone) for mutual tele-environment by real-time 3d image transfer with midair force feedback," in *Proceedings of the 2016 CHI Conference on Human Factors in Computing Systems*. ACM, 2016, pp. 1980–1990.

[10] K. Yoshida, T. Kamigaki, S. Inoue, K. Hasegawa, Y. Makino, and H. Shinoda, "Haptoclonear (haptic-optical clone with augmented reality) for mutual interactions with midair 3d floating image and superimposed 2d display," in *International AsiaHaptics conference*. Springer, 2016, pp. 473–477.

[11] Ultrahaptics. (2017) Bosch demonstrates Ultrahaptics' mid air haptics in concept car at CES. [Online]. Available: https://www.ultrahaptics.com/news/announcements/bosch-ces-concept-car

[12] B. G. PressClub. (2016) BMW HoloActive Touch. [Online]. Available: https://www.press.bmwgroup.com/global/article/detail/T0266649EN/the-bmw-group-at-ces-2017-in-las-vegas-bmw-holoactive-touch:-an-innovative-operating-concept-for-the-interior-of-the-future

[13] R. Wettach, C. Behrens, A. Danielsson, and T. Ness, "A thermal information display for mobile application," in *Proc. In in MobileHCI '07*, 2007, pp. 182–185.

[14] L. A. Jones, "Perspectives on the evolution of tactile, haptic and thermal displays, presence," *FORUM Short Paper*, vol. 25, no. 3, pp. 247–252, 2016.

[15] H. N. Ho and L. A. Jones, "Contribution of thermal cues to material discrimination and localization," *Perception Psychophysics*, vol. 68, pp. 118–128, 2006.

[16] K. Sato and T. Maeno, "Presentation of rapid temperature change using spatially divided hot and cold stimuli," *J.Robotics and Mechatronics*, vol. 25, no. 3, pp. 497–505, 2013.

[17] M. Sakaguchi, K. Imai, and K. Hayakawa, "Development of high-speed thermal display using water flow," *Human Interface and the Management of Information. Information and Knowledge Design and Evaluation, Lecture Notes in Computer Science*, vol. 8521, pp. 233–240, 2014.

[18] K. Hayakawa, K. Imai, R. Honaga, and M. Sakaguchi, "Highspeed thermal display system that synchronized with the image using water flow," *Haptic Interaction*, vol. 277, pp. 69–74, 2015.

[19] K. Sato, "Augmentation of thermal sensation on finger pad using stimuli for finger side," *EuroHaptics2016*, pp. 371–379, 2016.

[20] K. Hokoyama, Y. Kuroda, G. Kato, K. Kiyokawa, and H. Takemura, "Mugginess sensation: Exploring its principle and prototype design," *IEEE World Haptics Conference 2017 (WHC)*, pp. 563–568, 2017.

[21] S. Saga, "Thermal-radiation-based haptic display: Basic concept," *Proceedings of IEEE World Haptics 2015, WIP-28 (Work-in-Progress Papers)*, 6 2015.

[22] S.Saga, "Thermal-radiation-based haptic display - laser-emission-based radiation control -," *Proceedings of IEEE World Haptics 2019, WP2P.10 (Work-in-Progress Papers)*, 7 2019.

[23] J. Xu, Y. Kuroda, S. Yoshimoto, and O. Oshiro, "Non-contact cold thermal display by controlling low-temperature air flow generated with vortex tube," in *World Haptics Conference (WHC), 2019 IEEE, Technical Papers, Oral session 1B (TP1B.23)*. IEEE, 2019.

[24] C. L. Fernando, M. Furukawa, T. Kurogi, S. Kamuro, K. Sato, K. Minamizawa, and S. Tachi, "Design of telesar v for transferring bodily consciousness in telexistence," in *Proc. of IEEE/RSJ IROS2012*. IEEE/RSJ, 2012, pp. 5112–5118.

[25] Orbi Yokohama, https://orbiearth.jp/exhibition/mtkenya/.

[26] International Antarctic Center, https://www.iceberg.co.nz/.

[27] H. Palleis and M. Mickisch, "Henrich hussmann: A concept for 3d interaction on a curved touch display," in *Proc CHI EA 2015, Proceedings of the 33rd Annual ACM Conference Extended Abstractson Human Factorsin Computing Systems*. CHI,

2015, pp. 1163–1168.

[28] A. Matsubayashi, Y. Makino, and H. Shinoda, “Direct finger manipulation of 3d object image with ultrasound haptic feedback,” *Proceedings of the 2019 CHI Conference on Human Factors in Computing Systems*, 5 2019.

[29] A. Matsubayashi, H. Oikawa, S. Mizutani, Y. Makino, and H. Shinoda, “Display of haptic shape using ultrasound pressure distribution forming cross-sectional shape,” *Proceedings of IEEE World Haptics 2019*, pp. 419–424, 7 2019.

[30] M. Nakajima, K. Hasegawa, Y. Makino, and H. Shinoda, “Remotely displaying cooling sensation via ultrasound-driven air flow,” in *IEEE Haptics Symposium 2018, Oral Session 7B (Technical Papers)*. IEEE, 2018, pp. 340–343.

[31] E. H. Weber, “The sense of touch,” *Academic Press*, pp. 139–264, 1978.

[32] D. Sinclair, “Cutaneous sensation,” *Oxford Univ Press*, 1967.

[33] A. Patapoutian, A. M. Peir, G. M. Story, and V. Viswanath, “Thermotrps and beyond: Mechanisms of temperature sensation,” *Nature Reviews Neuroscience*, vol. 4, pp. 529–539, 2003.

[34] I. Darian-Smith, “Thermal sensibility,” *I. Darian-Smith (Ed.), Handbook of physiology: The nervous system, Bethesda, MD: American Physiological Society*, pp. 879–913, 1984.

[35] A. C. Brown, “Somatic sensation: peripheral aspects,” *H. D. Patton (Ed.), Textbook of Physiology, Philadelphia: Saunders*, pp. 298–308, 1989.

[36] D. C. Spray, “Cutaneous temperature receptors,” *Annual Review of Physiology*, vol. 48, pp. 625–638, 1986.

[37] J. C. Stevens and K. C. Choo, “Temperature sensitivity of the body surface over the life span,” *Somatosensory Moter Research*, vol. 15, pp. 13–28, 1998.

[38] D. R. Kenshalo, “Correlations of temperature sensitivity in man and monkey, a first approximation,” *Y. Zotterman (Ed.), Sensory functions of the skin with special reference to man, Oxford: Pergamon Press*, pp. 305–330, 1976.

[39] J. D. Hardy and T. W. Oppel, “Studies in temperature sensation. . the sensitivity of the body to heat and the spatial summation of the end organ responses,” *Journal of Clinical Investigation*, vol. 16, pp. 533–540, 1937.

[40] L. E. Marks, J. C. Stevens, and S. J. Tepper, “Interactions of spatial and temporal summation in the warmth sense,” *Sensory Processes*, vol. 1, pp. 87–98, 1976.

[41] R. H. Taus, J. C. Stevens, and L. E. Marks, “Spatial localization of warmth,” *Perception Psychophysics*, vol. 17, pp. 194–196, 1975.

[42] J. C. Stevens and L. E. Marks, “Spatial summation of cold,” *Physiology Behavior*, vol. 22, pp. 541–547, 1979.

[43] J. C. Stevens, “Thermal sensibility,” *M. A. Heller W. Schiff (Eds.), The Psychology of Touch, Hillsdale, NJ: Lawrence Erlbaum*, pp. 61–90, 1991.

[44] A. J. H. Vendrik and E. G. Eijkman, "Psychophysical properties determined with internal noise," *D. R. Kensharo (Ed.), The Skin Senses, Springfield, IL: Charles Thomas*, pp. 178–193, 1968.

[45] W. S. Cain, "Spatial discrimination of cutaneous warmth," *American Journal of Psychology*, vol. 86, pp. 169–181, 1973.

[46] P. W. Nathan and R. C. Rice, "The localization of warmth," *Neurology*, vol. 16, pp. 533–540, 1966.

[47] M. L. Simmel and A. Shapiro, "The localization of non-tactile thermal sensation," *Psychophysiology*, vol. 5, pp. 415–425, 1969.

[48] D. R. Kenshalo and H. A. Scott, "Temporal course of thermal adaptation," *Science*, vol. 151, pp. 1095–1096, 1966.

[49] E. Abbott, "The effect of adaptation on the temperature difference limen," *Psychological Monographs*, vol. 16, pp. 1–36, 1914.

[50] J. C. Stevens, W. C. Okulicz, and L. E. Marks, "Temporal summation at the warmth threshold," *Perception Psychophysics*, vol. 14, pp. 307–312, 1973.

[51] H. Fruhstorfer, H. Guth, and U. Pfaff, "Thermal reaction time as a function of stimulation site," *Pflugers Arch*, vol. 335, 1972.

[52] C. J. Fowler, K. Sitzoglou, Z. Ali, and P. Halonen, "The conduction velocities of peripheral nerve fibres conveying sensations of warming and cooling," *Journal of Neurology, Neurosurgery, and Psychiatry*, vol. 51(9), pp. 1164–1170, 1988.

[53] S. Saga, "Calibration method of thermal-radiation-based haptic display," *In Proceedings of EuroHaptics2016*, 2016.

[54] S.Saga, "Thermal-radiation-based haptic display - calibration and shape display -," *In Proceedings of AsiaHaptics 2016*, 2016.

[55] S. Saga, "Thermal-radiation-based haptic display - laser-emission-based radiation system -," *Proceedings of AsiaHaptics 2018*, 2018.

[56] R. Osczevski and M. Bluestein, "The new wind chill equivalent temperature chart. bulletin of the american meteorological society," *Bulletin of the American Meteorological Society*, vol. 86, pp. 1453–1458, 2005.

[57] I. L. Khodorkov, N. V. Poshernev, and M. A. Zhidkov, "The vortex tube—a universal device for heating, cooling, cleaning, and drying gases and separating gas mixtures," *Chemical and Petroleum Engineering*, pp. 409–415, 2003.

[58] T. Kamigaki, S. Suzuki, and H. Shinoda, "Noncontact thermal and vibrotactile display usingfocused airborne ultrasound," *In Proceedings of EuroHaptics2020*, 9 2020.

[59] S. Kanaya, Y. Matsushima, and K. Yokosawa, "Does seeing ice really feel cold? visualthermal interaction under an illusory body-ownership," *PLoS ONE*, vol. 7(11), 2012.

[60] T. Carter, S. A. Seah, B. Long, B. Drinkwater, and S. Subramanian, "Ultrahaptics: Multi-point mid-air haptic feedback for touch surfaces," in *Proceedings of the 26th Annual ACM Symposium on User Interface Software and Technology*, ser. UIST '13. New York, NY, USA: ACM, 2013, pp. 505–514. [Online]. Available: http://doi.acm.org/10.1145/2501988.2502018

[61] L. Jackowski-Ashley, G. Memoli, M. Caleap, N. Slack, B. W. Drinkwater, and S. Subramanian, "Haptics and directional audio using acoustic metasurfaces," in *Proceedings of the 2017 ACM International Conference on Interactive Surfaces and Spaces*. ACM, 2017, pp. 429–433.

[62] S. Nomura, K. Murakami, and Y. Sasaki, "Streaming induced by ultrasonic vibration in a water vessel," *Jpn. J. Appl. Phys., Part 1 39(6A)*, pp. 3636–3640, 2000.

[63] J. A. Cosgrove, J. M. Buick, S. D. Pye, and C. A. Greated, "Piv applied to eckart streaming produced by a medical ultrasound transducer," *Ultrasonics*, vol. 39(6), pp. 461–464, 2001.

[64] A. L. Bernassau, P. G. Jones, F. Gesellchen, M. Riehle, M. Hill, and D. R. S. Cumming, "Controlling acoustic streaming in an ultrasonic heptagonal tweezers with application to cell manipulation," *Ultrasonics*, vol. 54(1), pp. 268–274, 2014.

[65] M. F. Hamilton and D. T. Blachstock, "Nonlinear acoustics," *Academic Press, San Diego*, 1998.

[66] L. K. Zarembo, "Acoustics streaming," *in High-Intensity Ultrasonic Fields, Part III*, pp. 137–199, edited by L. D. Rozenberg(Plenum,1971).

[67] H. Kimoto, *Gekkan Fijikusu*, vol. 6, no. 3, pp. 187–191, 1985[in Japanese].

[68] B. Moudjed, V. Botton, D. Henry, H. B. Hadid, and J. P. Garandet, "Scaling and dimensional analysis of acoustic streaming jets," *Phys. Fluids.*, vol. 26, p. 093602, 2014.

[69] B. Moudjed, V. Botton, D. Henry, S. Millet, J. P. Garandet, and H. B. Hadid, "Oscillating acoustic streaming jet," *Appl. Phys. Lett.*, vol. 105, p. 184102, 2014.

[70] S. J. Lighthill, "Acoustic streaming," *Appl. Phys. Lett.*, vol. 61, pp. 391–418, 1978.

[71] K. Hasegawa, L. Qiu, A. Noda, S. Inoue, and H. Shinoda, "Electronically steerable ultrasound-driven long narrow air stream," *Applied Physics Letters*, vol. 111, no. 6, p. 064104, 2017. [Online]. Available: https://doi.org/10.1063/1.4985159

[72] J. Durnin, J. J. Miceli, Jr., and J. H. Eberly, "Diffraction-free beams," *Phys. Rev. Lett.*, vol. 58, p. 1499, 1987.

[73] R. M. Herman and T. A. Wiggins, "Diffraction-free beams," *J. Opt. Soc. Am. A*, vol. 8, pp. 932–942, 1991.

[74] K. Hasegawa, L. Qiu, and H. Shinoda, "Interactive midair odor control via ultrasound-driven air flow," *In SIGGRAPH Asia 2017 Emerging Technologies, SA '17*, pp. 8:1–8:2, 2017.

[75] K.Hasegawa, L. Qiu, and H. Shinoda, "Midair ultrasound fragrance rendering," *IEEE Transactions on Visualization and Computer Graphics*, vol. 24, no. 4, pp. 1477–1485, 2018.

[76] M. Fujiwara, "Remote measurement of mechanical property distribution using acoustic radiation pressure," Ph.D. dissertation, The University of Tokyo, 2014.

[77] Y. Nishiyama, T. Hoshi, and I. Torigoe, "Study on airflow accompanying airborne ultrasound tactile display," *Proceedings of the 2010 JSME Conference on Robotics and Mechatronics*, no. 10-4, June 2010.

[78] T. Kamakura, "Nonlinear phenomena in ultrasound (in japanese)," *Kyoto University Research Information Repository*, no. 993, pp. 1–10, 1997.

[79] Spraying Systems Co., https://www.spray.co.jp/automated_systems/jp_mist_cooling_systems.aspx.

[80] hi.takagi.co.jp, https://hi.takagi.co.jp/products/list.php?category_id=72.

[81] Saisyu Techno, https://www.saisyu.jp/info/?post_type=product&p=677.

[82] ETG (Eco Technology Group), https://www.etg-japan.com/products/fans/misting-fan/.

[83] HIRO CORPORATION, http://www.hiro-corpo.net/users/detail.asp?pn=000000037114.

[84] The Chemical Society of Japan, "Handbook of chemistry: Pure chemistry, 5th ed." *Maruzen Publishing*, 2 2004.

[85] Y. Yano, "Nanodroplets generated by ultrasound atomization," *Earozoru Kenkyu*, vol. 26, no. 1, pp. 18–23, 1 2011.

[86] S. C. Jiang, H. J. Ma, H. J. Li, and X. X. Zhang, "Effects of thermal properties and geometrical dimensions on skin burn injuries," *Burns*, vol. 28, pp. 713–717, May 2002.

[87] S. Alrutz, "On the temperature-senses:ii," *Mind*, vol. 7, no. 25, pp. 141–144, 1898.

[88] A.D.Craig and M.C.Bushnell, "The thermal grill illusion:unmasking the burn of cold pain," *Science*, vol. 265, pp. 252–255, 1994.

[89] F. Lindstedt, B. Johansson, S. Martinsen, E. Kosek, P. Fransson, and M. Ingvar, "Evidence for thalamic involvement in the thermal grill illusion: an fmri study," *PloS one*, vol. 6, pp. 252–255, 11 2011.

[90] P. Bach, S. Becker, D. Kleinbohl, and R. Holzl, "The thermal grill illusion and what is painful about it," *Neuroscience Letters*, vol. 505, no. 1, pp. 31–35, 2011.

[91] B.G.Green, "Synthetic heat at mild temperatures," *Somatosensory Motor Research*, no. 19(2), pp. 130–138, 2002.

[92] R. Watanabe, R. Okazaki, and H. Kajimoto, "Mutual referral of thermal sensation between two thermal-tactile stimuli," in *IEEE Haptics Symposium 2014*. IEEE, 2014.

[93] A. Moritz and F. Henriques, “Studies of thermal injury: Ii. the relative importance of time and surface temperature in the causation of cutaneous burns,” *Am J Pathol*, vol. 17, pp. 695–720, 1947.

[94] A. Moritz, “Studies of thermal injury: Iii. the pathology and pathogenesis of cutaneous burns. an experimental study.” *The American Journal of Pathology*, vol. 23, no. 6, pp. 915–941, Nov 1947.

List of Publications

International Referred Conference

1. Mitsuru Nakajima, Yasutoshi Makino and Hiroyuki Shinoda, “Remote Cooling Sensation Presentation Controlling Mist in Midair,”in Proc. 2020 IEEE/SICE International Symposium on System Integration, pp. 1238-1241, Jan. 12-15, 2020, Hawaii Convention Center, Honolulu, Hawaii, USA.
2. Mitsuru Nakajima, Yasutoshi Makino and Hiroyuki Shinoda, “Displaying Pain Sensation in Midair by Thermal Grill Illusion,”IEEE International Symposium on Haptic Audio-Visual Environments and Games (HAVE2019), Sunway, Malaysia, October 3-4, 2019.
3. Mitsuru Nakajima, Yasutoshi Makino and Hiroyuki Shinoda: Noncontact Pain Display by Temperature Control, Proc. 2019 IEEE World Haptics Conference (WHC), WP1P.10 (Work-in-Progress Papers), 9-12 July, Ochanomizu, Tokyo, Japan, 2019.
4. Mitsuru Nakajima, Keisuke Hasegawa, Yasutoshi Makino and Hiroyuki Shinoda: Remotely Displaying Cooling Sensation Using Ultrasound Mist Beam, Asia Haptics 2018, Live Demo Presentation, Incheon, Korea, Nov. 14- 16, 2018.
5. Shun Suzuki, Ryoko Takahashi, Mitsuru Nakajima, Keisuke Hasegawa, Yasutoshi Makino and Hiroyuki Shinoda, “Midair Haptic Display to Human Upper Body,”in Proc. SICE Annual Conference 2018, pp. 848-853, Sep. 11-14, 2018, Nara, Japan.
6. Mitsuru Nakajima, Keisuke Hasegawa, Yasutoshi Makino, and Hiroyuki Shinoda: Remotely Displaying Cooling Sensation via Ultrasound-Driven Air Flow, IEEE Haptics Symposium 2018, pp.340-343, Oral Session 7B (Technical Papers), 25-28 March, San Francisco, California, USA, 2018.

Domestic Conference

1. 中島允, 小丹枝涼哉, 牧野泰才, 篠田裕之, “集束超音波を用いた冷覚フィードバックを有するインタラクティブなフォグディスプレイ,”第 21 回計測自動制御学会システムインテグレーション部門講演会論文集, pp. 647-650, 福岡 (オンライン発表へ変更), Dec. 16-18, 2020.

2. 鈴木智也，神垣貴晶，中島允，二宮悠基，藤原正浩，牧野泰才，篠田裕之，”空中超音波を用いた水滴の触感の提示，”第 21 回計測自動制御学会システムインテグレーション部門講演会論文集，pp. 638-640，福岡 (オンライン開催), Dec. 16-18, 2020.
3. 中島允, 牧野泰才, 篠田裕之, “集束超音波による冷覚フィードバックを有するフォグディスプレイの基礎検討,”第 25 回バーチャルリアリティ学会大会, 2D2-1, オンライン開催, Sep. 16-18, 2020.
4. 小丹枝涼哉, 中島允, 神垣貴晶, 水谷沙耶, 藤原正浩, 牧野泰才, 篠田裕之“非接触な冷覚刺激による注意喚起システム”第 25 回バーチャルリアリティ学会大会, 2D2-1, オンライン開催, Sep. 16-18, 2020.
5. 日浦宏哉，鈴木颯，中島允，藤原正浩，牧野泰才，篠田裕之“液面境界刺激による水中感覚の再現”第 25 回バーチャルリアリティ学会大会, 2C3-4, オンライン開催, Sep.16-18, 2020.
6. 中島允, 長谷川圭介, 牧野泰才, 篠田裕之, “収束焦点を用いた遠隔冷覚提示,”ロボティクス・メカトロニクス講演会 2020 論文集, No20-2, 2P1-M03(1)-(3)(オンライン発表に変更), 石川県産業展示館３号館, 金沢, May 27-30, 2020.
7. 中島允, 長谷川圭介, 牧野泰才, 篠田裕之, “超音波ミストビームと収束焦点を用いた冷覚と振動覚の遠隔同時提示,”第 20 回計測自動制御学会システムインテグレーション部門講演会（SI2019）論文集, pp. 70-72, サンポート高松, 香川, Dec. 12-14, 2019.
8. 中島允, 牧野泰才, 篠田裕之, “空中ミストの制御による遠隔冷覚提示,”第 24 回バーチャルリアリティ学会大会, 5A-04, 東京大学本郷キャンパス, 東京, Sep. 11-13, 2019.
9. 中島允, 長谷川圭介, 牧野泰才, 篠田裕之, “サーマルグリル錯覚を用いた遠隔痛覚提示”, 第 63 回システム制御情報学会研究発表講演会（SCI 19）論文集, pp. 111-115, 中央電気倶楽部, 大阪, May. 22-24, 2019.
10. 中島允, 長谷川圭介, 牧野泰才, 篠田裕之, “超音波ミストビームによる遠隔冷覚提示,”第 19 回計測自動制御学会システムインテグレーション部門講演会（SI2018）論文集, pp. 530-533, 大阪工業大学梅田キャンパス, 大阪, Dec. 13-15, 2018.
11. 中島允, 長谷川圭介, 牧野泰才, 篠田裕之, “超音波走査による匂いディスプレイ,” 第 23 回バーチャルリアリティ学会大会, 34B-2, 東北大学青葉山新キャンパス, 仙台, Sep. 19-21, 2018.
12. 中島允, 長谷川圭介, 牧野泰才, 篠田裕之, “超音波フェーズドアレイによる匂いのセンシング,”第 35 回センシングフォーラム資料, pp. 73-76, Aug., 2018, 山口大学・常盤キャンパス, 山口.
13. 中島允, 長谷川圭介, 牧野泰才, 篠田裕之, “音響ビームによる任意方向への冷気の誘導に基づく遠隔冷覚提示,”第 18 回計測自動制御学会システムインテグレーション部門講演会論文集, pp. 1996-1997, 仙台, Dec. 20-22, 2017.

14. 中島允, 長谷川圭介, 牧野泰才, 篠田裕之, “音響流ベッセルビームを用いた遠隔冷覚提示,”第 22 回バーチャルリアリティ学会大会, 1D3-03, 徳島大学常三島キャンパス, 徳島, Sep 27-29, 2017.

Awards

1. 2019 年度計測自動制御学会学会賞学術奨励賞・研究奨励賞 (第 19 回計測自動制御学会システムインテグレーション部門講演会で発表) [2020.2.28]

A

Appendix A: Remote Simultaneous Displaying Cooling and Vibrotactile Sensation

This research also aims to realize a system in which cold and vibrotactile sensation can coexist. This appendix describes an approach of a midair haptic display that provides cooling and vibrotactile sensation simultaneous. For that purpose, the system used ultrasound-driven cold air flow and focal point cooled by mist vaporization. Figure A.1 shows the schematic image of system. This system is based on chapter 3. As an approach to display cooling and vibrotactile sensation at the same time, ultrasound beam and focused ultrasound are alternately irradiated at short time intervals. The ultrasound beam is used to transport mist in the air and display cooling sensation. On the other hand, the focused ultrasound is used to display vibrotactile sensation.

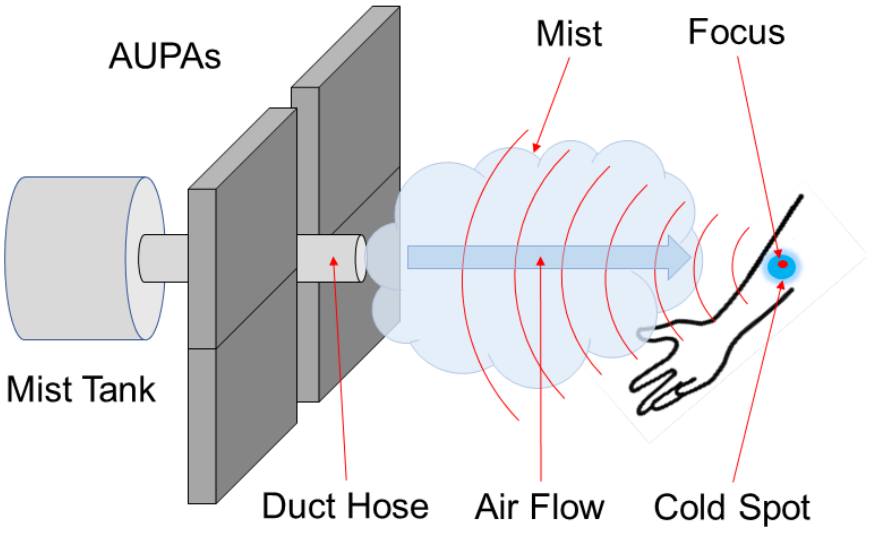

Fig. A.1. System overview in this appendix.

We conducted a comparative experiment on the cooling effect among the following three cases: irradiation of ultrasound beam, focused ultrasoud, and these alternately for $0.5\ s$ each.

A.1 Experimental Setup

The prototype used in the experiment is the same as that used in chapter 6 and 7(Fig. A.2). AUPAs can irradiate ultrasound with time intervals by adjusting the duty ratio. Therefore, it is possible to irradiate alternately by applying the irradiation time of ultrasound beam and focused ultrasound. In this experiment, it is irradiated alternately at $0.5\ s$ intervals by setting the duty ratio to 0.5.

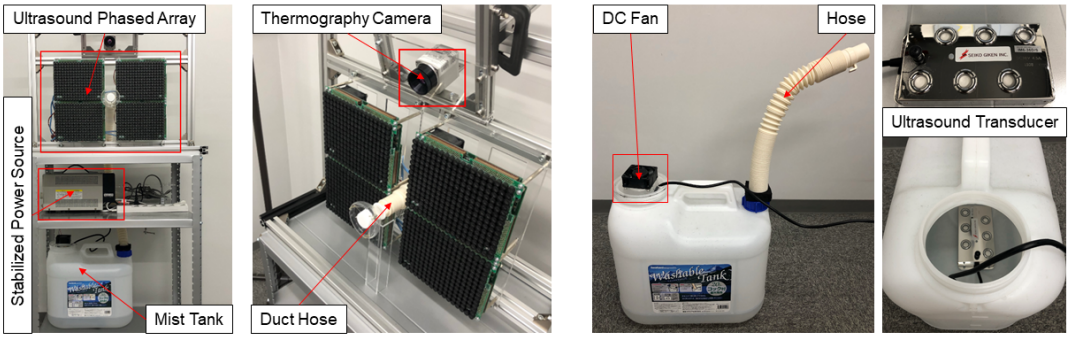

Fig. A.2. Prototype display. Reprinted from figures 6.2 and 6.3.

.

A.2 Measuring procedures

For each of three cases, as shown in Fig. A.3, we placed our hand $50\ cm$ away from the AUPAs surface. We adjusted the position so that ultrasound beam or focused ultrasound irradiates the center of the palm.

We evaluated the cooling effect in three cases by the temperature change on the skin surface after irradiation. In each case, we measured the temperature change for $20\ s$ from the start of irradiation with a thermographic camera (OPTOI450O 29T900, Optris) in a video format.

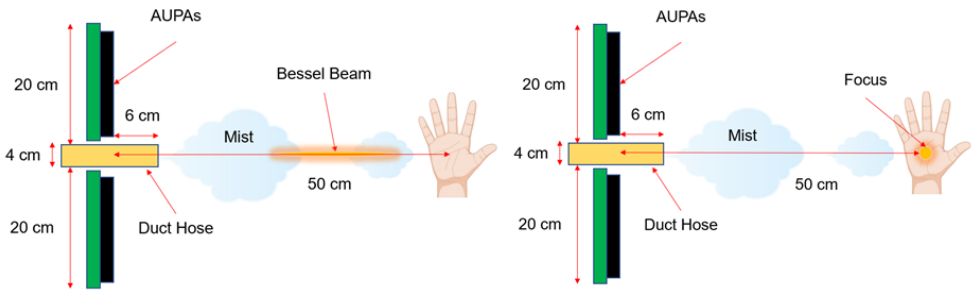

Fig. A.3. Schematic image of experimental setup and view from above. (Left)Using the ultrasound beam. (Right)Using the focused ultrasound.

A.3 Result

Figure A.4, A.5, and A.6 show the long-term temperature change while cold spot is generating. A sharp drop in temperature was observed when the system used the focused ultrasound. In Figure A.5, it can be seen that a cold spot has generated 1 s after the start of irradiation when using the focused ultrasound. Furthermore, in figure A.6, it can be seen that a cold spot has generated in 500 to $750\,\mathrm{ms}$.

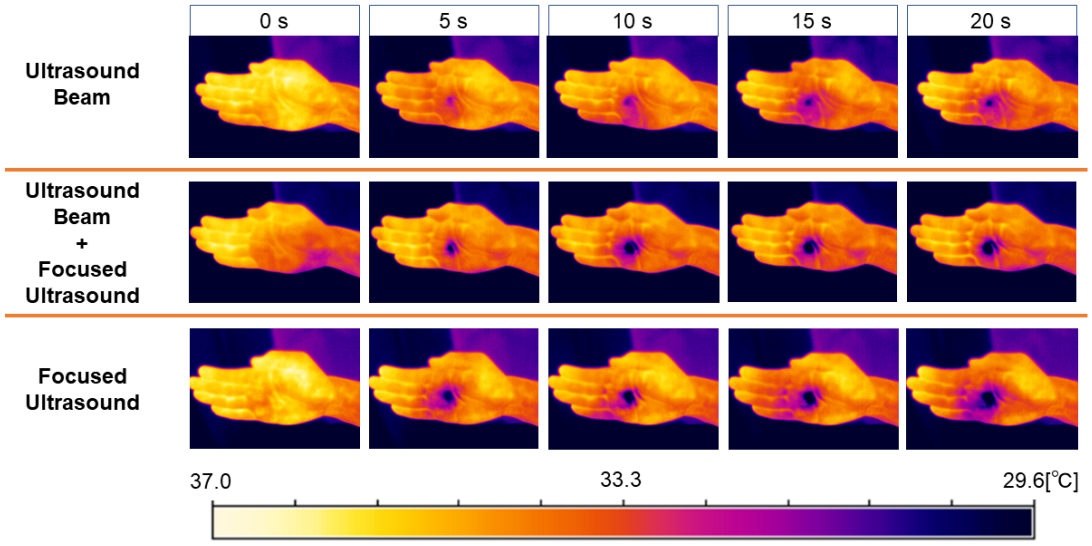

Fig. A.4. Temperature change of the skin surface cooled by mist with (Upper)the ultrasound beam, (Lower)the focused ultrasound, and (Middle)both of them. They are shown images when irradiated for 20 s from the start of irradiation.

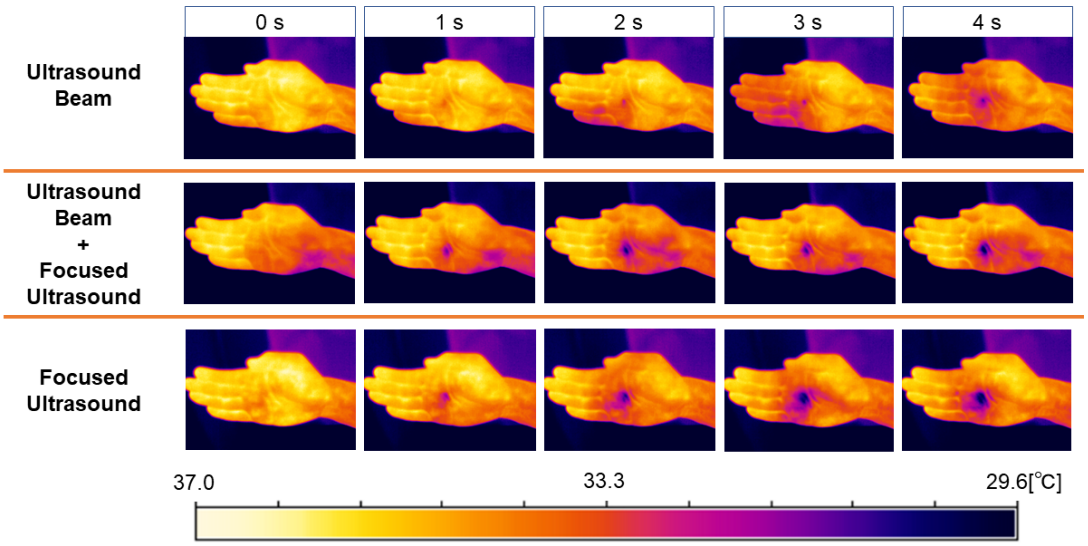

Fig. A.5. Temperature change of the skin surface cooled by mist with (Upper)the ultrasound beam, (Lower)the focused ultrasound, and (Middle)both of them. They are shown images when irradiated for $4\ s$ from the start of irradiation.

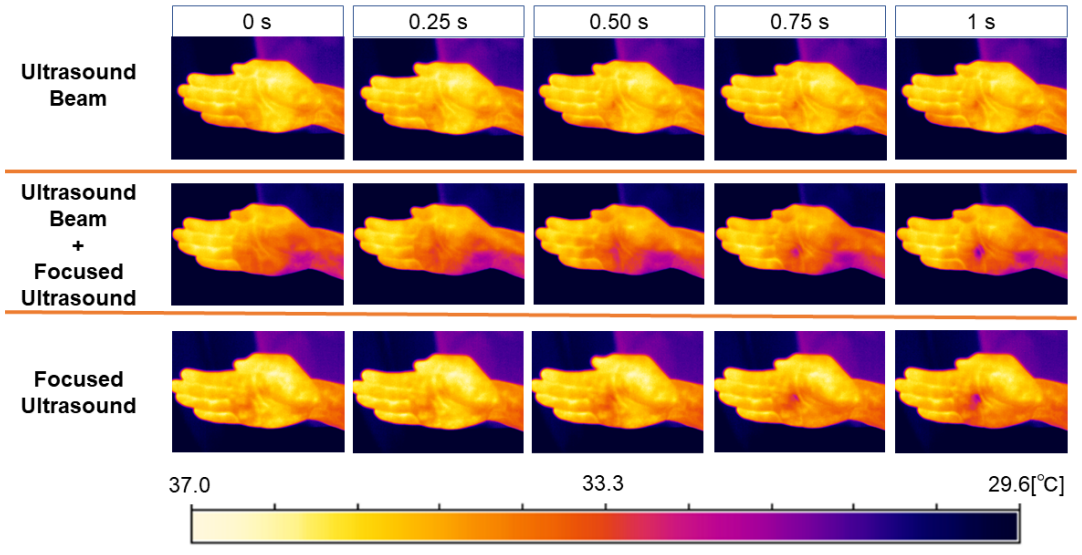

Fig. A.6. Temperature change of the skin surface cooled by mist with (Upper)the ultrasound beam, (Lower)the focused ultrasound, and (Middle)both of them. They are shown images when irradiated for $1\ s$ from the start of irradiation.

When ultrasound beam and focused ultrasound are used under the same conditions, the latter clearly causes a rapid temperature drop and cold spot. It is possible that focused ultrasound is promoting the vaporization of mist, as in chapter 7.

Figure A.7 shows the minimum value of temperature against time in the target area shown in figure 6.7. It was found that the temperature dropped by 2.9 to 3.1 °C in $2\,\mathrm{s}$ after the focused ultrasound was applied. In the long term, the temperature continues to drop with ultrasound beam and focused ultrasound. Immediately after the start of irradiation, there was no significant difference in temperature drop when using focused ultrasound only and two types of ultrasound.

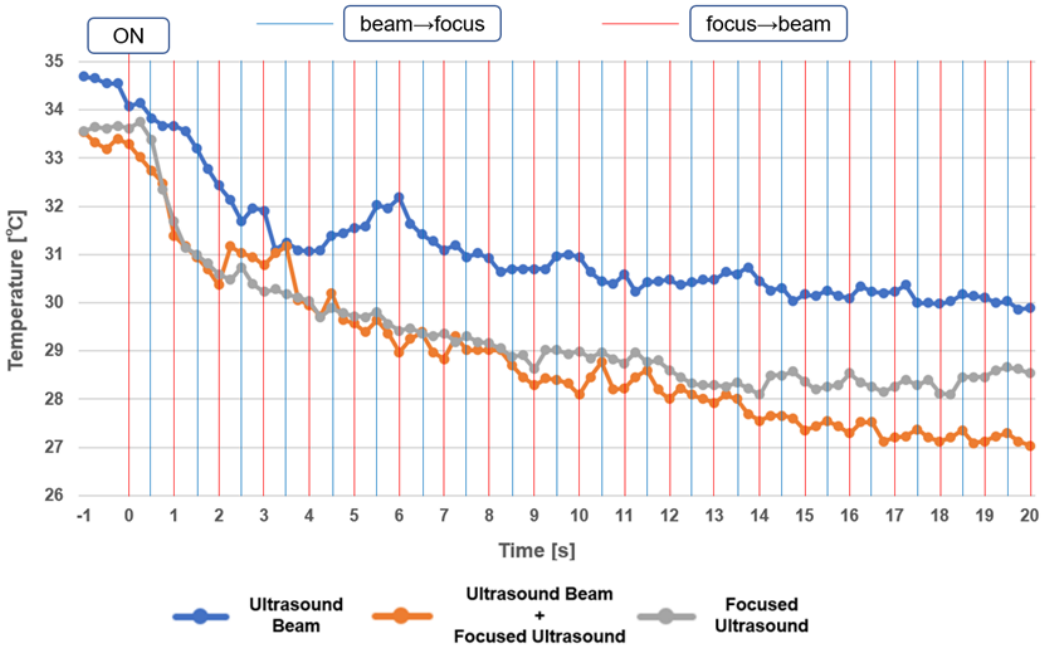

Fig. A.7. Temperature change in the palm using ultrasound beam only, focused ultrasound only, and by irradiating them alternately.

A.4 Conclusion

In this appendix, we proposed a method of a midair haptic display that provides cooling and vibrotactile sensation simultaneous. For that purpose, we approached a method of alternating irradiation by controlling the duty ratio of the irradiation time of ultrasound beam and focused ultrasound. In the experiment, we conducted comparative experiment on temperature change when using ultrasound beam only, focused ultrasound only, and by irradiating them alternately. As a result, the cooling effect was high when focused ultrasound was used. Since the cooling effect was high even when only focused ultrasound was used, it is expected that cooling and vibrotactile sensations coexist by adjusting the modulation of ultrasound. Subjectively, we felt cooling and vibrotactile sensations at the same time when focused

ultrasound was applied.

In the future, we will examine the evaluation of sensation when cold and vibrotactile sensation are displayed at the same time through the psychophysical aspects.

B

Appendix B: Noncontact Pain Display by Thermal Grill illusion

This appendix describes a method to display a pain sensation in noncontact manner. For that purpose, we use the phenomenon of the thermal grill illusion. This phenomenon produces a pain sensation without damage of the skin by simultaneously displaying the cooling and heating sensation. For displaying cooling sensation, we apply the system in chapter 5. On the other hand, for displaying heating sensation, we use the light beam irradiation of halogen lamp. Figure B.1 shows the schematic image of system. First, using these system, we examine temperature change of the skin surface. Second, we observed the temperature change up to the generation of pain sensation.

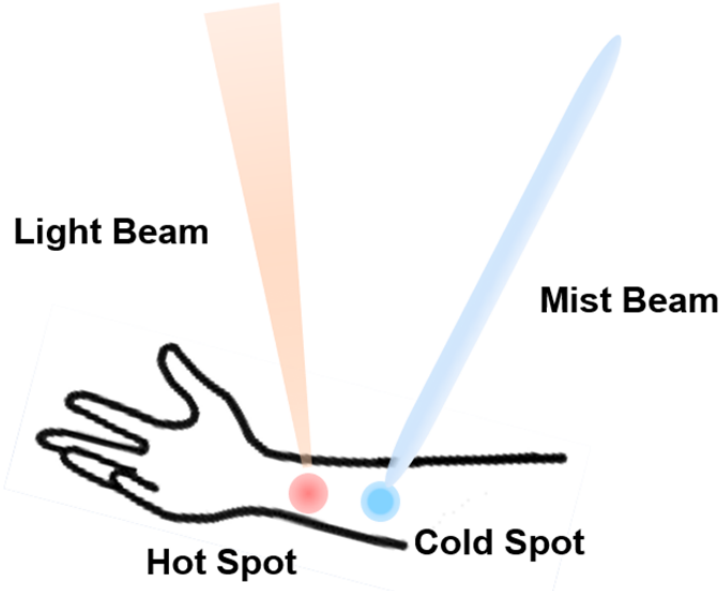

Fig. B.1. System overview in this appendix. Displaying a pain sensation using thermal grill illusion.

B.1 Thermal Grill Illusion(TGI)

Thermal grill illusion(TGI) is an illusion phenomenon that produces a unique sensation accompanied by pain and burning sensation when hot and cold stimuli are simultaneously presented to the skin surface as shown in figure B.2[87][88][89].

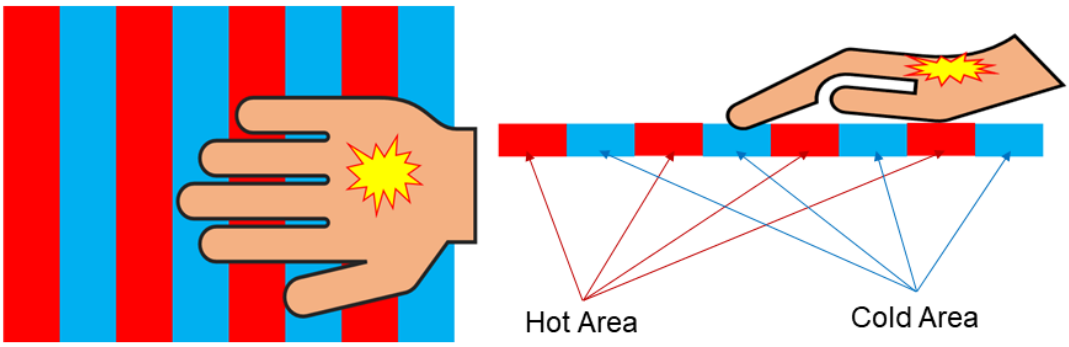

Fig. B.2. Image diagram of thermal grill illusion(TGI).

TGI can cause a pain sensation without damaging the user's skin surface[90][91]. Since it can occur safely without damaging the skin surface, it is suitable for psychological experiments on pain. There are some pain displays based on TGI in contact manner using Peltier elements[92].

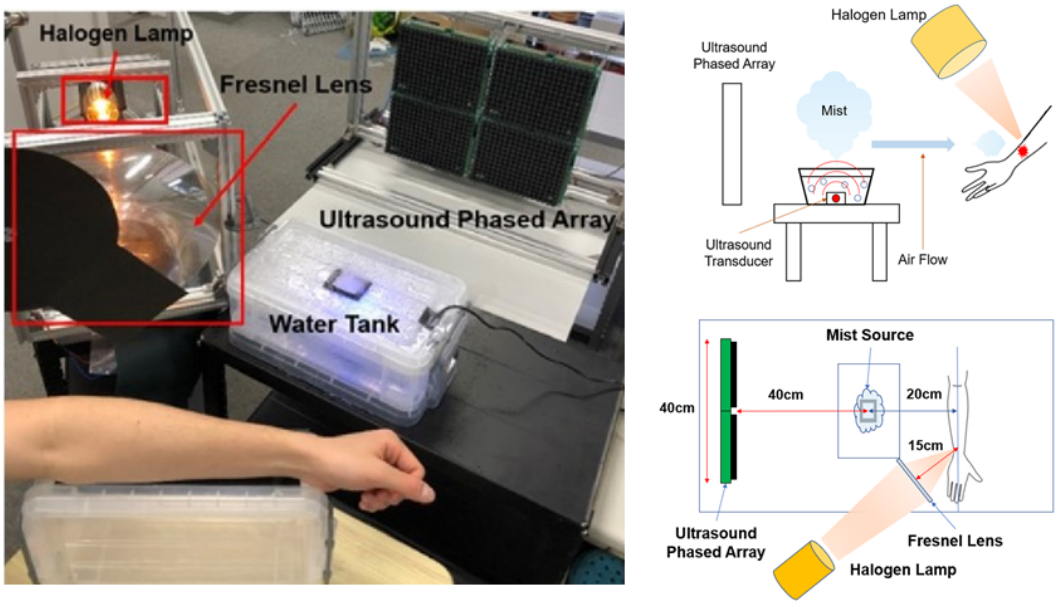

Fig. B.3. Experimental setup.

B.2 Experimental Setup

The overall system is shown in figure B.3. This system is composed of the airborne ultrasound phased arrays (AUPA) driven at $40\,\mathrm{kHz}$, ultrasound transducer for generating mist (IM1-24/LW SEIKO GIKEN INC), water tank, and halogen lamp. For remote cooling sensation, we use the method in chapter 5. For remote heating sensation, we use a halogen lamp (HSH 60, Fintech Tokyo). The focal length is $105\,\mathrm{mm}$ and the maximum power consumption is $105\,\mathrm{W}$. By properly controlling the applied voltage, it is set to prevent skin damage from burns. The power consumption used in the experiment is $28\,\mathrm{W}$. A Fresnel lens (NTKJ CO.LTD.) is used to adjust the condensing of the halogen lamp. The focal length of lens is $150\,\mathrm{mm}$, which makes a light spot of $3.5\,\mathrm{cm}$ in diameter. As shown in figure B.4, there is shutter near the front of the lens. In this experiment, we control the irradiation time by rotating shutter to block the light beam. The shutter is connected to servo motor synchronized with the AUPAs for displaying cooling sensation. This system has a timing controller that can be operated with a single computer, and provides both heating and cooling sensation.

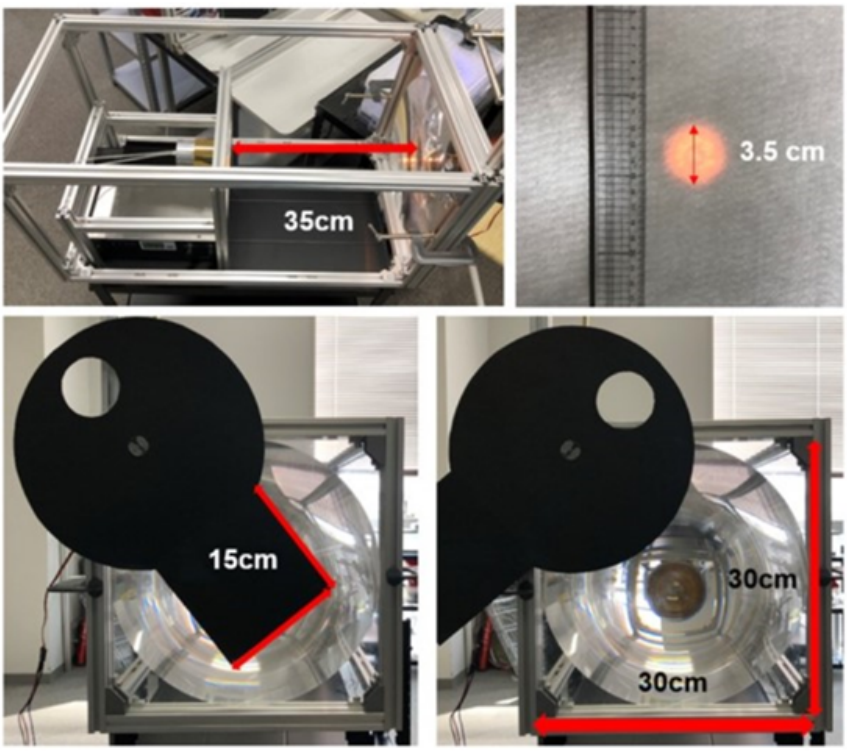

Fig. B.4. Setup of remote displaying heating sensation.

B.3 Experiment 1

In this section, we examine temperature change of the skin. As shown in figure B.3, the experimenter put the arm on the table. We adjusted the ultrasound and light beams to irradiate the forearm. While both beams were irradiating the targets, we captured the entire arm with a thermographic camera (OPTOI450O 29T900) in a video format for measuring temperature changes on the skin surface.

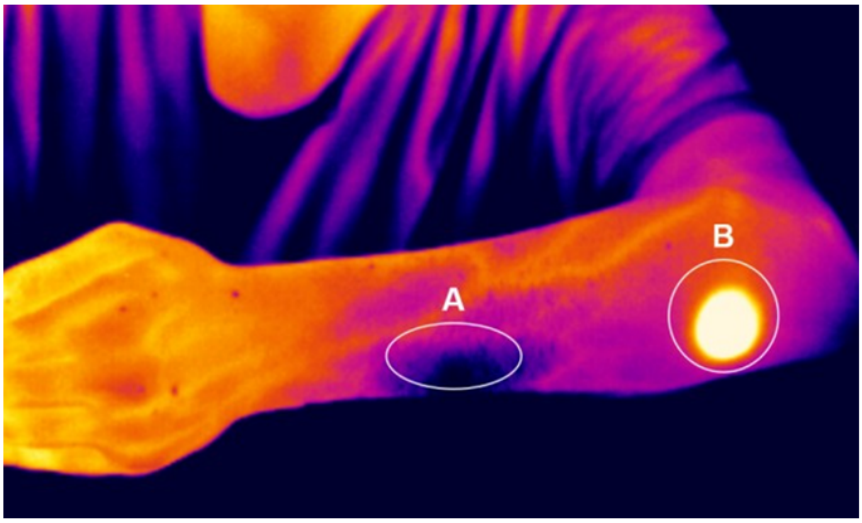

Fig. B.5. Target parts on user's arm shown in the thermographic image.

B.3.1 Measuring procedures 1

As shown in figure B.5, there are two areas where the forearm is heated and cooled. At Area A, the mist hits by ultrasound-driven airflow. Area B corresponds to the position where the light irradiation of the halogen lamp converged on the lens as shown in figure B.4. The measurement dimension is as described in figure B.3 and B.4. The distance between the centers of Area A and Area B is approximately $10\,\mathrm{cm}$.

We measured the temperature change for $30\,\mathrm{s}$. Simultaneously with the start of measurement, light beam irradiation and ultrasound beam irradiation are activated. Here, in order to ensure safety, it is necessary to keep the temperature so as not to damage the skin surface. It has been found that thermal burns occur in a hot period of 6 hours at a skin surface temperature of $44\,^{\circ}\mathrm{C}$ and a shorter burning time when the temperature is $45\,^{\circ}\mathrm{C}$ or more[93][94]. In this experiment, the system operates for $15\,\mathrm{s}$ so as not to exceed $43\,^{\circ}\mathrm{C}$.

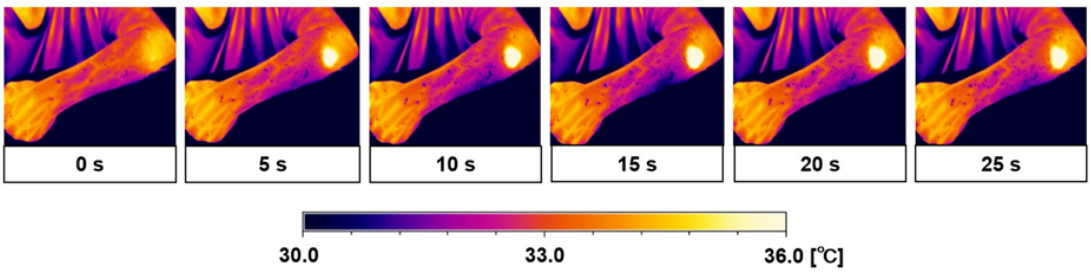

Fig. B.6. Temporal change of the skin irradiated by the mist and light beam.

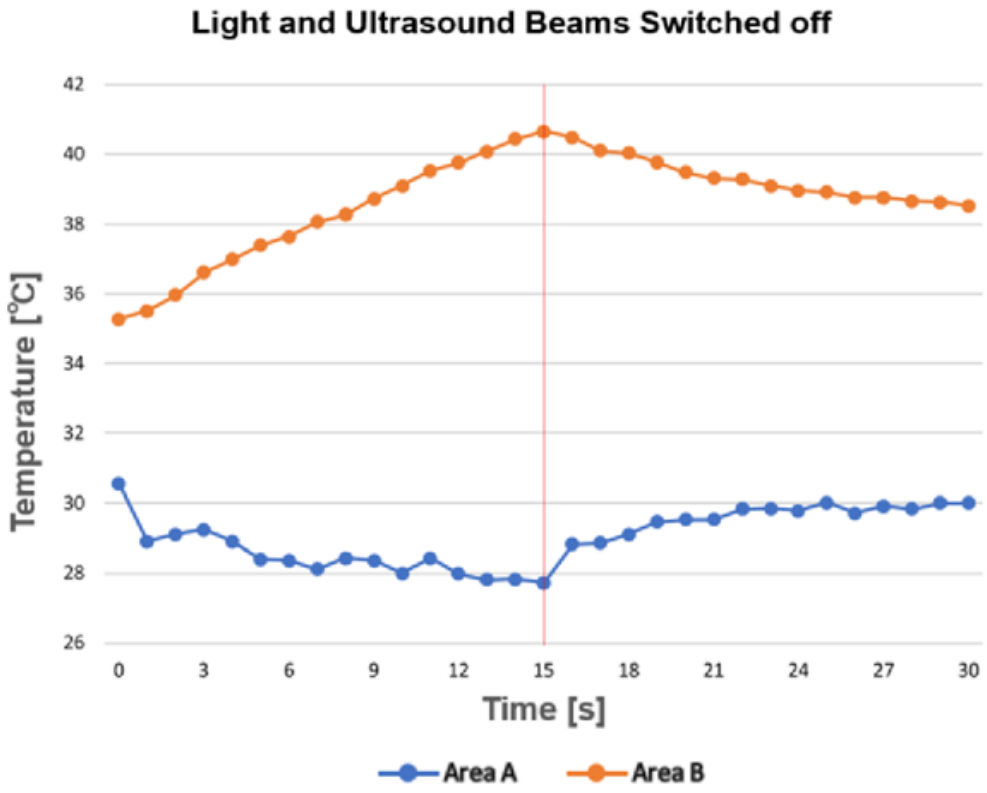

Fig. B.7. Temperature change by the hot and cold stimuli.

B.3.2 Result 1

Figure B.6 shows the long-term temperature change in Area A and B. Figure B.7 shows the minimum value of the temperature in Area A and the maximum value of the temperature in Area B. It is shown that the temperature difference between Area A and Area B gradually increases when light and ultrasound beam are irradiated.

On the other hand, when the irradiation of both beams is stopped, the temperature difference decreases with the time constant of 18.0. Since it does not exceeds $43\ ^{\circ}$C during operation, it ensures the safety in the experiment of next section.

B.4 Experiment 2

Using the system similar to section B.3, we observed the temperature change until the pain sensation was generated by the TGI. 7 participants(male 6 name, female 1 name, average age 25 year old) participated in the experiment. Participants had no skin disease. For the experimental environment, the room temperature and humidity were $23\ ^{\circ}$C and $60\ \%$, respectively.

Before the experiment, we told participants to experience a preliminary experiment. Participants were verbally asked whether they felt a clearly different pain from the feeling of heat by the light beam. Based on the answers, participants who clearly felt pain and those who did not were distinguished preliminary.

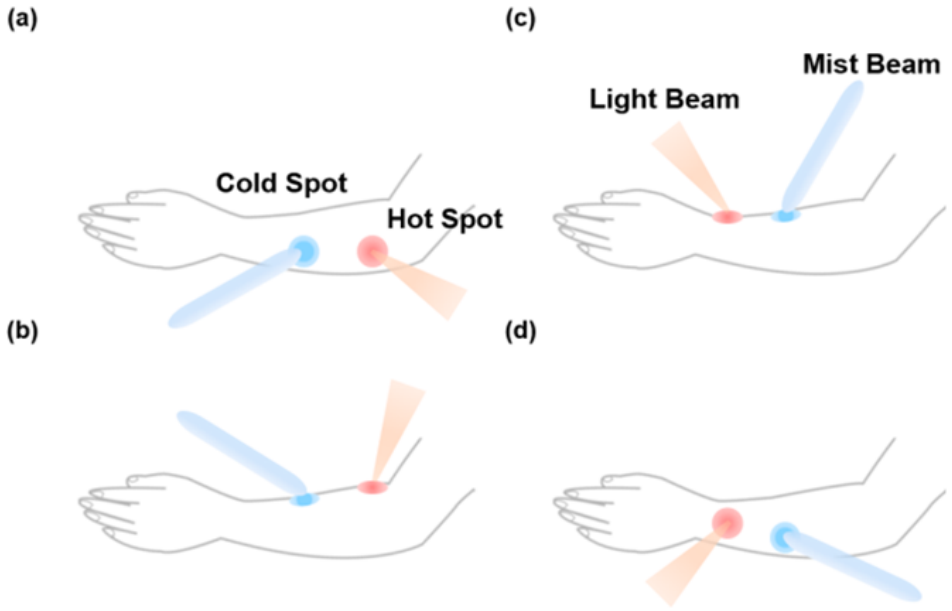

Fig. B.8. Irradiation positions of the light and mist beams.

B.4.1 Measuring procedures 2

The participant puts his arm on the table. We adjusted the position so that the light and mist beam hit his forearm. The light and mist beam are irradiated at the same time as the measurement starts. If the participant feels pain, he moves his finger

to send a signal. As shown in figure B.8, we measure the time for pain generation and the temperature of that moment for the total of 4 cases which is distinguished inside or outside of the forearm, in the positions of the hot/cold spots.

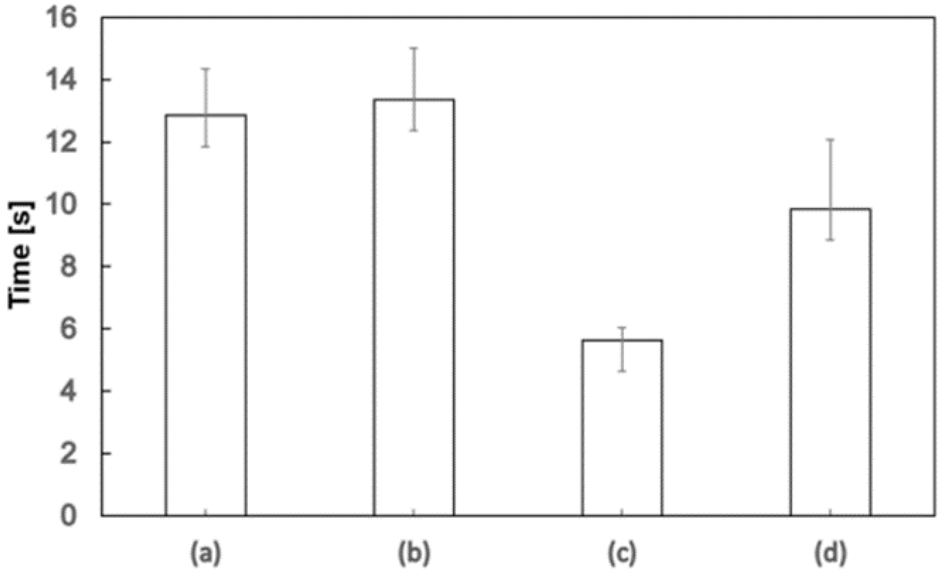

Fig. B.9. Average time required for pain generation.

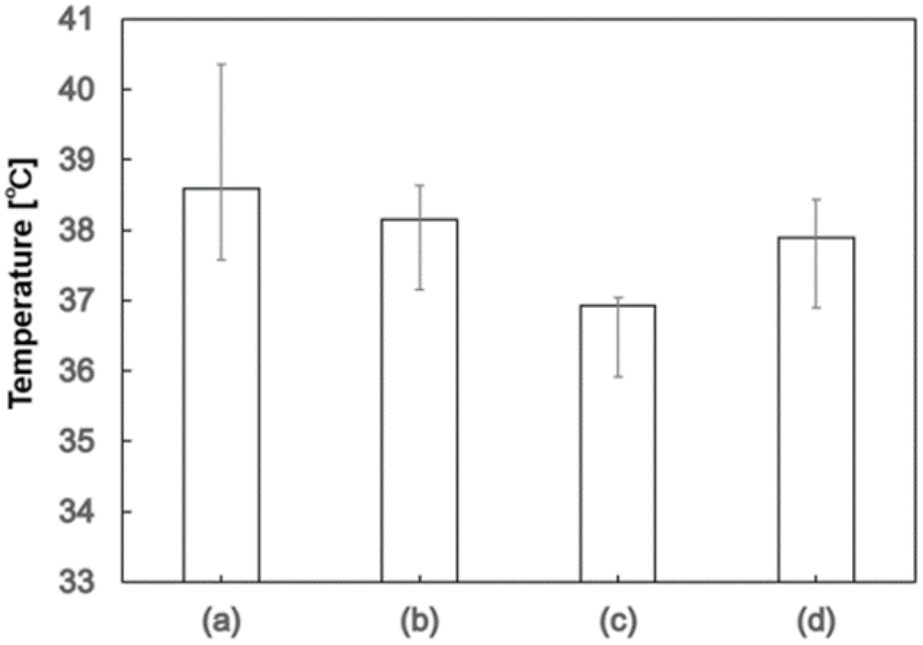

Fig. B.10. Average hot-spot temperature (the maximum value in the hot spot) for pain generation.

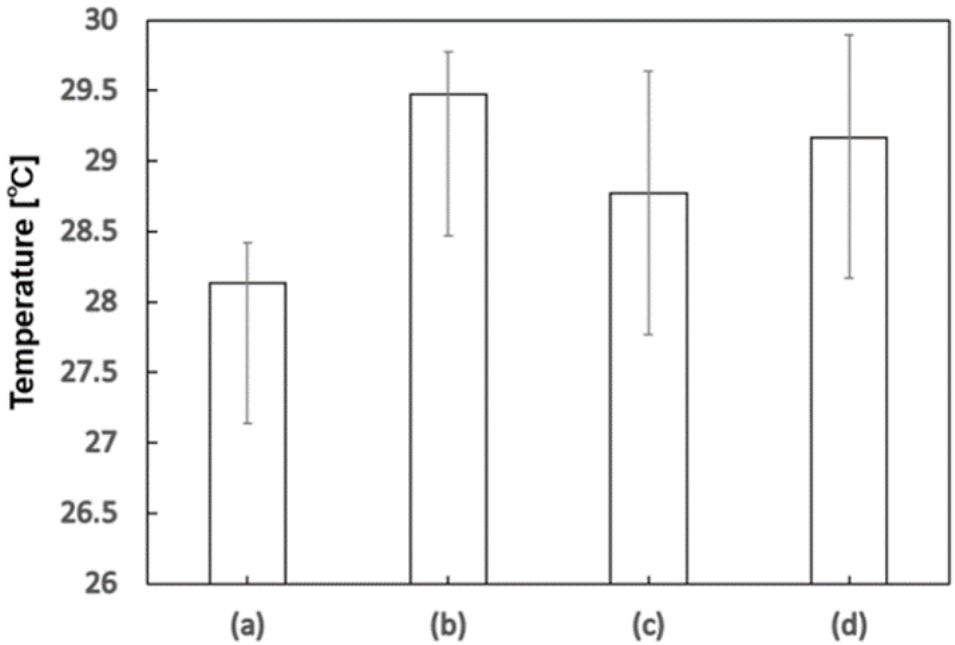

Fig. B.11. Average cold-spot temperature (the minimum value in the cold spot) for pain generation.

B.4.2 Result 2

Figure B.9 shows the average time until pain occurs. Figure B.10 and B.11 shows the average value of the hot-spot and cold-spot temperatures when pain occurs. The hot-spot temperature indicates the maximum value in the hot spot. The cold-spot temperature indicates the minimum value in the cold spot.

There was difference in the response time among the 4 cases:(a), (b), (c), and (d). It is suggested that not only the position of the forearm but also the positions of hot/cold spots affects the pain sensation. It can be seen that it is effective when there is a hot-spot on the wrist side of the forearm. Furthermore, from case (c), it has been clear that the irradiation on the inside of the forearm is higher than that on the outside. As a result, it is shown that the pain occurred earlier when the hot-spot was on the wrist side of the forearm. The case (c) is the most sensitive case of pain sensation.

In the experiment, 4 out of 7 participants could not clearly distinguish between the pain and heating sensation, while 3 participants (one is an author) could clearly distinguish. The most sensitive participant experienced clear pain at high and low temperature of $36.6\,^{\circ}$C and $27.8\,^{\circ}$C, respectively. Another participant felt pain clearly, but it was out of the standard temperature range provided by the system. The tem-

peratures required for the participants were $42.3\,^{\circ}$C and $28.9\,^{\circ}$C. The experiment has revealed a wide range of pain sensitivities. In the experimental system, the temperature change of the hot-spot was lowered to $0.4\,^{\circ}$C/s for safety and the precision of the temperature measurement.

B.5 Conclusion

In this appendix, we proposed a method to display pain sensation by controlling the temperature on the skin surface in a noncontact manner. For that purpose, based on the TGI, we used the light and ultrasound beam. We constructed a system that irradiates the skin surface with a light beam for heating and an ultrasound beam for cooling based on chapter 5. We measured the temperature change of the skin surface. It was confirmed that hot spot of $40.7\,^{\circ}$C and cold spot of $27.7\,^{\circ}$C were produced simultaneously in the local areas on the skin. We used this system to experiment with pain sensation. The result shows that the noncontact system caused a pain sensation when the hot and cold spot temperatures in average reached $36.9\,^{\circ}$C and $27.2\,^{\circ}$C respectively. At the same time, 4 of 7 participants did not feel pain, while the rest of participants felt a pain sensation clearly.

In the future, we will construct a system that displays pain sensation to any position on the user's body. Also, we will investigate the individual differences and conditions for effective displaying pain sensation.

C

Appendix C: Sensing and Displaying Odor

In this appendix, we propose a method to actively generate odors by irradiating ultrasound beams and transporting them to a desired position. By using this method, it is possible to remotely sense the position of the odor source. At the same time, it enables to display the odors to the user at any time in a desired position. Figure C.1 shows the concept of the proposed method.

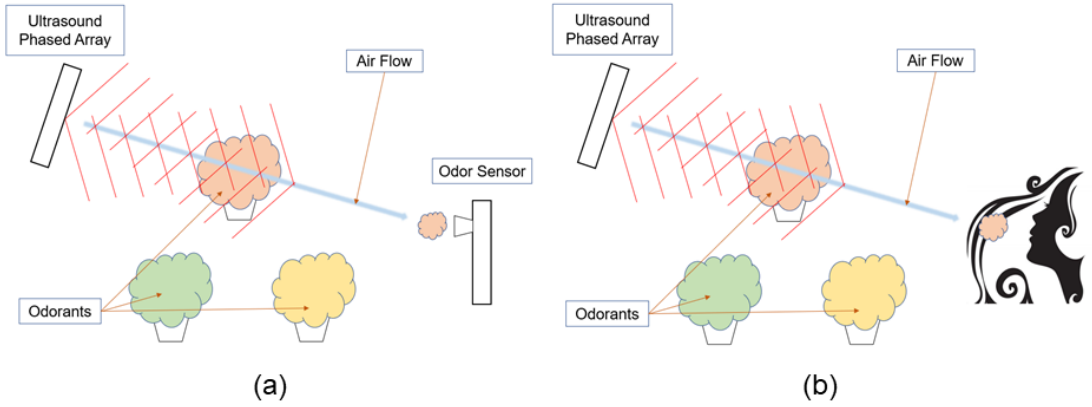

Fig. C.1. The concept of system in this appendix. (a)Sensing the odor. (b)Displaying the odor.

C.1 Background

・Sensing Odors

Since the odorant is diffusely transported, it is generally difficult to sense the position of the odor source. It may be possible to detect the odor source by spatially scanning the odor sensor. However, remote measurement is difficult when the distance between the odor source and the sensor is long. If multiple odors are mixed, it is difficult to distinguish which source each odor is produced from.

We propose a measurement system that transmits only the odor generated from a specific location to the sensor by transporting the odor substance using ultrasound-driven airflow based on chapter 5. This makes it possible to identify the location of the odor source and selectively distinguish the odor source in an environment with multiple sources.

・Displaying Odors

With the development of VR technology, information displaying technology targeting not only audiovisual stimulation but also tactile stimulation has been actively researched in recent years, and a high-quality information environment has been constructed. Research on smell and taste is also developing, although it is rare compared to audiovisual and tactile sensations. There is seamlessness between the real space and the VR space, and it is important to understand not only audiovisual and tactile sensations but also taste and smell sensations.

Comparing taste and smell, taste basically conveys information about objects in the oral cavity and conditions inside the body. Also, the sense of smell conveys environmental information in the same way as the audiovisual and tactile sensations. For example, in addition to touching an object, it can be identified from a distance without touching it by smelling the odor peculiar to the target object. At the fire scene, even if you are blind or deaf, you can smell the outbreak of a fire.

C.2 Our Approach

It has been confirmed that odorous substances can be transported in the air by using AUPAs, and odors can be displayed remotely [74][75]. In chapter 5, it has also been shown that it is possible to remotely display cooling sensation by using mist and transporting it by AUPAs.

Therefore, by irradiating the odor source with an ultrasound beam, the diffusion of odorous substances is promoted. Furthermore, we propose a method of transporting the generated odorous substances to a remote sensor using another ultrasound beam. By combining these two principles, it is possible to measure the concentration of an odorous substance existing at a specific position in the air. By scanning the irradiation point of the ultrasound beam, the spatial distribution of odorous substances can be measured from a distance.

A similar system can also be used as the system of displaying odor. When there are multiple odor sources in a room, the ultrasound beam irradiates the odor sources to promote diffusion. When it is transported near the user's nasal cavity, a specific odorous substance can be generated at any time and the odor can be displayed. Most of the proposed odor displays are limited to directly displaying a prepared odor

source to the user. In addition, it does not have a function to dynamically generate odors.

By simultaneously generating and transporting odorous substances with ultrasound beams, we aim to realize the sensing of the position of the odor source and the display of the odor.

C.3 Prototype

Figure C.2 shows the prototype of the proposed system. It mainly consists of ultrasound phased arrays (AUPAs), an odor source, and an odor sensor. Four AUPAs make up one unit, and there are two units. These two units are constructed so that they irradiate directly below (Unit A) and sideways (Unit B). In unit A, the odor source is irradiated to diffuse the odorous substance. In unit B, the odorous substances diffused by the ultrasound-driven airflow are converged and transported to the odor sensor in the air.

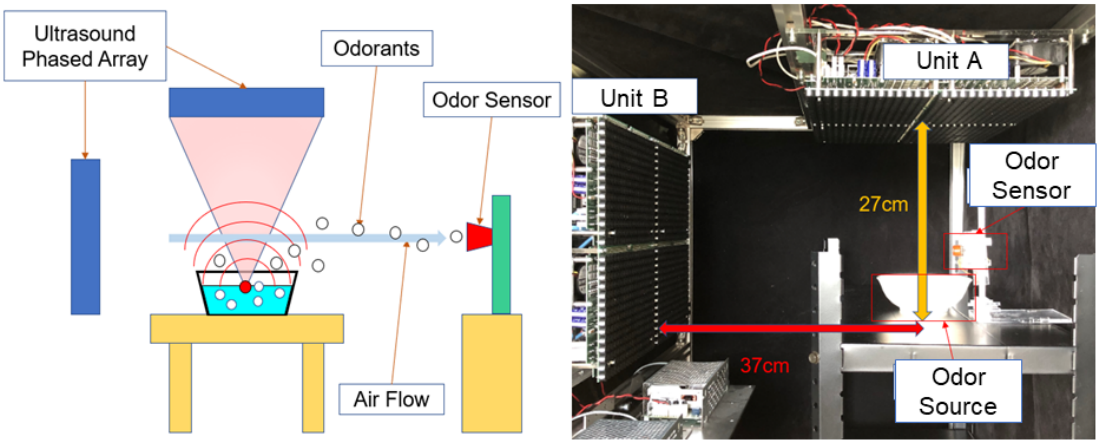

Fig. C.2. The schematic of prototype.

・Odor Sources

An aqueous solution of aroma oil ($15\,\mathrm{ml}$, main components: water, ethanol, surfactant, fragrance, methylparapen) and water ($15\,\mathrm{ml}$) was used as the odor source. By irradiating the aqueous solution with unit A, the odorous substance is diffused in the air.

・Odor Sensor

An alcohol sensor (MQ-3 Spark Fun) was used to measure the odor concentration of odorous substances transported in the air by unit B. Since the aroma oil contains alcohol, this was adopted as the most suitable for measurement. Figure C.3 shows

the prototype of the created alcohol sensor and the equivalent circuit.

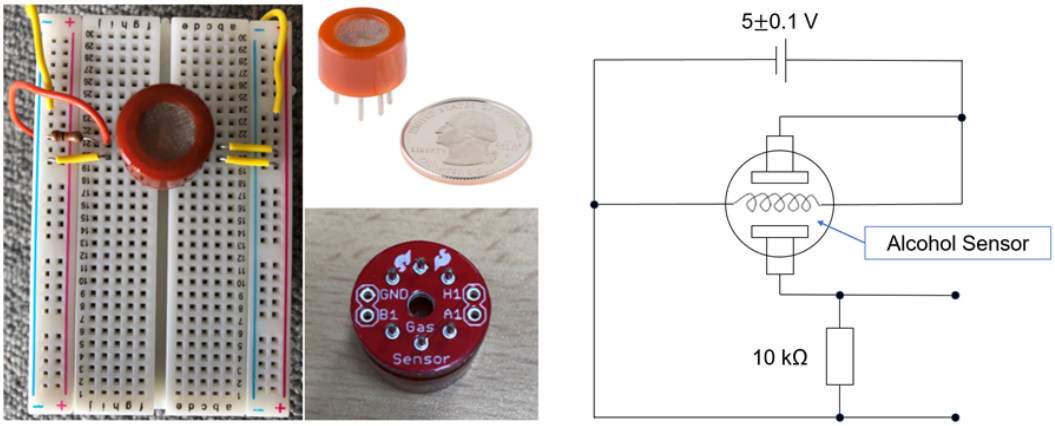

Fig. C.3. (Left)The prototype of odor sensor (cited and reprinted from https://www.sparkfun.com/products/8880). (Right)Equivalent circuit.

C.4 Experimental Setup

Figure C.4 shows the schematic diagram of the experimental system. The alcohol sensor used as the odor sensor is placed so that it is horizontal to the center position of unit B. The container containing odor source is placed so that the center of unit A and the center of the container are located vertically.

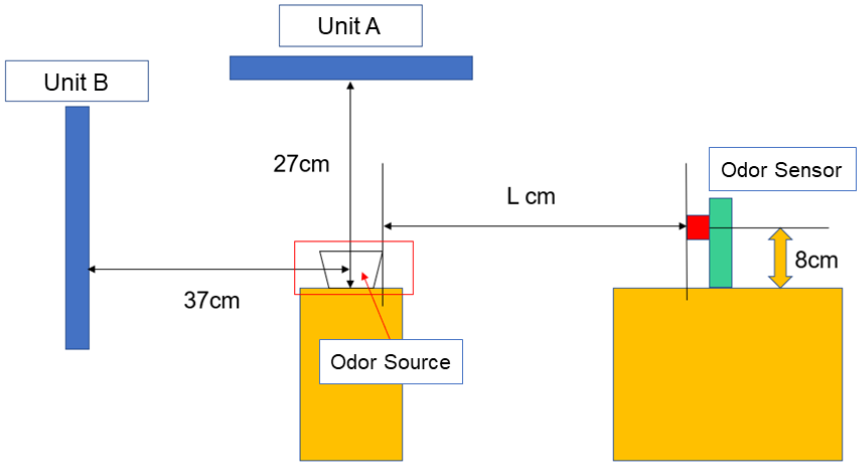

Fig. C.4. The schematic diagram of experimental setup.

The voltage supplied to the entire circuit of the alcohol sensor is $5\,\mathrm{V}$, and it is connected to the microcomputer (Arduino Uno). When the odorous substance is

brought close to the sensor, the AD conversion value can be read from the analog input, and the output voltage is derived.

C.5 Experiment 1

C.5.1 Measuring procedures 1

From the previous section, we measured the odor concentration relative to the distance between the odor source and the sensor. First, $30\,\mathrm{s}$ after the start of measurement, the ultrasound beam is irradiated from unit A to diffuse the odorous substance. Furthermore, after $30\,\mathrm{s}$, the beam is irradiated from unit B, the diffused odor is transported in the direction of the sensor, and the measurement is conducted for $40\,\mathrm{s}$. As shown in figure C.4, the distance between the sensor and the odor source is $L\,\mathrm{cm}$, and we measured the 6 patterns of $L = 40, 50, 60, 70, 80, 90\,\mathrm{cm}$.

C.5.2 Result 1

Figure C.5 shows the odor concentration change in 6 patterns of $L\,\mathrm{cm}$. It is stable at 0.34 to $0.36\,\mathrm{mg/L}$ for each distance for $60\,\mathrm{s}$ from the start of measurement. On the other hand, after the irradiation of unit B, the value of odor concentration increased for $3\,\mathrm{s}$ for each distance.

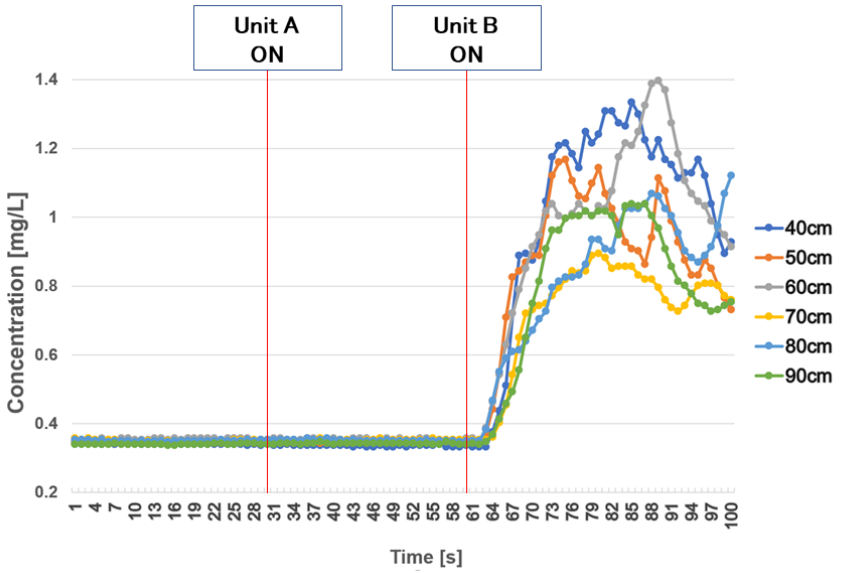

Fig. C.5. The odor concentration change with respect to distance from the odor source.

Figure C.6 shows the maximum value of the odor concentration at each distance from the start of measurement. When the odorous substances reaches the sensor

from figure C.5, the measured value of the odor concentration increases. However, from the figure C.6, there was no significant difference in the quantitative relationship of the odor concentration with respect to the distance between the sensor and odor source. It can be seen that odorous substances are transported in the air without diffusing, regardless of that distance. It is suggested that the odor concentration is uniformly distributed up to a certain distance from the odor source when unit B is operated. It is also considered that the odorous substances reached the sensor at high speed due to the velocity of the ultrasound-driven airflow.

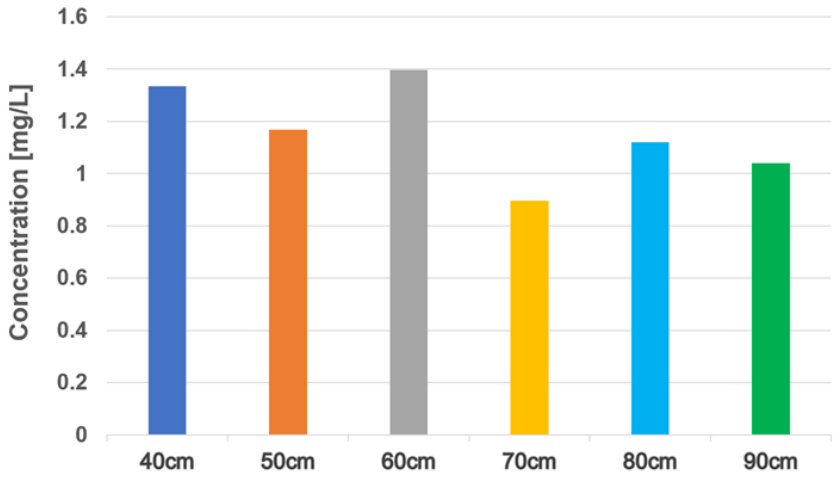

Fig. C.6. The maximum odor concentration at each distance.

C.6 Experiment 2

Using the same system as in Experiment C.5, we measure the concentration of odorous substances transported in the air by switching the irradiation to different odor sources. We use 2 types of odor sources.

C.6.1 Measuring procedures 2

As shown in figure C.7, the odor source and the odor sensor are placed. The distance between the center of unit A and the odor source is $10\,\mathrm{cm}$ each. In order to distinguish the odor sources, the odor sources are named Ⅰ and Ⅱ.

The odor source is the same as that used in Experiment C.5. The odor sources Ⅰ and Ⅱ have different fragrances which we can distinguish odors.

As for the measurement procedure, first, $20\,\mathrm{s}$ after the start of measurement, an ultrasound beam is irradiated from unit B. After $20\,\mathrm{s}$, unit A irradiates the odor source Ⅰ for $30\,\mathrm{s}$, and the irradiation is stopped. Next, $30\,\mathrm{s}$ after the pause, the odor source Ⅱ

is irradiated for $30\,\mathrm{s}$. After that, irradiation is stopped, and measurement is finished $20\,\mathrm{s}$ later. The measurement time is $150\,\mathrm{s}$.

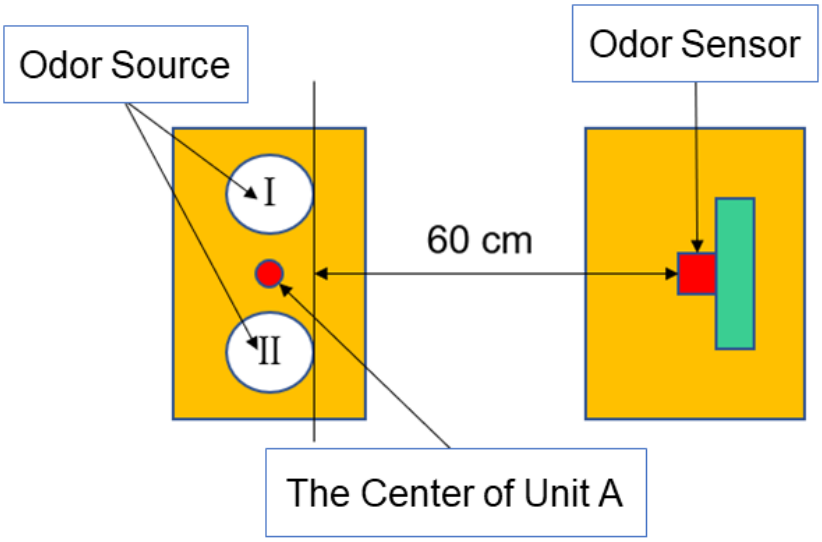

Fig. C.7. The positional relationship between the odor source and the sensor.

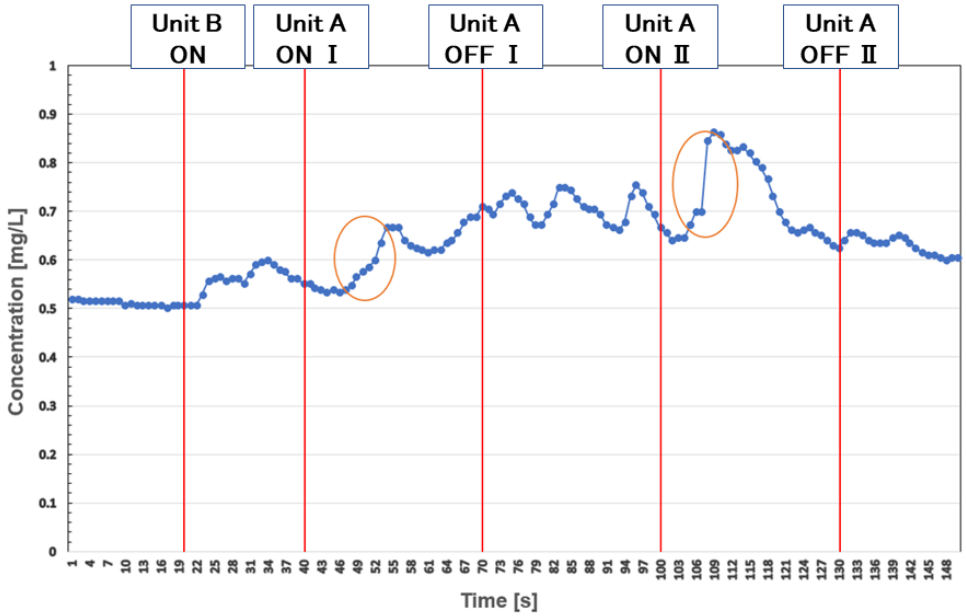

Fig. C.8. The odor concentration change with switching from odor source Ⅰ to Ⅱ. Circles indicate that odors Ⅰ and Ⅱ are responding to the sensor.

C.6.2 Result 2

Figure C.8 shows the results of the measurement method in the previous section C.6.1. When the odor sources I and II were irradiated, an increase of $0.14\,\mathrm{mg/L}$ and $0.22\,\mathrm{mg/L}$ was observed after a dozen seconds, respectively. In addition, a time response was confirmed by switching the irradiation of the ultrasound beam. On the other hand, no time response was observed after the irradiation was stopped. It is suggested that odorous substances floating around the odor source may remain.

C.7 Conclusion

In this appendix, we proposed a method of diffusing odorous substances by irradiating the odor source with an ultrasound beam and transporting them to a sensor or user's nasal cavity with another beam.

In Experiment C.5, we measured the odor concentration with respect to the distance between the odor source and sensor. A few seconds later, the odor sensor responded to the generation of ultrasound-driven airflow. It was found that odorous substances are transported in the air without diffusing, regardless of the distance between the odor source and the sensor.

In Experiment C.6, using two types of odor sources, different odor substances were generated by switching the irradiation direction of a ultrasound beam, and each odor was transported in the air by another beam. We measured the odor concentration transported in the air by the odor sensor similar to Experiment C.5. Then, we measured the odor concentration change with irradiation time and switching beam. As a result, the time response by switching of irradiation was confirmed. However, the time response by stopping the irradiation was not observed.

In the future, we will consider a method to clarify a proper quantitative relationship between the odor concentration and the distance to the sensor. As for displaying odor, we will construct a system for improving the response change of odor concentration by switching and stopping the irradiation to the odor source.